

## **INFORMATION TO USERS**

This manuscript has been reproduced from the microfilm master. UMI films the text directly from the original or copy submitted. Thus, some thesis and dissertation copies are in typewriter face, while others may be from any type of computer printer.

**The quality of this reproduction is dependent upon the quality of the copy submitted.** Broken or indistinct print, colored or poor quality illustrations and photographs, print bleedthrough, substandard margins, and improper alignment can adversely affect reproduction.

In the unlikely event that the author did not send UMI a complete manuscript and there are missing pages, these will be noted. Also, if unauthorized copyright material had to be removed, a note will indicate the deletion.

Oversize materials (e.g., maps, drawings, charts) are reproduced by sectioning the original, beginning at the upper left-hand corner and continuing from left to right in equal sections with small overlaps.

Photographs included in the original manuscript have been reproduced xerographically in this copy. Higher quality 6" x 9" black and white photographic prints are available for any photographs or illustrations appearing in this copy for an additional charge. Contact UMI directly to order.

Bell & Howell Information and Learning  
300 North Zeeb Road, Ann Arbor, MI 48106-1346 USA  
800-521-0600

**UMI<sup>®</sup>**



University of Alberta

**The Winnipeg Hailstorm of 16 July 1996:  
Synoptic Analysis and Radar Observations**

by

Amin Erfani



A thesis submitted to the Faculty of Graduate Studies and Research in partial  
fulfilment of the requirements for the degree of Master of Science

Department of Earth and Atmospheric Sciences

Edmonton, Alberta

Fall 1999



National Library  
of Canada

Acquisitions and  
Bibliographic Services

395 Wellington Street  
Ottawa ON K1A 0N4  
Canada

Bibliothèque nationale  
du Canada

Acquisitions et  
services bibliographiques

395, rue Wellington  
Ottawa ON K1A 0N4  
Canada

*Your file Votre référence*

*Our file Notre référence*

The author has granted a non-exclusive licence allowing the National Library of Canada to reproduce, loan, distribute or sell copies of this thesis in microform, paper or electronic formats.

The author retains ownership of the copyright in this thesis. Neither the thesis nor substantial extracts from it may be printed or otherwise reproduced without the author's permission.

L'auteur a accordé une licence non exclusive permettant à la Bibliothèque nationale du Canada de reproduire, prêter, distribuer ou vendre des copies de cette thèse sous la forme de microfiche/film, de reproduction sur papier ou sur format électronique.

L'auteur conserve la propriété du droit d'auteur qui protège cette thèse. Ni la thèse ni des extraits substantiels de celle-ci ne doivent être imprimés ou autrement reproduits sans son autorisation.

0-612-47024-5

University of Alberta  
Library Release Form

Name of Author: Aminollah (Amin) Erfani

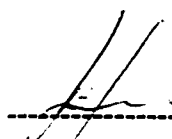
Title of Thesis: The Winnipeg Hailstorm of 16 July 1996:  
Synoptic Analysis and Radar Observations

Degree: Masters of Science

Year this Degree Granted: 1999

Permission is hereby granted to the University of Alberta Library to reproduce single copies of this thesis to lend or sell such copies for private, scholarly, or scientific research purposes only.

The author reserves all other publication and other rights in association with the copyright in the thesis, and except as hereinbefore provided, neither the thesis nor any substantial portion thereof may be printed or otherwise reproduced in any material from whatever without the author's prior written permission.

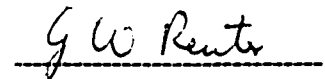
  
-----  
Amin Erfani  
306-936 Chancellor Dr  
Winnipeg, Manitoba  
R3T-2K1

20 July 1999

University of Alberta

Faculty of Graduate Studies and Research


The undersigned certify that they have read, and recommended to the Faculty of Graduate Studies and Research for acceptance, a thesis entitled The Winnipeg Hailstorm of 16 July 1996: Synoptic and Radar Observations submitted by Amin Erfani in partial fulfilment of the requirements for the degree of Master of Science.



G. W. Reuter, Supervisor



A. B. G. Bush



M. D. Sacchi

Date 23 July 1999

## **Abstract**

The 16 July 1996 hailstorm over Winnipeg, Manitoba was analysed using radar observations, sounding data, and synoptic charts. Data were part of the operational observations of Environment Canada. Warm humid air was advected by a low level jet, resulting in the classical “loaded gun” sounding with a large potential for instability (CAPE was  $4220 \text{ Jkg}^{-1}$ ). The hailstorm started as a multicell complex, triggered by the southerly low level jet converging with outflow from pre-existing showers. The development was fed by the low level jet and the release of the convective instability.

Within 30 minutes the multicell storm structure developed into a supercell with a persistent hook echo, overhang and Bounded Weak Echo Region. Radar reflectivity echoes that exceed 52 dBZ at 7 km altitude matched closely with surface observations of the hailstones having diameter of 40 mm or more. The storm closely resembled the conceptual models of severe hailstorms.

## **Acknowledgements**

I am sincerely grateful to many individuals without whose encouragement and guidance this thesis could not have been completed. In particular, I wish to thank:

- Dr. G. W. Reuter, my thesis supervisor. His suggestions, guidance and continued interest were invaluable and very much appreciated.
- Environment Canada for supplying me data and for the financial support provided during this undertaking.
- My colleagues in the Prairie Storm Prediction Centre for their comments and ideas.
- Mr. Ron Goodson for the time he spent to familiarise me with the mesoscale numerical model ARPS.
- Ms. Nina Erfani for her proof reading and encouragement.
- My parents for their encouragement.
- My wife, Carla, whose patience and enduring support contributed much to the accomplishment of this thesis.

I am indebted to you all.



## **Table of contents**

|   | page |
|---|------|
| 1. Introduction                                 | 1    |
| 1.1 Background                                  | 1    |
| 1.2 Conceptual model of a severe hailstorm      | 2    |
| 1.3 Case studies of hailstorms in North America | 4    |
| 1.4 Objectives                                  | 10   |
| 1.5 Outline                                     | 10   |
| 2. Data Sets                                    | 12   |
| 2.1 Synoptic weather charts                     | 12   |
| 2.2 Upper air balloon soundings                 | 12   |
| 2.3 Hourly observations                         | 13   |
| 2.4 Ground truth                                | 13   |
| 2.5 Vivian radar imagery                        | 13   |
| 2.6 Empirical Z-R relationship                  | 17   |
| 3. Analysis of the Winnipeg hailstorm           | 19   |
| 3.1 Overview                                    | 19   |
| 3.2 Synoptic scale air flow pattern             | 20   |
| 3.3 Triggering of the Winnipeg hailstorm        | 26   |
| 3.4 Developing stage of the hailstorm           | 29   |

|   |     |
|---|-----|
| 3.5 Maturing stage of the hailstorm                       | 31  |
| 3.6 Dissipating stage of the hailstorm                    | 36  |
| 3.7 Hail analysis of the hailstorm                        | 37  |
| 3.8 Summary of events                                     | 40  |
| 4. Comparison of Winnipeg hailstorm to conceptual models  | 43  |
| 4.1 Overview  | 43  |
| 4.2 Fawbush, Miller and Starrel's conceptual model        | 43  |
| 4.3 Chisholm and Renick's (CR) hailstorm conceptual model | 51  |
| 4.4 Lemon's conceptual model of a supercell hailstorm     | 56  |
| 4.5 Conclusion  | 58  |
| 5. Discussion and conclusion                              | 59  |
| 5.1 Summary of major findings                             | 59  |
| 5.2 Comparison to conceptual models                       | 63  |
| 5.3 Discussion  | 65  |
| 5.4 Recommendation for further research                   | 67  |
| Bibliography  | 119 |
| Appendix  | 124 |

## **List of Tables**

| <b>Table</b> |  | <b>page</b> |
|--------------|--|-------------|
| 1            | Maximum hailsize and damage as reported by weather watchers in Winnipeg.   | 68          |
| 2            | Area of 45 dBZ at 7 km (CAPPI) and its longest width perpendicular to the track of the hailstorm, together with the peak echo within area and along the width.         | 69          |
| 3            | List of 14 atmospheric parameters ranked (in order of importance) by Miller (1972) and their magnitude. (mb is equivalent to hPa, Kts = knots and nm = nautical miles) | 70          |

## **List of Figures**

| Figure  | page |
|---|------|
| 1.1 Average annual number of days with hail in Canada. (from Environment Canada, 1977)  | 71   |
| 2.1 Illustration of how a CAPPI is made. The radar beam is corrected for the earth's curvature and normal refraction. (from Crozier et al., 1986)   | 72   |
| 2.2 Geometric relation of the heights (z) of a point above the ground and its radial range (r) from the antenna. (from Environment Canada, 1997)  | 72   |
| 3.1 Relative locations of Shilo upper air station, Winnipeg and Vivian radar (range 240 km) with respect to the hailstorm's initiation position.  | 73   |
| 3.2 Time line for the evolution of the Winnipeg hailstorm.  | 74   |
| 3.3 250 hPa heights at 1200 UTC, 16 July 1996 and 0000 UTC, 17 July 1996 depicting contour heights (solid lines, dam), area of maximum winds (shaded, knots) and velocity (dashed lines). | 75   |
| 3.4 500 hPa heights at 1200 UTC, 16 July 1996 and 0000 UTC, 17 July 1996 depicting contour heights (solid lines, dam), vorticity (dashed lines).  | 76   |
| 3.5 700 hPa heights at 1200 UTC, 16 July 1996 and 0000 UTC, 17 July 1996 contour heights (solid lines, dam) and temperature (dashed lines, °C).   | 77   |
| 3.6 850 hPa heights at 1200 UTC, 16 July 1996 and 0000 UTC, 17 July 1996 contour heights (solid lines, dam) and temperature (dashed lines, °C). The axis of dilatation is shown as DD'.   | 78   |
| 3.7 Surface analysis at 1200 UTC, 16 July 1996 depicting isobars and upper front.   | 79   |

|      |   |    |
|------|---|----|
| 3.8  | Surface analysis at 0000 UTC, 17 July 1996 depicting isobars and surface front.   | 80 |
| 3.9  | Tephigrams for soundings at Shilo (WLO) taken at 1200, 1700 UTC 16 July 1996 and 0100 UTC, 17 July 1996 depicting temperatures (thick solid curves) and dewpoint (dotted curve). Horizontal lines are isobars (hPa), straight lines skewed to the right are isotherms (°C), straight lines skewed to the left are dry adiabatic (°C), long dashed lines are moist adiabatics (°C) and short dashed lines are mixing ratio (g/kg). | 81 |
| 3.10 | Hodographs for the soundings at Shilo (WLO) taken at (a) 1200 UTC, (b) 1700 UTC, 16 July 1996 and (c) 0100 UTC, 17 July 1996 depicting the winds profile (blue line). Heights are in thousands of feet. Rings are in 5 knots intervals.   | 82 |
| 3.11 | Modified Shilo (WLO) sounding at 0100 UTC 17 July 1996. Measurements from the 1200 UTC 16 July 1996 sounding above 400 hPa is attached to that of 0100 UTC below 400 hPa. Thick dashed line is the track of the lifted parcel along the corresponding wet adiabat.  | 83 |
| 3.12 | Vivian Radar CAPPI at 1.5 km for 0025 UTC, 17 July 1996. Rings are spaced 50 km apart. The colour scheme of rainfall rates (in mm/h) is shown in Fig. 3.32.   | 84 |
| 3.13 | Conceptual diagram for the triggering of the Winnipeg hailstorm   | 85 |
| 3.14 | Five minutes sequence of 1.5, 3, 5, 7 km Vivian radar CAPPIs from 0025 to 0035 UTC, 17 July 1996.   | 86 |
| 3.15 | Vivian radar (WVJ) CAPPIs at 1.5 km for (a) 0035, (b) 0045, (c) 0055 and (d) 0105 UTC.  | 87 |
| 3.16 | Five minute time sequence of 1.5, 3, 5 and 7 km Vivian radar CAPPIs from 0050 to 0105 UTC 17 July 1996.   | 88 |
| 3.17 | Time variation of height of maximum radar storm tops, 17 July 1996.   | 89 |
| 3.18 | Track of the strongest reflectivity on the southwest flank of the Winnipeg hailstorm and the orientation of the low level jet (not in   | 90 |

scale). Blue circles show the locations of the peak echoes and the their path is shown by small dashed lines.

|      |  |    |
|------|--|----|
| 3.19 | (a) 1.5 and 7 km Vivian radar CAPPIs at 0050 UTC, (b) cross section presented by RDSS through the southwest flank of the storm (shown as xx' in (a)).  | 91 |
| 3.20 | Vector composite for the velocity of the low level jet, mean environmental wind and the hailstorm at its developing an maturing stage.   | 92 |
| 3.21 | Vivian radar CAPPIs at 1.5 km for (a) 0115, (b) 0125, (c) 0135, (d) 0145, (e) 0155 and (f) 0205 UTC.   | 93 |
| 3.22 | 16 July 1996 Winnipeg hailstorm - photo by Eugene Kowaluk.   | 94 |
| 3.23 | Vivian radar CAPPIs at (a) 1.5, (b) 3, (c) 5.0 and (d) 7 km for 0120 UTC, 17 July 1996. Areas of maximum reflectivity are labelled by Z Max.   | 95 |
| 3.24 | Vivian radar CAPPIs at 0120 UTC for 1.5 km altitude (left top) and 7 km altitude (right top). The colour scheme for rainfall (in mm/h) is shown in Fig. 3.32. (b) Vertical cross section showing radar reflectivity in dBZ along the line segment xx' shown in (a). (c) Vertical cross section along yy'.                                    | 96 |
| 2.25 | Hodograph illustrating the environmental wind relative to the storm at 0100 UTC (red). Heights are indicated in km AGL (red numbers), wind speed relative to storm are in knots (black numbers).   | 97 |
| 3.26 | Schematic air flow in the direction (a) and across (b) the plane of the hailstorm's motion, 0120 UTC 17 July 1996, superimposed on the vertical cross sections displayed by RDSS (refer to Fig. 3.24). Wind components relative to the storm (in the plane and across of storm motion) are shown on the left side of each display (a and b). | 98 |
| 3.27 | Five minutes sequence of cross sections (through the southwest flank of the storm) displayed by RDSS from 0110 to 0135 UTC, 17 July 1996. Formation and decay of three cells (1-3) are shown in the severe hailstorm complex.  | 99 |

|      |  |     |
|------|--|-----|
| 3.28 | Vivian radar CAPPIs (WVJ) at 1.5 km for (a) 0215 and (b) 0245.   | 101 |
| 3.29 | The location of the reported large hailstones over the city of Winnipeg. Refer to Table 3.1 for the size and the possible damage caused to property.   | 102 |
| 3.30 | Five minutes sequence of 45 dBZ boundary (red) obtained from 7 km CAPPIs and peak echoes (blue) on the southwest flank of the storm at 1.5 km. The dashed line is the path of the storm, the solid line is the longest width of the 45 dBZ at 7 km perpendicular to the track of storm and the cross indicate the maximum echo along the width.  | 103 |
| 3.31 | Track of the longest width of 45 dBZ at 7 km (thick black) perpendicular to the storm's motion (aa') (refer to Fig. 3.29). The crosses are the maximum echoes along the width. The thin dashed line (black) is the track of the maximum echoes. Red circles are the location of the hailstones greater than 40 mm.   | 104 |
| 3.32 | Colour scheme for converting radar reflectivity (in dBZ) to rainfall rate (in mm/h) based on the Marshall Palmer Z-R relationship.   | 105 |
| 4.1  | (a) Classical pattern of a mid-latitude, synoptic scale situation favourable for the development of a severe thunderstorm. Thin line denote sea level isobars. Broad arrows represent low level jet (LLJ), polar jet (PJ) in the upper troposphere, and subtropical jet (SJ) at a slightly higher level in the upper troposphere. Severe storm's (hatched areas) are most likely to start near "x". (from Barnes and Newton, 1986)<br>(b) The composite dynamic features, in the synoptic scale, that were present over southern Manitoba at 0000 UTC, 17 July 1996 (approx. 30 minutes prior to the hailstorm initiation) | 106 |
| 4.2  | (a) The classical "loaded gun" sounding of temperature and dewpoint plotted on a tephigram (from Johns and Doswell 1992).<br>(b) The Winnipeg hailstorm sounding (from Shilo at 0100 UTC 17 July 1996).  | 107 |
| 4.3  | (a) Typical 500 hPa heights (solid, dam) and 100-500 hPa thickness (dashed, dam) fields associated with severe convective outbreaks in Alberta.  | 108 |

- (b) East - west daytime cross section showing exaggerated mountain plain circulation produced by the upper level cooling and surface heating over the foothills. ( from Smith and Yau, 1993b)
- 4.4 Schematic horizontal sections of the radar showing the radar structure of a supercell storm at 1, 4, 7, 10 and 13 km AGL. Reflectivity contours are in dBZ. Note the indentation on the right front quadrant of the storm at 1 km which appears as a BWER at 4 and 7 km. On the left hand side of the BWER, is a Z maximum, extending from the top of the BWER to the surface. (from Chisholm and Renick, 1972) 109
- 4.5 Schematic vertical sections through a supercell storm:  
 (a) normal to the plane of storm motion. The cross section is taken through the line AB in Fig. 4.6 and viewed in the upwind direction. Note that the BWER extends to a height of 9 km AGL and the high gradient of reflectivity on the LH side of the BWER.  
 (b) in the plane of storm motion, along the line CD of Fig. 4.6. Note the Z maximum caps the BWER and extends to the surface on the rear of the BWER. (from Chisholm and Renick, 1972) 110
- 4.6 Five minute time sequence, from 0110 to 0135 UTC, of 7 km CAPPI. 111
- 4.7 The location (circles) of the BWER centres from 0110 to 0135 UTC. These centres are obtained from the 7 km CAPPIs shown in Fig. 4.6. The solid lines joining the centres illustrate the track and the dashed line, aa', is the best fit line through the centers. 112
- 4.8 (a) Classical supercell wind hodograph (from Chisholm and Renick, 1972)  
 (b) Winnipeg hailstorm wind hodograph (at 0100 UTC 16 July 1996). 113
- 4.9 Schematic airflow pattern for a supercell hailstorm (refer to figure 4.6 for location of cross sections). (from Chisholm and Renick, 1972) 114
- 4.10 (Above) Vertical sections as it might be observed on radar scope during the (a) early, (b) middle, and (c) mature phases of a supercell storm. Low-level inflow, updraft, and outflow aloft (solid lines) are superimposed on the radar reflectivity (dashed lines). The updraft becomes more intense as the storm evolves to its 115



mature phase. WER implies a weak echo region and BWER implies a bounded weak echo region. (Below) Composite tilt sequences. Solid lines are the low-level reflectivity contours, dashed lines outlines the echo > 20 dBZ derived from the middle-level elevation scan, and the black dot is the location of the maximum top from the high-levels scan. (from Weisman and Klemp 1986)

- |      |  |     |
|------|--|-----|
| 4.11 | Vivian radar CAPPIs for 1.5, 3, 5, 7 km AGL at 0035 UTC 17 July 1996 (triggering stage).   | 116 |
| 4.12 | (a) 1.5 and 7 km Vivian radar CAPPIs at 0100 UTC , (b) cross section presented by RDSS through the southwest flank of the storm (shown as xx' in (a)). | 117 |
| 4.13 | (a) 1.5 and 7 km Vivian radar CAPPIs at 0120 UTC, (b) cross section presented by RDSS through the southwest flank of the storm (shown as xx' in (a)).  | 118 |

## **1. Introduction**

### **1.1 Background**

In this thesis we investigate the severe hailstorm that developed on 16 July 1996 over Winnipeg, Manitoba. The front page of the Winnipeg Free Press, on 17 July 1996, summarised the event as follows:

“Gale-Force winds, torrential rains and golf ball-sized hail tore through Winnipeg last night, leaving behind blackouts, thousands of dented cars and millions of dollars in damages. Charleswood and St. James took the brunt of the hail, which piled up like snow. Rain deluged streets and underpasses—where some drivers sought shelter from the hail—leaving cars stranded in water as deep as 1.5 metres. In some areas, the 100-minute storm smashed gardens and ripped so many leaves off trees it looked like the seasons had suddenly changed from summer to fall. Although the entire city was hit by thundershowers and winds up to 100 kilometres per hour, the hail cut a swath southeast from Headingley, through St. James, Charleswood and Waverly Heights before moving through south St. Vital”.

The Winnipeg hailstorm had the following characteristics: very rapid development, intense rainfall causing flash floods, large hailstones (up to 70 mm in diameter) and strong winds. The storm caused extensive damage to cars, roofs and windows of houses, and vegetation, and was responsible for an estimated insured loss of 111 million dollars to Winnipeg. The extreme characteristics and impact of the hailstorm warrants a detailed investigation. As an introduction to this area of investigation, a brief review of some conceptual models of severe hailstorms is provided, followed by a discussion of some hailstorm case studies that have been conducted in the past. A more

detailed discussion of conceptual models in relation to the Winnipeg hailstorm is provided in chapter 4.

## **1.2 Conceptual model of a severe hailstorm**

Hail consists of spherical lumps of ice and snow which fall from very active thunderstorms. The lumps of ice may range in size from pea to larger than a baseball. The damage caused by hailstones depends largely on their size, as the kinetic energy of the impacting hailstone increases with increasing size. Largest hailstones are usually formed in a supercell storm (Summer, 1972; Paul, 1973; Browning and Foote, 1976; Nelson, 1976).

The supercell storm is characterised by a strong rotating updraft, high water content, large cloud-drop size, and deep vertical development. These characteristics are produced when warm humid air from below the cap is released into the deep conditionally unstable air aloft. The strong environmental wind shear with veering winds with height aids the formation of a strong quasi-steady updraft and downdraft circulation couplet within the storm's complex. This circulation couplet produces a long lived self propagating mechanism (Chisholm and Renick, 1972). A "high positive correlation between vertical velocity and vorticity" (Doswell, 1985, p70) is a qualitative distinction between the supercell and multicell storm types. This correlation produces a long-lasting rotating updraft that propagates the storm to the right, or occasionally to the left, of the mean environmental winds. Supercells are often seen to evolve from multicell storms (Lemon, 1980), and even during their quasi-steady phase may comprise several rain centres, which evolve similarly to multicell storm types (Browning, 1977; Weisman, 1986).

In a supercell, the warm humid air supplies the buoyant energy needed to maintain the updraft and downdraft circulations (Djuric, 1994). Condensation of water vapour and the formation of precipitation occurs in the updraft (Browning, 1977). The precipitation then falls in the downdraft. The downdraft originates from dry air in the mid-levels of the troposphere. This air often enters the storm's complex at an angle to the right of the inflow, corresponding to the environmental wind shear. The downdraft air is cooled by the evaporation of precipitation (Roger and Yau, 1989). This descending air spreads out at the surface forming a gust front.

A supercell storm is potentially the most dangerous of all the convective storm types. In addition to large hailstones, it may produce high winds and long lived tornadoes over a wide path (Weisman and Klemp, 1986). The structure and evolution of supercell storms have been investigated in various geographical regions: Wokingham, England (Browning and Ludlam, 1962), Alberta, Canada (Chisholm and Renick, 1972), the former Soviet Union (Marwitz, 1972), and the central United States (Lemon, 1980). In all regions the supercell storms evolved in an atmospheric environment that had a capped "loaded gun" thermodynamic profile and a strong vertical wind shear with winds veering with height (John and Doswell, 1992).

The initial hailstones, or embryos, begin as rain in the lower layers of the storm's structure. The updraft carries the raindrops to the higher and colder portions of the cloud (the so-called embryo formation region). The updrafts in the embryo formation region must be relatively weak to allow the embryos sufficient time to grow into large particles. After the embryos have formed and grown in their formation region, they fall into the main updraft region of the supercell (known as the hail growth zone). Here, updrafts must be at least  $15 \text{ ms}^{-1}$  in order to support the hailstone and to prevent it from falling to the ground prematurely. Once the hailstone has grown to a sufficiently large size, it falls to

the ground. The strength of the updraft in the hail growth zone determines the size of the hailstones (English, 1973).

The radar echo pattern of precipitation in supercell storms has distinctive characteristics. On weather radar displays, a supercell is identified by a pendent or “hook” echo at low levels, a Bounded Weak Echo Region (BWER) or echo free vault at mid levels, and an overhang at mid to high levels of the storm’s structure (Chisholm, 1973; Browning and Foote, 1976). The hook echo is caused by precipitation being drawn into the cyclonic rotating wind. The formation of the hook on the southwest flank of the storm’s complex indicates a mesocyclone. The precipitation free area ahead of the hook is where the warm humid air flows into the storm (Browning, 1964). The presence of the BWER and the overhang indicates a strong rotating updraft.

### **1.3 Case studies of hailstorms in North America**

Case studies of hailstorms have determined the major synoptic and mesoscale condition necessary for the formation of severe hailstorms. Most cases had the following characteristics; 1) high latent energy (moisture) in the planetary boundary layer, 2) conditionally unstable air at low to mid levels, 3) strong vertical wind shear with veering of the winds with height and 4) a triggering mechanism to lift a parcel at lower levels to its level of free convection (e.g. Strong, 1986; Smith and Yau, 1993). Common triggering mechanisms are surface heating, dry lines, frontal boundaries, outflow boundaries from existing thunderstorms, orographic lifting or low level jets (Cotton, 1989).

Case studies of severe hailstorms have also determined the internal flow and precipitation fields within the hailstorm’s complex. The evolution of the flow from the developing to the dissipating stages were characterised (Chishom, 1973).

The data used in case studies of severe storms include synoptic weather charts, and observations from weather radars, satellites and radiosondes. Some case studies also had research aircraft measurements and high resolution surface observations. The spatial and temporal data sampling frequencies have been mainly designed for each individual case study. Weather radar has been the ideal tool (Doswell, 1985) for the following aspects of hailstorms:

- 1) the echo intensity representing hailstones,
- 2) the reflectivity distribution with respect to internal flow pattern,
- 3) the rate of intensification and growth of isolated intense echoes (cells) and their evolution relative to the hailstorm's main complex,
- 4) the interaction of individual cells with the storm's immediate environment throughout their evolution, and
- 5) the determination of storm type based on cellular evolution.

In North America the major centres for hailstorm studies have been Illinois, Oklahoma, South Dakota, Colorado and Alberta. These locations have all been identified as being prone to severe hailstorms (Strong, 1986). Selected case studies of severe hailstorms in North America will be summarised to illustrate past approaches and results that have been obtained from such investigations.

**a) 28 July 1968 Hailstorm in Alberta, Canada (Chisholm, 1973)**

On 28 July 1968 a hailstorm developed on the foothills of Alberta, Canada. Radar reflectivities of  $\geq 50$  dBZ were present in this storm over the course of several hours. The evolution of this storm had three distinct phases.

Phase 1 - The storm was essentially motionless while situated over the eastern range of the Rocky Mountain foothills. The radar cross section of the storm at this stage was characterised by a Weak Echo Region (WER) (Chisholm and Renick, 1972) on its downwind side. The WER was divided from a vertical column of echo maximum by a sharp reflectivity gradient. The radar characteristics and the storm relative winds revealed that the air was entering the storm from the west at low levels, traversed up through the WER and was tilted downstream as it encountered moderately strong cross winds at higher levels. There was a sharp reflectivity gradient between the echo maximum and WER indicating that the largest precipitation particles were falling closest to the updraft. The air flow depicted for this storm was only possible as long as it remained anchored to the foothills. Once the storm began to move the WER dissipated and the storm reflectivity changed over the course of 30 minutes and resulted in phase 2.

Phase 2 - As the storm moved to the southeast, radar cross sections showed that the storm was characterised by a BWER on its southwest flank, indicating the orientation of strong rotating updraft. Echo values in excess of 48 dBZ were also detected above the BWER. The BWER was progressively developing and decaying. The high echo values above the BWER descended back through the updraft, bringing about the demise of the BWER.

Phase 3 - At approximately 2 hours into the life of the storm, the BWER collapsed completely and the storm changed its configuration once more. At this stage the radar cross sections showed a WER region on the leading edge of the storm, indicating that the air was entering the storm from the east at low levels. During this phase the storm moved to the east.

Chisholm labelled the different phases: Phase 1 as a stationary or back feeding storm. Phase 2 as a “short lived supercell storm”. Phase 3 as a “squall line” (Newton 1963).

**b) 19 July 1973 Hailstorm in Colorado (Chalon et al., 1976)**

On 19 July 1973 a hailstorm evolved in northeastern Colorado. The storm had a lifetime of nearly 2 hours and comprised of at least seven distinct cells. It attained a maximum radar top of 14 km, reflectivity echo maximum of 68 dBZ and produced hailstones as large as 15 mm in diameter. The radar structural analysis of the storm revealed that new cells were developing on the southern flank of the storm's main complex at an average frequency of every 15 minutes. The new cells were initially detected at an altitude of 7 km ( $-12^{\circ}$  C) and at a distance of 5 to 10 km away from the main complex. In the early stages of their development they grew rapidly in size and intensity, and moved slower than the existing cells, but as the older cells decayed they became the main storm component. At any instant as many as 3 cells were found to coexist in varying stages of development. The average life time of the individual cells from initiation to dissipation was 45 minutes. At a particular stage in the evolution of each cell, a vertical radar cross section showed a BWER and a forward overhang typical of supercell storms. In contrast to supercell storms, the features were transitory as the result of the new echoes joining with the main echo soon after their formation as discrete entities. The overall motion of the storm was to the south at an average speed of  $10 \text{ ms}^{-1}$ . This was primarily due to the propagation of the cells on the southern flank. Once each cell began to dissipate, their upper portion moved with the mid-level tropospheric wind and were carried out in the anvil to the northeast. Chalon et al. (1976) classified this storm as a multicell.



### **c) 22 June 1976 Hailstorm in Colorado (Fankhauser, 1982)**

On 22 June 1976 an approaching 500 hPa long wave trough from the western United States generated a low pressure system over southern Wyoming. The low produced southeasterly flow over northern Colorado where the terrain rises. The southeast winds were bringing moist air from the gulf of Mexico to the regions. A localised surface convergence in the warm sector and the upslope flow triggered a storm over northeastern Colorado. The storm remained quasi-steady during its 90 minute lifetime and produced copious rainfall and widespread hail.

In the early stages of the storm development radar cross sections showed that, while the old cells were moving to the north, new cells were being generated to the south at a rate of one every 10 minutes. The new cells were developing as the result of the convergence between the outflow from the older cells and the warm moist air advection from the south, much like a multicell storm (Chisholm and Renick, 1972). Within approximately 30 minutes into the storm lifetime a cell to the south became more intense than the other existing cells and dominated the entire cluster. This cell lead the storm to its maturing stage. The intensified storm became stationary and its three dimensional radar structure displayed the characteristics of a supercell (Browning, 1964; Marwitz, 1972; Chisholm and Renick, 1972). During this stage an extensive overhang appeared to the south and east of the main body of the storm. A significant amount of precipitation echoes (greater than 50 dBz) were suspended above the 6 to 8 km altitude in this region. A persistent BWER was observed for more than 40 minutes within the overhang. The BWER appeared to fluctuate in size and shifted in its horizontal position. These were presumably the result of corresponding oscillations in the updraft which in turn were probably due to local precipitation loading. Adjacent to the BWER was a column of echo maximum extending to the ground with a high reflectivity gradient in between. After 90 minutes of intense quasi-steady structure, the storm's complex disorganised and the

overall intensity of the reflectivity declined. Fanhkauser (1982) categorised this storm as an intense multicell.

**d) 22 July 1976 hailstorm Colorado (Foote and Charles, 1982)**

On 22 July 1976 a stationary surface front extended from northeast to southwest through Kansas beneath a 500 hPa diffluent region. Light southeasterly winds south of the stationary front provided a flux of low level moisture into northeastern Colorado. A lee trough had also formed to the east of the Rocky Mountains over eastern Colorado. Convection was initiated during the afternoon in northeastern Colorado, as a result of the localised heating and convergence associated with the lee trough. The storm moved to the southeast and lasted for approximately 5 hours and displayed echoes greater than 60 dBZ on radar. The representative sounding of the environment showed that the air was potentially unstable at mid levels and the vertical wind shear was weak. The winds with respect to the storm's motion veered with height below 9 km.

The radar structural analysis of this storm revealed that the storm started as a series of organised multicells and evolved into a steadier stage. The latter stage was characterised by a periodic (every 10 to 18 minutes) formation of new cells on the southern flank of the storm. The new cells eventually merged with the main storm's complex. The successive formation of new cells propagated the storm to the south. This stage of the storm displayed some characteristics of a supercell storm. Foote et al. (1982) argued that the dichotomy of organised multicell versus supercell is often developed in terms of qualitative structural characteristics (Marwitz, 1972; Chisholm and Renick, 1972; Barnes, 1978). On the other hand, Browning (1977) has proposed that classification be according to cell life time. This can be somewhat more objective. However, since the cells in many storms will neither be short-lived nor long-lived, but somewhere in

between, the scheme is not likely to encompass all cases. The hailstorm of 22 July is an example of such a case.

## **1.4 Objectives**

An analysis of the average annual number of days with hail in Canada, Fig. 1.1 (Environment Canada, 1977), shows that southern Manitoba is an area with a relatively high frequency. To our knowledge, no investigation of a hailstorm developing over southern Manitoba has been carried-out in the past. This thesis examines the evolution of the 16 July 1996 hailstorm over southern Manitoba from the triggering to dissipating stages. The approach taken in performing this study is similar to the case studies summarised in the previous section. Specifically the main objectives of this thesis are:

- 1) to evaluate whether a complete analysis of this hailstorm can be conducted using the operational observations collected by Environment Canada;
- 2) to determine the major dynamic processes that affected the evolution of the hailstorm in three dimension;
- 3) to determine to what extent the development and structure of the Winnipeg storm compares to conceptual models of severe hailstorms.

## **1.5 Outline**

We conclude this chapter by outlining the contents of the remaining chapters of this thesis. In chapter 2, the weather observations used in this thesis are briefly described. The emphasis is on the data collected by the Vivian weather radar. In Chapter 3, the synoptic scale atmospheric condition over southern Manitoba, prior to the hailstorm's initiation, will be evaluated and the most likely triggering mechanism of the hailstorm

will be determined. The radar structural characteristics of the storm at its triggering, developing, maturing and dissipating stages will be examined. The major synoptic scale parameters that contributed to the evolution of the hailstorm will also be defined. The radar signature indicating large hailstones will be evaluated against the hailstone reports. In Chapter 4, the findings of chapter 3 will be compared to conceptual models of hailstorm studies. These conceptual models are then used to reveal further insights about the development and evolution of the severe hailstorm. Chapter 5 summarises the results and delineates the conclusion of this thesis. Some suggestions for future research will also be offered.

## **2. Data Sets**

### **2.1 Synoptic weather charts**

The three dimensional structure of the troposphere is recorded by radiosonde released at 0000 and 1200 UTC daily. The soundings sample temperature, pressure, humidity and the horizontal wind vector. The radiosonde data collected all over the world are made available to government weather forecasting agencies. The synoptic sounding data are processed by the Canadian Meteorological Centre (CMC) in Montreal. The data are interpolated and assimilated for consistency. For example, the temperature and pressure data are related by the hydrostatic balance equation. The synoptic fields are contoured on constant pressure levels ( 850, 700, 500 and 250 hPa pressure levels).

For this case study, the CMC weather charts are used to describe the synoptic scale evolution of the atmosphere. The wide spacing between upper air sites and the long sampling intervals of 12 hours prohibit these charts from displaying mesoscale features such as the airflow within the Winnipeg hailstorm.

### **2.2 Upper air balloon soundings**

The only upper air site in southern Manitoba is located at Shilo (WLO). This site is operated by the Canadian defence forces when required by military operations. For the Winnipeg hailstorm of 16 July, three soundings were released within a period of 13 hours. The last sounding was obtained at approximately 30 minutes of the hailstorm's initiation. Shilo soundings will be analysed on a tephigram.

## **2.3 Hourly observations**

Surface weather observations are reported at least once per hour by observers at a number of sites. The data collected are temperature, dewpoint temperature, wind speed, wind direction, surface pressure, precipitation, cloud heights and cloud amounts. The methods and standards of these measurements are established by the World Meteorological Organisation. There are also some unmanned observing site that automatically generate hourly observations. Automatic weather stations record temperature, dewpoint temperature, wind speed and direction and pressure. In this case study, changes in temperature, pressure and wind are important for both the synoptic and smaller scale (thunderstorm scale) analysis.

## **2.4 Ground Truth**

A convective storm, due to its small horizontal scale, often cannot be detected by the coarse network of surface observing stations. To improve the network of observations, volunteer weather observers have been recruited by Environment Canada to report weather events to the Prairie Storm Prediction Center in Winnipeg. The observers are located across southern Manitoba and report storm information by telephone. Although they are not trained observers, the information they provide to the forecasters confirm the severity of the weather events.

## **2.5 Vivian radar Imagery**

### **2.5.1 Radar characteristics**

The radar observations used for this case study were obtained by the weather radar located at Vivian (WVJ), Manitoba. The Vivian radar transmits energy pulses at a frequency of 5.625 GHz, which corresponds to a wavelength of 5.32 cm (C-band). The

transmitted pulses have a peak power of 250 kW, a repetition frequency of 250 Hz , and a duration of 2  $\mu$ s. The antenna is parabolic, has a diameter of 3.7 m with a beam width of 1.1° and rotates at a scan rate of 6 rpm. Within every five minutes, 360° scans of reflectivity data are made at 24 different elevation angles ranging from 0.5° to 30°. The radial range was 240 km. The data are recorded in 2 km length bins for every elevation angle with the exception of 0.5°, where for the first 120 km radial range they are recorded in 1 km length bins. This scanning process is referred to as the “volume scan”.

### **2.5.2 Radar data processor (RDP) products**

The volume scan data of the reflectivity values of the Vivian radar is provided to the RDP (Radar Data Processor). The RDP products that are used in this study are CAPPI (Constant Altitude Plan Position Indicator), and Echo tops. These displays are now described:

- 1) CAPPI - As the antenna is rotated uniformly in azimuth and raised in elevation by fixed steps after each revolution, by selecting any appropriate range interval for each elevation, a series of annular rings can be swept out centred on any selected altitude. Data from the set of annular rings, which are in range-azimuth ( $r, \theta$ ) co-ordinates, are then meshed together to synthesize a near horizontal surface. The data is converted from the polar to cartesian co-ordinate system and displayed with a horizontal resolution of 2 km by 2 km (pixel size). The RDP algorithm assigns a peak reflectivity value to each pixel. Fig. 2.1 shows the vertical antenna beam axes locations for the syntheses of CAPPI displays at 2 different altitudes, that is, 1.5 and 4 km. It is apparent that the CAPPI-surface slices in reality are composed of a series of annular volumes which are slightly tilted and whose thickness and width increases with range. The figure accentuates

the layer irregularity due to the difference in scale ordinate axes, but these discontinuities are nevertheless present and explain occasional aberrations which will occur with certain echo patterns. It can also be seen from this figure that the lower level CAPPI becomes less useful beyond approximately 120 km, due to the surface of the earth.

- 2) Echo tops - The highest altitude of the minimum detectable signal is obtained from a volume scan and converted to cartesian data display elements (2 km by 2 km). One limitation to this method of detection is that precipitation echoes may have varying heights relative to the beam axis. Depending on where the precipitation is located and how many other precipitation structures are present, certain echoes may be underestimated due to partial beam filling.

### **2.5.3 Radar Decision Support System (RDSS) products**

The volume scan data of reflectivity data are also processed using the RDSS software to generate vertical cross sections. The RDSS algorithm divides the atmosphere, within the range of radar, into cubes of 1 km length sides that extend from the surface of the earth to the top of the atmosphere (Environment Canada, 1997). Reflectivity values are stored at the centre of each cube. The data value at every bin of a volume scan closest to the centre of the box is assigned to that grid centre.

$$z = [(R + h)^2 + r^2 - 2 r (R + h) \cos (90 + \theta)]^{1/2} - R - h \quad (2.1)$$

where;

$R$  = earth's radius at sea level



$h$  = height of radar above sea level  
 $z$  = height of point above the ground  
 $r$  = direct range from radar to point above ground  
 $\theta$  = radar elevation angle

Equation 2.1 defines the relation between the height of a point in space (  $z$  ) above the ground and its range (  $r$  ) from the radar (Fig. 2.2). A cross section is a display of echoes represented by the center point of the corresponding cubes from the ground to the top of the atmosphere and are displayed in 1 km by 1 km resolution. The cross section taken automatically by the RDSS are through the vertical plane that has the highest radar reflectivity, called the centroid of the echo complex.

#### **2.5.4 Limitations and shortcomings of radar data**

For a discussion of limitations of radar observations we refer to Crozier et al. (1986). Here we deal only with the major issues related to the Vivian radar for severe convection.

- 1) Conical beam spreading - The volume scanned by the beam increases as the range from the radar increases.
- 2) Beam width distortion - The radar beam is shaped like a cigar with an axis along the beam. If there exists a target at any part of the beam, that target will be displayed as though it were on the beam axis.
- 3) Pulse length distortion - If some targets are not separated from one another by a distance more than one-half the distance occupied by a pulse in space, the targets will appear as one instead of two or more.

- 4) Wind shear distortion - The vertical variation of wind vector with height between the base and the top of a thunderstorm has an influence on the shape and inclination of the precipitation with height. This distortion causes the range of the storm to appear larger than they are in reality.
- 5) Anomalous propagation - When there exists variations in temperature and moisture profiles in the atmosphere (which lead to variation in the index of refraction with height), the radar beam bends as it traverses through different profiles. Atmospheric conditions like these are especially present in weather events such as thunderstorms.
- 6) Attenuation for radar detecting in the 5 cm wave length - Actual values of returned echoes are at times difficult to determine as intervening targets can attenuate the signal. This occurs in heavy precipitation.

## **2.6 Empirical Z-R relationship**

To relate the rainfall rate to the radar reflectivity the Vivian radar system uses the empirical relationship:

$$Z = 200 R^{1.6} \quad (2.2)$$

Z is reflectivity (dBZ) and R is rainfall rate (mmh<sup>-1</sup>). This is the Marshall and Palmer Z-R. This relation is consistent with the exponential size distribution for raindrop diameters (Roger and Yau, 1989). The reflectivity depends on the drop-size distribution, (Roger and Yau, 1989; Rinehart, 1997):

$$Z = \sum_i N_i D_i^6 \quad (2.3)$$

where  $N$  is the drop size density and  $D$  is diameter of the droplet. Thus  $Z$  depends on the sixth power of raindrop size. When rain is associated with hail, most of the reflectivity comes from hail due to its size. Later in this thesis it will shown that echoes  $\geq 45$  dBZ indicate hail in the case study storm.

### **3. Analysis of the Winnipeg hailstorm**

#### **3.1 Overview**

In this chapter we will investigate the build up of the synoptic flow pattern prior to the hailstorm's initiation, and its evolution from its triggering to its dissipating stage. The main objectives are:

- 1) To evaluate the synoptic scale atmospheric condition over southern Manitoba prior to the hailstorm's initiation.
- 2) To determine the dynamic and thermodynamic processes leading to the triggering of the hailstorm.
- 3) To determine the major synoptic scale atmospheric parameters that contributed to the evolution of the hailstorm.
- 4) To document the precipitation structure of the hailstorm at the triggering, developing, maturing and dissipating stages (using radar data).
- 5) To evaluate the radar representation of hailstones (diameter  $\geq 20$  mm) within the hailstorm's structure at the maturing stage using the minimum radar criteria set by Lemon (1977)
- 6) To verify the echoes' representation of large sized hailstones (diameter  $\geq 40$  mm) using actual surface reports of large sized hails

The data to perform the tasks outlined above are obtained from synoptic weather charts produced by the Canadian Meteorological Centre, radar echoes detected by the Vivian radar and the soundings released from the Shilo upper air site. Fig. 3.1 shows the location of the City of Winnipeg and the vicinity of hailstorm's initiation point, Vivian radar and Shilo upper air station.

### **3.2 Synoptic scale air flow pattern**

In this section the synoptic scale evolution of the atmosphere over southern Manitoba will be analysed using synoptic weather charts and upper air soundings. The condition of the atmosphere at 0000 UTC 17 July 1996, just prior to the hailstorm's development, will be determined. Fig. 3.2 shows the time line of the storm's evolution.

#### **3.2.1 Analysis of the synoptic weather charts**

In this subsection the dynamic and thermodynamic processes of the synoptic air flow from 1200 UTC 16 July 1996 to 0000 UTC 17 July 1996 are examined using the 250, 500, 700 and, 800 hPa, and surface charts.

##### **a) 250 hPa chart (Fig. 3.3)**

At 1200 UTC 16 July 1996 a westerly jet stream with a core wind speed of 74 knots blows over central Alberta. The jet extends from central Manitoba to central British Columbia. At 1200 UTC a second air jet with a core wind speed of 67 knots over Minnesota extends into southern Manitoba. Twelve hours later, the first jet, with a diminished core speed of 69 knots, arches from Northwestern Ontario to central British Colombia. At 0000 UTC 17 July 1996 the secondary jet is located to the southeast, away from southern Manitoba.

##### **b) 500 hPa chart (Fig. 3.4)**

At 1200 UTC the wind over southern Manitoba blows from the northeast with a speed of approximately 30 to 45 knots. The wind speed has decreased to approximately 25 knots and its direction has changed from northwesterly to westerly at 0000 UTC, 17

July 1996. The weakening of the wind at 500 hPa is consistent with the departure of the second 250 hPa air jet from southern Manitoba (discussed above). There are no apparent relative vorticity maximum or minimum apparent in the 500 hPa flow over southern Manitoba at 1200 UTC or 0000 UTC.

**c) 700 hPa flow (Fig. 3.5)**

At 1200 UTC 16 July 1996 the wind over southern Manitoba is southwesterly with a speed of approximately 30 knots. A northwest to southeast 5° C isotherm is oriented perpendicular to the wind direction over southwestern Manitoba. Twelve hours later the wind blows from the southwest at about 25 knots, and the 5° C isotherm is shifted to central Manitoba. The northeastward movement of the 5° C isotherm indicates warm air advection at 700 hPa. The warm air advection will be discussed in more detail in the next section, in connection with the sounding.

**d) 850 hPa chart (Fig. 3.6)**

At 1200 UTC 16 July 1996 a northwest to southeast 15° C isotherm is shown. This isotherm moves from southwestern Manitoba to central Manitoba by 0000 UTC 17 July 1996 in a prevailing south to southwesterly flow. A tightening of geopotential heights over southern Manitoba from 1200 to 0000 UTC shows that the flow has strengthened and has formed into a jet by 0000 UTC. The orientation of the 15° C isotherm relative to the jet indicates warm air advection over southern Manitoba. The dew point spread in flow of the low level jet also indicates moisture advection. The dilatation axis (indicated by DD') and the 15° C isotherm, shown at 1200 and 0000 UTC, are almost parallel. This identifies an area of frontogenesis.

#### **e) Surface pressure charts (Fig 3.7 and 3.8)**

An upper warm front, associated with the 850 hPa flow is drawn on the 1200 UTC 16 July 1996 surface map (Fig. 3.7). The associated surface warm front at 0000 UTC 17 July 1996 is shown in Fig. 3.8. The strength and the exact position of the surface warm front cannot be determined accurately due to sparse observing sites over southern Manitoba. The dewpoint temperature over southern Manitoba has increased from 13° C (Fig. 3.7) to a peak value of 22° C (Fig. 3.8). The water vapor mixing ratio has increased from 9.5 gkg<sup>-1</sup> to 17gkg<sup>-1</sup>. We speculate that the dramatic increase in the mixing ratio came from moisture advection and evapotranspiration. The strong surface winds would cause strong moisture fluxes.

#### **3.2.2 Sounding analysis**

Balloon soundings were released from Shilo at 1200 UTC 16 July, 1700 UTC 16 July, and 0100 UTC 17 July. The hailstorm had developed approximately 120 km to the northeast of Shilo. With a west to southwesterly flow, Shilo soundings represent the storm environment adequately. The stability of the atmosphere below 500 hPa level from 1200 UTC 16 July to 0100 UTC 17 July will now be evaluated.

##### **a) 500 to 700 hPa layer (Fig. 3.9)**

At 1200 UTC, the 700 to 500 hPa layer is conditionally unstable. The dew point depression ( $T - T_d$ ) within this layer indicates that the air from 700 to 600 hPa is moist, while the air from 600 to 500 hPa is relatively dry. From 1200 to 0100 UTC the 700 to 500 hPa becomes warmer. The hourly increase in temperature at 700, 600 and 500 hPa are 0.4°, 0.3° and 0.4° Ch<sup>-1</sup>, respectively. The strata is maintaining its prevailing conditionally unstable temperature profile at 0100 UTC. The decrease in the dewpoint

values between 500 and 700 hPa levels, from 1200 to 0100 UTC, indicate that the layer has become drier.

**b) 700 hPa to surface layer (Fig. 3.9 and 3.10)**

At 1200 UTC, the air from 700 to 900 hPa is conditionally unstable. Below 900 hPa a radiation inversion is indicated. The dewpoint depression ( $T - T_d$ ) values within this layer indicate that air is mainly dry, except for the air at the inversion and near the 700 hPa level. The veering of the wind with height from the surface to 700 hPa (approx. 10000 ft/3000 m AGL) at 1200 UTC (Fig. 3.10) indicates the presence of warm air advection within the lower levels.

At 0100 UTC the conditionally unstable layer is maintained between 700 to 880 hPa. From 880 to 900 hPa, however, a capping inversion forms and the layer below 900 hPa becomes conditionally unstable. The dewpoint depressions, from 1200 to 0100 UTC, indicate that the moisture has increased from 700 hPa to the surface. A comparison of the soundings for 1200, 1700 and 0100 UTC shows that the moisture has increased largely from 1700 to 0100 UTC. The most significant rise in dewpoint appears to be near 850 hPa. The warm air advection and the rate of increase in dewpoint at this level, from 1200 to 0100 UTC, is  $0.5^\circ$  and  $0.8^\circ \text{ Ch}^{-1}$  respectively. The formation of the capping inversion and the increase in moisture at lower levels indicates the presence of a surface warm front. The significant increase of moisture below 700 hPa is caused by advection and lifting of moist surface air. Another source of moisture, in addition to advection, over the prairies could be the evapotranspiration from agricultural areas (Radditz, 1998).

A change in wet bulb potential temperature with height within a layer determines the potential stability of the air (Rogers and Yau, 1989, p.34). If the change is negative (i.e.  $\partial\theta_w/\partial z < 0$ ), that layer is “potentially unstable”. Such a layer may become absolutely



unstable once lifted to saturation. At 0100 UTC, the layer between 880 to 730 hPa is potentially unstable (Fig. 3.9).

The wind profiles obtained from the Shilo sounding (Fig. 3.10), indicate that the wind speed has increased to 30 knots ( $55.6 \text{ kmh}^{-1}$ ) near 1700 m AGL (approx. 850 hPa) by 0100 UTC. At 1200 UTC the wind direction at this level is  $230^\circ$ . By 0100 UTC the wind direction becomes  $195^\circ$ . The increase in wind speed and change in direction is consistent with the strengthening southerly flow (low level jet) at 850 hPa discussed in the previous section. Fig. 3.10 illustrates that the low level jet has increased the environmental wind shear at lower levels by 0100 UTC, and winds are veering with height.

### **3.2.3 The pre-storm atmospheric conditions of the Winnipeg hailstorm**

From our discussion above, we conclude that the air over southern Manitoba had the following conditions just prior to the hailstorm:

- 1) presence of capping inversion near 880 hPa,
- 2) potential instability between 880 to 730 hPa,
- 3) build up of moisture at and below the cap,
- 4) presence of a low level jet near 850 hPa over southern Manitoba,
- 5) warm air advection over southern Manitoba at 700 hPa and 850 hPa,
- 6) no apparent relative vorticity maximum and minimum affected southern Manitoba at 500 hPa,
- 7) no jet core influenced southern Manitoba at 250 hPa.

### 3.2.4 Convective Available Potential Energy (CAPE) for the Winnipeg hailstorm

In order to estimate the CAPE, a complete temperature profile of the Shilo sounding from the surface to the top of the atmosphere is required. The soundings obtained at 1700 and 0100 UTC were from the surface to 400 hPa only. To construct a complete sounding, the 1200 UTC measurements above 400 hPa are attached to the 0100 UTC sounding. The modified Shilo 0100 UTC temperature profile is shown in Fig. 3.11. The Convective Available potential Energy (CAPE) is given by;

$$CAPE = R \int_{P_{LFC}}^{P_e} [T(P) - T_a(P)] d \ln P \quad (3.1)$$

where,

$T(P)$  = temperature of the lifted parcel at pressure  $P$

$T_a(P)$  = is the ambient ( or environmental) temperature at pressure  $P$

$R = 287 \text{ m}^2 \text{ s}^{-2} \text{ K}^{-1}$  is the gas constant for dry air

The integration is done from the pressure of the Level of Free Convection ( $P_{LFC}$ ) to the equilibrium level ( $P_e$ ). In our case,  $P_{LFC} = 850 \text{ hPa}$  and  $P_e = 180 \text{ hPa}$  (12.3 km AGL). Using (3.1), we estimate  $CAPE = 4220 \text{ J kg}^{-1}$ . This is much higher than typical  $CAPE = 500 - 2000 \text{ J kg}^{-1}$  for airmass thunderstorms.

An estimation of the maximum vertical motion ( $W_{\max}$ ) in the storm can be obtained with the assumption that the CAPE is converted into the kinetic energy of the vertical motion. As an upper bound on  $W_{\max}$ , we assume that

$$\frac{1}{2} (W_{\max})^2 = \text{CAPE}$$

or

$$W_{\max} = (2 \text{ CAPE})^{1/2} \quad (3.2)$$

For  $\text{CAPE} = 4220 \text{ m}^2 \text{ s}^{-2}$ , we estimate  $W_{\max} = 92 \text{ ms}^{-1}$ . This is supposedly the vertical motion with which an adiabatic air parcel reach the equilibrium pressure level. However, this estimate does not account for (1) loading of condensed water in the parcel; (2) non-hydrostatic perturbation pressure gradient forces that tend to reduce the upward buoyancy by about 33%; and (3) the mixing of air into the lifted parcel that tends to dilute the upward buoyancy by friction. It is not easy to account for these effects that all counter act the thermal buoyancy. Usually, a fast estimate of the peak storm updraft is obtained by taking half of the adiabatic  $W_{\max}$  value (e.g. Weisman and Klemp, 1986). For the Winnipeg hailstorm this would yield a peak storm updraft of about  $46 \text{ ms}^{-1}$ . Allowing for the overshooting above equilibrium level, the storm top is estimated to reach 16.6 km AGL (see page 287 in Djuric, 1994). The mean shear from the Lifted Condensation Level ( $\text{LCL} = 1.3 \text{ km AGL}$ ) to the storm top (16.6 km AGL) had a value of  $12 \text{ ms}^{-1}/(15.3 \text{ km}) = 0.78 \text{ ms}^{-1}\text{km}^{-1}$ . The shear direction is  $280^\circ$ .

### **3.3 Triggering of the Winnipeg hailstorm**

In the previous section it was determined that the air over southern Manitoba became potentially unstable at lower levels prior to the hailstorm development.

Once the capping inversion is broken, the CAPE will be released resulting in severe convection. To break the inversion cap, a trigger is needed with sufficient lifting for air to reach the level of free convection. We will now focus on the possible triggering of the Winnipeg storm.

The storm started to form west of Winnipeg at approximately 0030 UTC 17 July 1996 (Fig. 3.1), 30 minutes prior to the storm's initiation, the highest recorded temperature and dewpoint values at the surface were 26° C and 20° C west of the city. Based on the 0100 UTC sounding (Fig. 3.11), the surface temperature had to have exceeded 35° C for a parcel to be lifted from the surface to the LFC for the measured dewpoint temperature of 20° C. The highest recorded temperature on that day, in the vicinity of the hailstorm's development, was 29° C. This indicates that the surface heating clearly was not sufficient to raise a parcel from the surface to LFC. Evidently, other lifting mechanisms (besides surface heating) must have been present to initiate the hailstorm.

For southern Manitoba in vicinity of Winnipeg, orographic effects are minimal for storm triggering, since the topography is flat. However, triggering mechanisms can arise from surface convergence and outflow boundaries. Areas of surface convergence and outflow boundaries were impossible to detect due to sparse surface observations. Some assessment, however, is possible from analysing the data of the Vivian radar.

Prior to the triggering of the hailstorm, two clusters of pre-existing precipitation cells were monitored on the Vivian radar over southern Manitoba (Fig. 3.12). The clusters were moving in a west-southwesterly direction, consistent with the 700 hPa level flow (Fig. 3.5). These pre-existing showers had likely developed from an upper level lift in the conditionally unstable layer between 700 and 500 hPa. Later, at a location to the south of the cluster, the capping inversion was broken and the Winnipeg hailstorm was formed.

The location of the two clusters of pre-existing showers, at 5 minutes prior to the hailstorm's initiation, is shown in Fig. 3.12. Some relatively weaker reflectivity echoes are apparent to the south of these clusters. These echoes may have formed from the outflow convergence originating from the pre-existing showers. The approximate region of outflow convergence is illustrated by two cold fronts. As discussed in the previous section, a low level jet from the south was influencing southern Manitoba near the time of hailstorm's initiation. The continuous feed of warm moist air by the jet was raising the wet bulb temperatures ( $T_w$ ) of the air parcels at and below the capping inversion as seen in Fig. 3.9. With a sufficient lifting mechanism of air at lower levels, a parcel with the highest wet bulb potential temperature,  $\theta_w$ , is raised to LFC. The triggering of the hailstorm was caused by the convergence of the approaching low level jet and the outflow from the pre-existing showers. The convergence produced the necessary lift to raise the parcel with the highest  $\theta_w$  to the Level of Free Convection (LFC) (see Fig. 3.11).

The effects of the collective convergence (Fig. 3.13) are evident from the hatched area just to the west of the city (Fig. 3.14). The analysis will be conducted by considering the presence of more intense echoes at higher elevations as a sign of intensification of a convection. At 0025 UTC weak echoes are seen at levels 1.5, 3, 5 km (Fig. 3.14a,d and g) with no reflectivity at 7 km (Fig. 3.15j). By 0030 UTC more intense echoes appear at levels 1.5, 3, 5 km (Fig. 3.14 b,e and h) and the first reflectivity appears at 7 km (Fig. 3.14k). At 0035 UTC this reflectivity weakens, but a new and more intense reflectivity appears to the southwest (Fig. 3.14l). The collapse of the first echo may have contributed to the new growth. The echoes at levels 1.5, 3 and 5 km shown in Fig. 3.15c,f and i are much stronger than in Fig. 3.14b,e and h. As will be discussed in the next section, the convection grew rapidly from this stage to produce a severe hailstorm.

We conclude that the outflow convergence from the pre-existing showers is the most likely triggering mechanism of the Winnipeg hailstorm. This storm was initiated between 0025 and 0035 UTC.

### **3.4 Developing stage of the hailstorm**

Fig. 3.15 shows CAPPIs at 10 minute intervals from 0035 to 0105 UTC. A rapid increase of echoes with time is evident. At 0055 UTC, a peak echo value of 52 dBZ is detected and the reflectivity gradient has increased on the southwest flank of the storm (peak value of 42 dBZ). By 0105 UTC the reflectivity gradient has risen further (peak value of 52 dBZ) and displays the strongest reflectivity within the entire hailstorm's structure at 1.5 km. It appears that a new cell is generated on the southwest flank of the storm by 0055 UTC and the cell becomes organised and intensified by 0105 UTC.

The evolution of the hailstorm structure from 0050 to 0105 UTC at (5 minute intervals) is shown in Fig. 3.16. There are 3 cells on the 7 km CAPPI at 0050 UTC (Fig. 3.16d). The structure of cell 1 and 2 are tracked to lower levels at 0050 UTC (Fig. 3.16a to d). Since there is no evidence for cell 3 at 1.5, 3 and 5 km CAPPIs, suggesting that it has formed at 0050 UTC. Between 0055 and 0100 UTC, cell 3 intensifies and appears at lower levels (Fig. 3.16e to l). At 0105 UTC cell 3 shows intense reflectivity values at all CAPPI levels (Fig. 3.16m to p).

Fig. 3.17 shows the rapid growth of the hailstorm from 0035 to 0105 UTC. From 0105 to 0155 UTC the echo tops remained steady. The rise in cloud tops is consistent with the rapid increase of echoes displayed at the 1.5 km CAPPIs (Fig. 3.15a to d). Therefore, the period from 0035 to 0105 UTC will be referred as the “developing stage” of the hailstorm (Fig. 3.2). The rate of ascent of the radar echo tops ( $W_{top}$ ) can be estimated from  $W_{top} = \Delta H / \Delta t$ , where  $\Delta H$  is the change in echo top heights during the

time interval  $\Delta t$ . For the 30 minutes time interval from 0035 to 0105 UTC the ascent rate of echo top is about  $4 \text{ ms}^{-1}$ .

### **3.4.1 The influence of the low level jet**

In this subsection the role of the low level jet on the development of the hailstorm is examined by comparing the velocity of the hailstorm relative to the low level jet at different times. The track of the most intense echoes on the southwest flank of the hailstorm, on the 1.5 km CAPPIs, and the orientation of the low level jet are displayed in Fig. 3.18. The echoes veer from 0045 to 0105 UTC. However, from 0105 to 0205 UTC the storm maintains a steady northwesterly track. By considering the southerly flow of the low level jet, it appears that the hailstorm developed a component of its motion towards the jet flow at 0045 UTC. From 0105 to 0205 UTC, the storm became organised and maintained a steady velocity with a component upwind of the jet. This suggests that the low level jet played a role in the development of the hailstorm.

#### **a) Structural evolution of the hailstorm**

A new cell (labelled cell 3) developed on the southwest flank of the hailstorm at 0050 UTC (Fig. 3.19a). This cell developed to the southwest of an existing cell 2. A vertical cross section at 0050 UTC, through the southwest flank of the storm, is shown in Fig. 3.19b. A peak echo of 45 to 54 dBZ at approximately 7 km AGL is formed on the southwest flank. This peak reflectivity shows cell 3. The column of reflectivity maximum immediately to its right shows cell 2. The orientation of the peak echo aloft on the southwest flank and the southerly direction of the low level jet reveal that cell 3 was probably formed from the air carried by the jet. This cell may have formed when the cool

outflow of the older cells in its vicinity had encountered the approaching warm humid air from the jet. Within the next 15 minutes, as this cell intensified and became well organised, its representative echoes at 1.5 km CAPPI moved to the south (Fig. 3.16e,i and m).

The hailstorm's mean velocity at the developing stage is estimated from the displacement of the maximum echo from 0035 to 0055 UTC (Fig. 3.18) to be at a speed of 15.7 knots from 280°. The steady path from 0105 to 0205 UTC (18.6 knots from 300°) is associated with the "maturing stage" of the hailstorm. This stage of the storm will be discussed in more details in the following section. A composite depiction of the mean environmental wind, the low level jet, the storm's mean velocity at the developing stage and the maturing stage are shown in Fig. 3.20. The maturing storm veers to the right of the mean environmental wind with a steady component of its velocity upwind of the low level jet.

### **3.5 Maturing stage of the hailstorm**

In this section the characteristics of the maturing stage of the Winnipeg hailstorm, as identified on radar, will be determined. Based on these characteristics and the storm's relative environmental wind the probable flow pattern within its structure will be evaluated. The influence of the low level jet on the maintenance and motion of the maturing stage of the hailstorm will also be examined.



### **3.5.1 Radar characteristics of the hailstorm at its maturing stage**

The Winnipeg hailstorm had formed a high reflectivity gradient on the southwest flank of its structure during the developing stage (Fig. 3.15). At 0115 UTC the reflectivity gradient increased further (peak echo of 57dBz) and formed into a “hook echo” (Fig. 3.21a). A hook echo has been associated with small scale circulation and is typically accompanied by tornadoes or funnel clouds (Doswell, 1985, p.68). Fig. 3.22 indicates that a funnel cloud is indeed associated with the hailstorm. An area of maximum reflectivity is also detected a few kilometers to the northeast of the hook. Fig. 3.21a to f shows that the hook echo and the associated maximum echo to the northeast moves collectively to the southeast from 0105 to 0205 UTC. This indicates that they are part of an organised cellular structure.

The echo tops on the southwest flank of the storm are at their peak values between 0105 and 0155 UTC, and decline by 0205 UTC (seen Fig. 3.17). The peak echo tops are consistent with the persisting high reflectivity gradient (hook echo) on the southwest flank of the hailstorm, as seen in Fig. 3.21a to f. Therefore, the period between 0105 to 0205 UTC is considered the hailstorm’s most intense stage and will be referred to as the “maturing stage”.

Fig. 3.23 shows a series of selected Vivian radar CAPPIs at 0120 UTC to illustrate the major features of this mature storm’s structure. They are as follows:

- 1) Radar reflectivity maximum - This feature is most obvious in 5 and 7 km CAPPIs (Fig. 3.23c and d) with values of 52 and 60 dBZ respectively, and it can be traced to lower levels. It is indicative of heavy precipitation (hail and/or heavy rain) extending through the depth of the storm. The vertical cross sections taken (Fig. 3.24b and c) along xx’ and yy’ shown in Fig. 3.24a, shows

a column of reflectivity between 45 and 54 dBZ that extends from approximately 10 km to the surface. Some areas of more intense echoes (55 - 64 dBZ) are also illustrated at higher and lower levels.

- 2) Overhang - An overhang is associated with the maximum echo (Fig. 3.23c and d) which extends downwind from the maximum radar echo at lower levels (Fig. 3.23a and b). The vertical cross sections through the southwest flank (xx') and along the motion (yy') of the hailstorm (Fig. 3.24b and c respectively) illustrate the extent of the overhang. The overhang is an indication of a strong updraft. The rising air within the updraft is cooled and forms precipitation large enough to be detected by the radar at higher elevations. The precipitation within the overhang is maintained aloft as long as its downward weight is equal to or lower than the upward buoyancy force.
- 3) Bounded Weak Echo Region (BWER) - Figure 3.23d shows an area of weak echoes surrounded by stronger reflectivities. This BWER also shows up in the vertical cross sections shown in Fig. 3.24. The BWER has been postulated to be a sign of a strong rotating updraft. Such a strong updraft does not allow precipitation to form fast enough for it to develop a radar detectable echo until the parcels have ascended to relatively great heights (Doswell, 1985). Hence, the core updraft is within the BWER.

### **3.5.2 The structural flow pattern of the hailstorm at its maturing stage**

Fig. 3.25 is a wind hodograph showing the environmental winds relative to the storm. This figure is based on the original wind sounding and a storm velocity of  $300^\circ$  at  $9.6 \text{ ms}^{-1}$  (18.6 knots). From this hodograph, it is apparent that the environmental wind

relative to the storm is not in the plane of the storm motion at all levels, but it diverts at different levels.

Using the storm relative environmental wind, the three dimensional storm reflectivity structure and the major features of the hailstorm identified above, the air flow pattern of the hailstorm is estimated at 0120 UTC.

#### **a) Orientation of the updraft axis relative to the hailstorm's structure**

Fig. 3.26 shows the main area of updraft (solid black lines) and its axis (short hatched line pointing up). The updraft originates from below the overhang and its axis traverses through the BWER. The cloud base was reported as 1 km AGL at the hailstorm maturing stage. The flow in the plane of the storm motion illustrated in Fig. 3.26a shows that there is a wind component directed towards the storm in the lowest 1.5 km AGL. Thus, the schematic airflow shown in Fig. 3.26a indicates inflow air entering the storm from the downwind side. The relative environmental wind in the direction of the storm between 1.5 to 5 km AGL increases from 0 to  $18.5 \text{ ms}^{-1}$  (Fig. 3.26a). The orientation of the BWER (Fig. 3.26a) suggest that the relative environmental wind seems to have little effect on the axis of the updraft at lower levels on this plane. Hence, from below the cloud base to 5 km AGL the updraft axis remains almost vertical. The relative environmental winds above 5 km AGL show an increase from  $18.5$  to  $38.5 \text{ ms}^{-1}$  between 5 to 12 km. This cross wind may have tilted the updraft to the right (Fig. 3.26a) at higher levels. At 15 km AGL the updraft exits the storm and joins the environmental wind. With the same reasoning used above, the orientation of the updraft in Fig. 3.26b is identified. This cross section is through the strongest echoes along the southwest flank of the hailstorm. In this plane there is a relatively strong wind ( $15 \text{ ms}^{-1}$ ) at lower levels, and it is directed into the core of the storm. This is where the low level jet is injecting the warm humid air into the storm updraft.

### **b) Orientation of the downdraft**

The outflow downdraft occurs at the downwind side of the storm (e.g. Reuter and Yau, 1987). In Fig. 3.26a and b, the main regions of downdraft are expected to be to the left and to the right of the main updraft respectively (short hatched lines pointing down). As discussed above, the column of higher reflectivity echo is representative of a shaft of intense rain and/or hail. For illustrative purposes, the cool air associated with the outflow downdraft has been separated from the updraft by a cold front. The cool air is due evaporative cooling of the precipitation. There is a cluster of echoes to the right of the main downdraft ( Fig. 3.26b) suggesting areas of relatively weaker updraft and downdraft within the hailstorm complex.

### **3.5.2 Propagation of the hailstorm during its most intense period**

A sequence of cross sections at 5 minute intervals through the southwest flank of the hailstorm is shown in Fig. 3.27. These cross sections were taken through the most intense echoes. As a result, their orientation through the southwest flank of the storm are changing slightly. The main updraft/downdraft couplets are separated by a cool outflow boundary. The depicted downdraft also shows a column of intense reflectivity approaching the lower levels. This is indicated by cell 1 in Fig. 3.27a. Five minutes later, the spatial concentration of the echoes in the overhang reduces and the column of the high reflectivity descends to lower levels (Fig. 3.27b). At 0115 UTC, the intensity of the precipitation rate increases near the ground, which is likely associated with the cool outflow at lower levels. At 0120 UTC (Fig. 3.27c) the echoes within the overhang increase and start to subside. The lowering of the precipitation within the overhang seems to have diminished the inflow of the warm humid air that previously fed the core of the updraft in cell 1. A new updraft cell 2 appears just to the left of the collapsing overhang. The newly formed echoes are in the range of 45 to 54 dBZ between 5 to 10 km AGL,

which signifies the presence of another strong updraft (Fig. 3.27c). By 0125 UTC (Fig. 3.27d) cell 1 collapses while cell 2 grows stronger. From Fig. 3.27d ,e and f, cell 2 appears to have gone through a similar growth and decay cycle as cell 1 and a new updraft emerges (cell 3).

The evolution of cells indicates that a new cell is formed on the southwest flank of the storm at approximately every 10 to 15 minutes while the old cells are decaying. These new cells were most likely formed from the convergence of the cool outflow from the decaying cells and the approaching warm and moist air from the low level jet. The net effect was a steady movement of the hailstorm to the southeast at its maturing stage (Fig. 3.18).

### **3.6 Dissipating stage of the hailstorm**

During the developing stage (0035 to 0105 UTC) of the Winnipeg hailstorm, the reflectivity gradient on the southwest flank of the storm shown by 1.5 km CAPPIs in Fig. 3.15a to d), increased rapidly. At the maturing stage (0105 to 0205 UTC), with further intensification of echoes in the southwest flank, the storm became organised and formed a “hook echo” (Fig. 3.21). The hailstorm had now veered to the right of the mean environmental wind, and with a persisting hook echo it continued to move to the southeast. By 0215 UTC (Fig. 3.28), however, the hook echo disappeared and the whole reflectivity of the storm become disorganised. Fig. 3.28a and b illustrates a weakening trend of the echoes along with an overall easterly motion. A complete track of the peak reflectivity on the southwest flank of the hailstorm, from the developing to dissipating stage, is shown in Fig. 3.18.

### **3.7 Hail analysis of the Winnipeg hailstorm**

In this section, the observed hail fall will be presented. Then, Lemon's (1977) minimum radar criteria for evaluation of severe hailstorms (hailstones diameter  $\geq 20$  mm) will be applied to the Winnipeg hailstorm. The possible echo intensity of large hailstones are compared to reports of large hailstones at the surface.

#### **3.7.1 Surface hail fall reports**

Fig. 3.29 shows the locations of hailstones reported by Environment Canada's volunteer weather observers. The hailstones' corresponding sizes and the reported damages are summarised in Table 1. The majority of hailstones fell on the southwestern section of the City of Winnipeg. The Manitoba Public Insurance Corporation has estimated incurred damages of \$51.2 million to public automobiles. The Insurance Bureau of Canada has estimated incurred damages of \$60 million to private and commercial buildings, as the result of the Winnipeg hailstorm. In total the damage to public property is estimated to be near \$111.2 million.

Below are selected quotes taken from the newspaper Winnipeg Free Press issue dated 17 July 1996, describing the events and incurred damages in the southwestern sections of Winnipeg. The entire article can be found in appendix 1.

"Although the entire city was hit by thundershowers and winds up to 100 kilometres per hour, the hail cut a swath southeast from Headingley, through St. James, Charleswood and Waverly Heights before moving through south St. Vital."

"Golf ball-sized pits were left in the metal of cars."

"The hail was so strong we know it took out some car windshields in Charleswood,"

“Kevin Houd, an assistant pro at the Charleswood Golf Club, said he braved the golf ball-sized hail to protect equipment on the course. “I got hit a few times, but I’m OK,” he said. “For a while there it looked like snow out there on the course. It was white covered over the course. It took 20 minutes to melt.”

“Meteorologists said hail was ankle deep in some parts of Winnipeg. Home owners were amazed at the force of the hail. “I really thought the hail was going to break the windows,” Island Lakes resident Debra Preece said. “It just sounded like rocks hitting the window.” Gary Johnson of Haney Street in Charleswood said he saw hail half the size of a baseball outside”.

“Keith Hoas said “the hail sounded like bombs hitting the side of the building” at his South Park Drive apartment. “the ice was hitting and just exploding,” said Hoas, ....“When you have 2 inch hail, some holes in the screen you can stick your pinkie right through”. He was outside surveying the damage after the storm. “I’ve got some chrome damage and 20 or 30 nice dimples in my roof,” he said of the assault on his 1984 Dodge Ram pickup truck. “Some people with fiberglass bodies had holes in them.”

### **3.7.2 Detection of hail using radar**

Lemon (1977) established minimum radar criteria for detecting hailstones with diameters greater than 20 mm. His criteria were based on 10 years of S-band radar and hailfall observations. His criteria are:

- 1) Peak mid-level (5 to 12 km AGL) reflectivity must be  $\geq 45$  dBZ.

- 2) Mid to high level overhang must extend at least 6 km beyond the strongest reflectivity gradient of the low-level ( $\leq 1.5$  km AGL) echo. The strongest reflectivity gradient usually occurs at the outer edge of the radar echo.
- 3) The highest echo top must be located on the storm flank that possesses the overhang and must lie above the low-level reflectivity gradient between the echo core and the echo edge or lie above the overhang

The minimum criteria developed by Lemon will be used to examine the Winnipeg hailstorm at its maturing stage. Then the track of peak echoes obtained from 7 km CAPPIs, during the maturing stage, will be compared to the surface hails swath.

The cross sections in Fig. 3.24b and c show echoes of 45 dBZ or more within the overhang at heights of 5 km or higher. The overhang (at mid-levels) is at least 6 km beyond the highest peak echoes near the surface, and the echo top lies above the overhang. The sequence of cross sections taken at 5 minutes intervals, from 0110 to 0135 UTC, through the southwest flank of the storm (Fig. 3.27a to f), indicate that the criteria of Lemon were satisfied throughout the 25 minutes, indicative for hail with diameters of 20 mm or larger.

#### **a) Comparison of peak radar echoes at 7 km AGL to actual hailstone observations**

Figure 3.30 shows the time sequence of the 45 dBZ echo at 7 km (red boundary) and maximum reflectivity at 1.5 km (blue dot) on the southwest flank, at 5 minute intervals. As the 45 dBZ threshold boundary moves to the southeast along with the 1.5 km peak echo, it fluctuates in size. These fluctuations appears to peak every 10 to 15 minutes from 0105 to 0145 UTC (Table 2). During the maturing stage of the hailstorm, the spatial concentration of the echoes in the overhang were periodically reducing and the



column of the high reflectivity were descending to lower levels (Fig. 3.27a to f). Since the echoes at 7 km AGL lie within the overhang, the variations in spatial concentration of echoes would also be apparent at this level. The peak areas of 45 dBZ shown at 0120 and 0130 UTC (Fig. 3.30 and Table 2) coincide with the descent of peak echoes identified from the corresponding cross sections (Fig. 3.27c and e). Therefore, it appears that the peak spatial concentration of echoes detected at 7 km CAPPI represent hailstones that are formed at and above this level.

The largest width of 45 dBZ at 7 km perpendicular to the storm's motion (Fig. 3.30), is overlaid on the hailstone reports for the period 0105 to 0145 UTC (Fig. 3.31). The majority of the available reported hailstones lie directly below the area covered by the 45 dBZ path. This indicates that the quasi-periodic descent of the overhang consisted of falling hailstones. The swath of hailstones having diameters of 40 mm or more lies within approximately 2 km from the track of the maximum echoes along the largest width of 45 dBZ. From the track of maximum echoes (Fig. 3.31), it is likely that the radar reflectivity values of above or equal to 52 dBZ at 7 km AGL represent hailstone with diameters of 40 mm or more.

### **3.8 Summary of events**

Earlier on 16 July 1996 two clusters of showers had developed from an upper level lift of conditionally unstable air within mid-levels. These pre-existing showers moved with the 700 hPa flow. A southerly jet at 850 hPa advected warm and humid air and increased the low level windshear. The most significant rise in moisture had occurred during the afternoon of that day (1700 to 0100 UTC). The moisture increase could have been due to evapotranspiration in addition to advection. Within 30 minutes prior to the hailstorm's development a capping inversion had formed near 880 hPa (1.3 km AGL) and the air between 880 and 730 hPa had become potentially unstable.

Based on our analysis, it appears that the crossing of the low level jet and the outflow convergence from the pre-existing showers had triggered the convection. They produced sufficient lift to raise a parcel from 880 hPa to LFC, breaking the capping inversion. The CAPE from this level were estimated to be  $4220 \text{ Jkg}^{-1}$ . This CAPE could produce a strong updraft of about  $45 \text{ ms}^{-1}$ . The convection grew rapidly, attained echo tops of 14 km AGL and formed into a severe hailstorm within 30 minutes. The maturing stage of the hailstorm lasted approximately 60 minutes, during of which the storm passed across southwestern sections of Winnipeg. Hailstones of 70 mm in diameter were observed. The damage was estimated to be \$111.2 million.

At the developing stage, the 1.5 km radar CAPPIs show that the storm intensified upwind of the low level jet. Our three dimensional radar analysis suggests that the warm humid air from the low level jet fed the storm. With further intensification, at the maturing stage, a hook echo appeared on the southwest flank. The hailstorm now became organised, with a persisting hook echo. It veered to the right of the mean environmental wind, with a component towards the low level jet. Cross sectional analysis through the southwestern flank of the storm indicated that a new cell formed roughly every 10 to 15 minutes. At this stage the storm moved to the southeast at  $9.6 \text{ ms}^{-1}$  as the low level jet generated new updrafts on its southwest flank. After 90 minutes from its initiation the echoes on the southwest flank dissipated.

The analysis of the hailstorm's structural characteristics and air flow pattern, at the maturing stage, revealed that the warm humid air from the low level jet entered the storm's updraft at lower levels (below 1.5 km AGL) from below the overhang. Then the strong updraft, with its axis through the BWER, carried the air to higher levels. Some precipitation were carried by the downdraft to lower levels on the downwind side of the air flow. Precipitation also formed the classical overhang above the updraft region. The

precipitation echoes in the overhang were periodically reducing and the column of high reflectivity descended to lower levels. The swath of hailstones with diameter  $\geq 40$  mm were within 2 km of the track of peak reflectivity at 7 km (within the overhang), along the direction of the hailstorm. The radar reflectivity values of 52 dBZ at 7 km probably were reflected from hailstones with diameters of 40 mm or more.

## **4. Comparison of Winnipeg hailstorm with conceptual models**

### **4.1 Overview**

In this chapter we compare the evolution of the Winnipeg hailstorm with conceptual models of severe hailstorms proposed by Fawbush, Miller, and Starrell (1951) and Smith and Yau (1993). These conceptual models postulate typical conditions of the pre-storm synoptic air flow. Further, the radar characteristics of the Winnipeg hailstorm will be compared to the conceptual models of severe hailstorm supercells proposed by Chisholm and Renick (1972) and Lemon (1980). These conceptual models deal particularly with long-lasting supercell storms in mid-latitudes. Our main objectives are:

- 1) To determine how the pre-storm synoptic scale atmospheric conditions of the Winnipeg hailstorm compare to those described by the conceptual models.
- 2) To determine how the Winnipeg hailstorm's precipitation structure compare to those described by the conceptual models.

### **4.2 Fawbush, Miller, and Starrell's conceptual model**

Fawbush, Miller, and Starrell (1951) offer the “classical” conceptual model of the environment that is favourable for the formation of severe convective storm (with possible tornadic outbreak). Fig. 4.1a shows the proposed orientation of a cyclone, a low level jet and a polar jet that combine to develop vigorous severe storm. The relevance of cyclone, low level jet and upper level jet are briefly discussed (see e.g. Barnes and Newton, 1986).

- 1) Cyclone: In mid latitudes, cyclones evolve downstream from the wave trough in the upper tropospheric polar jet stream (PJ) associated with the zone of temperature contrast between the large scale cold and warm air masses. The vorticity advection and warm air advection associated with cyclogenesis generate synoptic scale lifting.
- 2) Low Level Jet (LLJ): The low level jet advects the warm and humid air into the warm sector of the cyclone. This process increases the low-level wet bulb potential temperature ( $\theta_w$ ) of the airmass. An increase of  $\theta_w$  causes an increase in the amount of potential instability of the air mass.
- 3) Upper level Polar Jet (PJ): The region to the east of the trough in the polar jet is characterised by horizontal wind divergence, which implies lifting. This rising air motion contributes to the cooling in upper levels and therefore increases thermal instability. The ascending air east of the upper trough also increases the depth of the moist layer and therefore the amount of water vapour available for condensation. In some cases it lifts the air to saturation and actually initiate the convection.
- 4) Subtropical Jet (SJ): The subtropical jet stream is marked by strong vertical shear in the high troposphere. This parameter is usually present at a slightly higher elevation than the PJ. The subtropical jet is not always present, but if it is, upper level divergence is enhanced and squall lines between the two upper level jets become particularly intense.

The location “x”, as shown Fig. 4.1a, is favoured for the initiation of a severe convective outbreak. At this location the rapid advection of warm humid air by the low level jet and the upper level divergence combine to cause the most pronounced vertical

motion near the polar jet. This provides the maximum thermodynamic and dynamic support for deep convection.

Miller (1972) identified that there are 14 synoptic scale parameters that play a major role in production of severe thunderstorms (based on the atmospheric analysis of 328 cases of severe outbreaks). Table 3 lists the 14 parameters. Miller qualifies the parameters as weak, moderate and strong. The “classical” conceptual model of severe storm are usually associated with strong cyclones (surface pressure of  $\leq 1005\text{hPa}$  over the threat area), strong Low Level Jets (LLJ) at 850 hPa ( $\geq 35$  knots), and strong polar jet (PJ) at 250 hPa ( $\geq 85$  knots).

John and Doswell (1992) indicate that the “classical” conceptual model produces a “loaded gun” thermodynamic sounding, as shown in Fig. 4.2a. It also has strong veering winds with height. This profile allows the build up of moisture below the capping inversion. Once the capping inversion is broken the explosive release of the latent energy, set free during the condensation, produces a deep convection. This convection usually manifests itself as a supercell storm when a strong low-level veering occurs. A supercell is usually associated with large hailstones, heavy rainshowers, strong winds, intense lightning and some times tornadoes.

The “classical” conceptual model provides the following overall atmospheric characteristics over the regions where the potential for a severe thunderstorm form (e.g. Cotton, 1989 p524):

- 1) Warm humid air advection by the strong low level jet.
- 2) A deep layer of conditionally unstable air.
- 3) A strong capping inversion, as the result of a “loaded gun” profile, which inhibits the widespread outbreak of storms.

- 4) Moderate to strong vertical wind shear with winds veering with height.
- 5) A triggering mechanism to break the capping inversion.

The major triggering mechanisms are frontal lifting, surface heating, drylines, gravity waves, and lifting due to terrain effects.

#### **4.2.1 The “classical” conceptual model compared with the pre-storm atmosphere of the Winnipeg storm**

Fig. 4.1b shows the orientation of the warm front, the 850 hPa Low Level Jet (LLJ), and the 250 hPa Polar Jet (PJ) over Manitoba at 0000 UTC 17 July 1996, just prior to the hailstorm’s formation. The strength of the 850 hPa jet maximum (25 knots), 250 hPa jet maximum (69 knots) and the surface pressure (1006 hPa) in the pre-storm environment are all categorised as moderate (Table 3). These synoptic features are compared against those in the “classical” conceptual (see Fig. 4.1a).

A comparison of the synoptic parameters shown in Fig. 4.1a and b indicate that the location of the warm front relative to the low level jet is similar in both cases. The Polar Jet’s strength and orientation relative to the low level jet, however, differ somewhat from those of the “classical” conceptual model. In the Winnipeg case, the arcing of the polar jet signified the existence of an upper level ridge over Manitoba. This implied the presence of subsiding air at high levels. Our synoptic scale analysis, within 12 hours prior to the hailstorm’s development, showed that there was warming at low to mid levels ( $\leq 6$  km AGL) of the troposphere. However, as the result of the low level jet, warm air advection at low levels ( $\leq 3.0$  km AGL) was at a higher rate than at mid levels (3 to 6 km AGL). This caused the formation of a deep layer of conditionally unstable air (Fig 4.2b). There was a capping inversion in the low levels and the moisture was concentrated below the cap. A comparison of Fig. 4.2a to Fig. 4.2b indicates that the profile of temperature

and dewpoint over southern Manitoba had a classical “loaded gun” sounding characteristic prior to storm formation. Since the environment of the Winnipeg hailstorm was potentially unstable, the combination of Polar Jet and low level jet destabilised the atmosphere, consistent with the conceptual model.

Fig. 4.1b shows that, unlike the classical conceptual model (Fig. 4.1a), there was a relatively weak cyclone present near the storm’s formation. Maddox and Doswell (1982) reported several severe thunderstorm outbreaks that were not associated with a strong surface cyclone. They found that the most common synoptic scale parameter for the severe outbreaks were strong warm advection. Maddox and Doswell suggested that in the absence of a strong surface cyclone warm air advection in regions of conditionally unstable air signals the presence of large scale vertical motion. This ascending air, in some cases, can trigger severe outbreaks. Otherwise, a sufficient triggering mechanism is required. Their findings are applicable to the environment in which the Winnipeg hailstorm evolved. Our analysis revealed that the Winnipeg hailstorm was initiated as the result of the convergence of the low level jet and a possible outflow boundary. The low level jet advected warm humid air over southern Manitoba. Therefore, a strong surface cyclone was not needed.

The combination of the synoptic features (Fig. 4.1b) had produced the following pre-storm condition of southern Manitoba:

- 1) stronger warm air advection at low levels ( $\leq 3.0$  km AGL) relative to higher levels,
- 2) presence of a moderate low level jet had increased the windshear at lower levels and wind was veering with height (consistent with low level warm air advection),



- 3) the presence of a capping inversion at lower levels and a build up of moisture below the cap (i.e. “loaded gun” sounding), and
- 4) a deep layer of conditionally unstable air.

These characteristics agree well with those of the “classical” conceptual model.

#### **4.2.2 Smith and Yau’s conceptual model**

Smith and Yau (1993) present a conceptual model of the environment that is favourable for the generation of severe Alberta thunderstorms. In Alberta summer severe weather outbreaks are very common. On a yearly basis over 60 hail days and between 10 and 20 tornadoes are reported in this region. A conceptual model of the synoptic situation that leads to severe thunderstorm outbreaks in central Alberta has been presented by Smith and Yau (1993b). Their work is based on 11 days of observations gathered during the 1985 Limestone Mountain EXperiment (LIMEX-85). The setup of their conceptual model occurs in two stages over the course of approximately two days. The evolution of the synoptic and mesoscale environments leading to a severe convection is summarised as follows:

- 1) Stage 1: A height and thickness ridge over Alberta causes clear skies and a strong low tropospheric capping inversion. Surface heating during the morning hours of day 1 along the foothills is sufficient to weaken the inversion significantly, or it may remove the inversion locally and initiate some convection. The morning surface heating produces early pressure falls which induce shallow upslope flow near the foothills. However, due to the upper level warming and the stratification associated with the upper level ridge, these convections remain weak. Therefore, the horizontal and vertical growth of the mountain-plain circulation caused by the thermally generated

pressure falls, evolving slowly. The net effect is that a strong upslope flow along the foothills may not commence (if it develops at all) until late in the day. As a result, the moisture required to produce deeper convection may not reach the foothills from the plains in time for the maximum surface heating.

- 2) Stage 2: In the early hours of day 2, the upper level ridge moves eastward giving way to an advancing upper trough, as shown in Fig. 4.3a. Mostly clear skies prevail over Alberta but some stratocumulus cloud may also be present. Differential surface heating along the foothills once again develops some convections along the foothills, but on this day, the strong surface heating and cooling aloft, in the presence of weaker stratification, leads to deeper convection (Fig. 4.3b). As a result, the vertical and horizontal growth of the mountain-plain circulation grows rapidly and generates mesoscale upslope transport of moisture. At the same time the synoptic pressure gradient over the plains favours the easterly component of surface winds. This aids the advection of moisture to the foothills. Therefore, the moist air is lifted to higher levels of the atmosphere by the foothills resulting in vigorous convective storms. The strong southwesterly flow ahead of the trough and the intensifying low level upslope flow provide the vertical shear required for the growing storms. The joint meso-synoptic scale interaction resulting in an upslope moisture transport was the key factor in initiating deep convection on the severe day.

The dynamic and thermodynamic processes of Smith and Yau's conceptual model produce the following features:

- 1) Advection of warm humid air from the plains to the foothills at stage 2.
- 2) Destabilization of the atmosphere as a result of surface heating and cooling aloft, leading to a deep layer of conditionally unstable air at stage 2.
- 3) Setup of a strong capping inversion at the lower levels as a result of the upper ridge at stage 1.
- 4) Generation of vertical wind shear (veering) as a result of intensifying upslope flow and the strong southwesterly flow ahead of the upper trough at stage 2 .

The triggering mechanism for the initiation of deep convection is the orographic lifting.

The Alberta storm conceptual model agrees with the "classical" conceptual model, that the pre-storm environment must exhibit the following "fundamental" characteristics:

- 1) warm air advection at low levels,
- 2) vertical windshear with winds veering with height,
- 3) a capping inversion at low levels with loaded gun characteristics,
- 4) presence of deep conditionally unstable air.

To initiate a convection, a triggering mechanism is required to break the capping inversion. Once the cap is penetrated, the warm moist air from below is released to

produce a deep convection producing a severe thunderstorm. The Winnipeg pre-storm environment had all these characteristics. In the Alberta storms the triggering usually comes from the topographic lifting over the foothills. In contrast, the Winnipeg storm was triggered from convergence of the outflow of pre-existing showers with the low level jet.

### **4.3 Chisholm and Renick's (CR) hailstorm conceptual model**

Chisholm and Renick (1972) used 6 years of storm data obtained over Alberta to compare and contrast the different characteristic features and behaviour of individual hailstorm types. They postulated three major categories of convective storms: single cell storms (airmass thunderstorms), multicell storms and supercell storms. They also proposed a conceptual model for a supercell hailstorm. This supercell model will be compared to that of the Winnipeg hailstorm. CR's supercell hailstorm conceptual model calls for a pre-storm "loaded gun" sounding profile, as shown in Fig. 4.2a.

#### **4.3.1 Maturing stage**

Chisholm and Renick propose that supercells exhibit the following characteristic radar features:

- 1) The plan view of a supercell appears as a single cellular structure which is elliptical. It has a horizontal dimension of 20 to 30 km and a depth of 12 to 15 km (Fig. 4.4 and 4.5).
- 2) A persistent Bounded Weak Echo Region (BWER) on the southwest flank of the storm. The BWER typically has a horizontal dimension of 5 to 12 km, is conical in shape and extends to a height of one-half to two-thirds of the distance through the storm's depth (Fig. 4.5). The strong updraft (20

to  $40 \text{ ms}^{-1}$ ), causing the BWER, contains small cloud droplets and prohibits the entry of hailstones into this region from above. A BWER normally tilts towards the left hand storm flank and near the top leans in a down stream direction.

- 3) The radar reflectivity maximum core is on the left hand side of the storm and borders the BWER. This results in a high reflectivity gradient between the maximum echo and the BWER. The maximum echo is composed of precipitation, with large hailstones on the side closest to the BWER. The size of the hailstones decrease with the increasing distance from the BWER.
- 4) An extensive echo plume of 60 to 150 km is observed from the radar.

The radar structure of the Winnipeg hailstorm at 0120 UTC, as shown in Fig. 3.23, retains essentially the same basic characteristics from 0110 and 0205 UTC. The horizontal dimension of the hailstorm is 20 to 40 km and its plan view is elliptical in shape. The extent of the plume is estimated, from the 7 km CAPPI (Fig. 3.23d), to be at least 35 km. The hailstorm exhibits a concave indentation of radar returns at 1.5 and 3 km CAPPIs (Fig. 3.23a and b), indicative of the air entering the storm from the southwest flank. A BWER is found directly above at 7 km radar CAPPI (Fig. 3.23d). Immediately to the north of the BWER is an extensive radar reflectivity maximum. The path of the reflectivity maximum at 7 km is compared to the swath of largest hailstones (diameter  $\geq 40 \text{ mm}$ ) in Fig. 3.31. The largest hailstones observed at the surface lie within 2 km of the path. Fig. 3.24 shows the vertical cross sections through the hailstorm at 0120 UTC, along and almost perpendicular to the direction of the storm. An area of relatively stronger reflectivities appears to cap the BWER (Fig. 3.24b). These peak echoes extend towards the earth, on the right side of the BWER. Fig. 3.24c shows that the BWER

extends at least one-half of the distance through the storm's depth, is conical in shape and has a maximum horizontal dimension of at least 5 km. The BWER delineates the path of strong updraft (Chisholm, 1970). The radar characteristics of the Winnipeg hailstorm during the maturing stage were similar to those of CR's supercell conceptual model.

#### **4.3.2 Supercell behaviour**

Chisholm and Renick add that supercells retain the same basic characteristic features over a period of half an hour to as long as several hours. During this time the storm exhibits the following characteristics:

- 1) The maximum radar storm top may show only minor fluctuations, not usually in excess of  $\pm 1$  km about the mean.
- 2) The BWER tracks in a straight line at near constant speed and without rapid changes in direction.
- 3) The storm's movement is at an angle of 0 to 40° to the right of the mean wind within the 700 to 300 hPa layer.
- 4) The radar reflectivity maximum core may fluctuate but retains the same basic configuration and relative position to the BWER.

Fig. 3.17 shows that the maximum radar echo tops of the Winnipeg hailstorm remained steady at 14 km from 0110 to 0155 UTC. A five minute time sequence of 7 km CAPPIs, from 0110 to 0135 UTC (Fig. 4.6), indicate that the BWER and radar reflectivity maximum display minor fluctuations in size and intensity. Additionally, the position of the radar reflectivity maximum remains to the north of BWER. The mean path

of the BWERs centres is presented by the line aa' in Fig. 4.7. Each centre falls within 1.5 km to the line aa'. The average speed of the BWER, from 0110 to 0135 UTC, is estimated to be  $10 \text{ ms}^{-1}$ . From 0110 to 0205 UTC (maturing stage), the storm travelled at  $20^\circ$  to the right of the mean environmental wind (Fig. 3.20). The Winnipeg hailstorm was similar to the CR's supercell conceptual model.

#### **4.3.4 CR's conceptual model environmental windshear and the pre-storm environment of the Winnipeg hailstorm**

Chisholm and Renick found that supercell storms can only occur for very specific wind profiles of the pre-storm environmental air flow. The required wind profile has a strong vertical wind shear with extreme veering in the lowest layers. Fig. 4.8a shows the typical wind hodograph of a pre-storm environment that supports supercells. The low level southerly winds veers rapidly to a strong westerly aloft. The low level southerly air, enters the storm from the right flank (Fig. 4.9a and b). The air then accelerates upwards through the BWER. Due to the initial momentum and the influence of the environmental wind, the updraft leans towards the left hand storm flank and is sheared downstream near the top. The precipitation forming in the updraft is shed to the left hand of the updraft and does not pose a major effect on its core. This enables the updraft core and the precipitation fallout zone to coexist. However, the updraft is eroded progressively from the left hand flank by the precipitation. This results in a "continuous flow" phenomena within the structure of the supercell, and produces a "continuous propagation" of the hailstorm.

The Winnipeg pre-storm hodograph and the storm motion vector are displayed in Fig. 4.8b. Similar to the CR supercell wind hodograph (Fig. 4.8a), the Winnipeg hailstorm hodograph also shows southeasterly winds at the surface with strong low level veering. According to Chisholms and Renick , "the wind component from the south in the

low levels appear to be the distinguishing mark” (p. 29). They explain that the magnitude and direction of this wind causes the separation between the strong updraft and the precipitation fall out zone. The typical motion vector of a supercell is compared to that of the Winnipeg hailstorm in Fig. 4.8a and b. The cases show close resemblance.

#### **4.3.4 Discussion**

It is concluded that the Winnipeg hailstorm, at its maturing stage, shows radar characteristics and behaviour similar to those depicted in Chisholm and Renick’s conceptual model of a supercell. Further, the Winnipeg hodograph agrees closely with the supercell hodograph proposed by Chisholm and Renick. Therefore, the Winnipeg hailstorm at its maturing stage can be categorised as a supercell hailstorm.

The cross sectional analysis of the intense echoes (centroid) through the southwest flank of the Winnipeg hailstorm, from 0110 to 0135 UTC (Fig. 3.27a to f), suggested that new updrafts (cell 2 and 3) were being generated at 10-15 minute intervals. In accordance with Chisholm and Renick’s supercell conceptual model, the updraft core and the precipitation fall out zone to its left remain and coexist throughout its life time. However, they explain that the fall of the precipitation erodes the updraft from the left, which produces a continuous propagation of the storm. Therefore, since the cross sections taken for the Winnipeg hailstorm were through the centroids, the subsiding echoes within the overhang may just have been the eroding precipitation from the left of the updraft. Further, what appeared as generations of new cells on the southwest flank of the hailstorm may just have been the re-orientation of the updraft core as the result of the storm’s propagation.



#### **4.4 Lemon's (1980) conceptual model of a supercell hailstorm**

A refined conceptual model of a supercell storm has been developed by Lemon (1980). Fig. 4.10 shows the prototype supercell storm proposed by Lemon. At the initial stage of a storm (Fig. 4.10a) the echoes are almost vertically aligned and more intense aloft. The echo top height at this stage indicates the presence of weak to moderate updraft strength. Within the next 60 minutes, new cells develop on the updraft of the storm as they generally move with the mean environmental wind. This is the behaviour of a typical multicell storm structure (Chisholm, 1973). Each developing cell becomes stronger than the previous one as its updraft intensity increases. The strengthening cells eventually have their low level reflectivity shift towards the updraft flank (Fig. 4.10b). The echo tops concurrently shift towards the same direction and lie above the strong low level reflectivity gradient. At this developing stage of storm, the mid level reflectivity increases rapidly. An overhang is formed above a weak echo region (WER). The overhang extends out from the low level reflectivities by approximately 6 to 25 km. Continued development of new and larger cells on the updraft side of the storm's complex eventually lead to a strong and dominant cell. This cell, referred to as a supercell, sustains itself for long periods. The intense updraft associated with such a cell rises almost vertically despite the effect of environmental winds, and the storm top may rise above 18 km (Fig. 4.10c). At this stage, the large mid-level reflectivity continues to overhang. A BWER is usually detected within the overhang and is capped with strong reflectivities. The storm top is situated directly above. Beneath the overhang the low level echo is characterised by a "hook echo".

At the triggering stage of the Winnipeg hailstorm (Fig. 4.11), the radar echoes appear vertically aligned (illustrated with arrows) with more intense echoes displayed at 3 and 5 km. The echo top is approximately at 7 km AGL. In the next 30 minutes the low level echoes (Fig. 3.15) intensify rapidly and elongate to the southwest by 0105 UTC.

Concurrently the echo tops increase rapidly (Fig. 3.17). A five minute time sequence of radar CAPPIs at 1.5, 3, 5 and 7 km, from 0050 to 0105 UTC, is shown in Fig. 3.16. New echoes form on the southwest flank of the storm's complex, as the older ones are moving to the east. This behaviour resembles that of a multicell storm. The newly developed cell (Cell 3 in Fig. 3.16) intensifies rapidly at all levels and forms into an organised cellular structure. A cross section through the hailstorms complex at 0100 UTC 17 July 1996 is shown in Fig. 4.12b. The echo top lies above the strong low level reflectivity gradient. Also, an overhang stretches to the south (approx. 15 km) and a WER region develops below. Within the next 15 minutes the low level echoes intensify further and form a "hook echo" on the updraft flank (Fig. 3.21a). The same structure is maintained for the next 50 minutes. The vertical cross section through the southwest flank of the storm at 0120 UTC (Fig. 4.13a) shows a large overhang (approx. 25 km) and BWER. Intense echoes cap the BWER with the storm echo top above. The echo top extends to approximately 15 km, indicating the presence of a strong updraft. The storm moves to the right of the mean environmental wind (Fig. 3.20).

The Winnipeg hailstorm's evolution compares well to Lemon's conceptual model. The Winnipeg hailstorm had multicellular behaviour at the developing stage and evolved into a supercell storm at the maturing stage. Our analysis showed that the approaching low level jet and the associated instability were the main driving mechanisms of the Winnipeg hailstorm's evolution. As the type of storm depends on the environmental instability and windshear (Weisman and Klemp, 1985), the transition from a multicell to a supercell hailstorm may have resulted from the approaching low level jet.

## **4.5 Conclusion**

In this chapter, we showed that the pre-storm environment of the Winnipeg hailstorm exhibited the same characteristics as those of the “classical” and Alberta conceptual models (Faubush et al., 1951 and Smith et al., 1993 respectively). We further showed that the conceptual models of Chisholm and Renick (1972) and Lemon (1980) offer insight in the development, structure and movement of the Winnipeg hailstorm. Consequently, we speculate that the conceptual models can be used to describe other storms in southern Manitoba, despite the fact that models were based on storms in other areas of North America.

## **5. Discussion and conclusion**

### **5.1 Summary of major findings**

This thesis provides the first case study of a hailstorm developing over southern Manitoba. The hailstorm under investigation is the 16 July 1996 event over Winnipeg. The analysis was performed using data from the Vivian weather radar, radiosonde data from Shilo, Manitoba, and synoptic charts. These data were all part of the operational observations collected by Environment Canada.

The synoptic charts and radiosonde data were used to determine the synoptic scale atmospheric conditions over southern Manitoba, prior to the initiation of the hailstorm. The radar data was used to determine the cloud scale structural characteristics and behaviour of the hailstorm from the triggering to the dissipating stages. The radiosonde data was also used for the thermodynamic assessment of the storm's environment and the storm's relative winds.

#### **a) Synoptic scale condition prior to the storm's initiation**

Based on our synoptic scale analysis, we determined that the air over southern Manitoba exhibited the following features just prior to the hailstorm formation:

- 1) a capping inversion at 880 hPa,
- 2) potentially unstable air between 880 to 730 hPa,
- 3) build up of moisture at and below the cap,
- 4) presence of a low level jet near 850 hPa with increasing windshear at low levels, and

- 5) warm air advection below 500 hPa with more rapid advection at lower levels as the result of the low level jet.

The potential instability was caused by the advection of the warm humid air by the low level jet.

**b) Triggering stage of the storm (0025 to 0035 UTC, 17 July)**

Earlier on 16 July 1998, two clusters of showers developed from an upper level lift in the conditionally unstable air within mid levels ( $\geq 3$  km AGL). Radar echoes showed that the pre-existing showers were moving with the 700 hPa flow to the east across southern Manitoba. An area of weaker echoes, at a small distance to the south of the clusters, were also displayed on radar. These echoes appeared to have formed as the result of the outflow convergence of the existing showers. At approximately 15 km west of the city of Winnipeg, Manitoba, a relatively intense echo appeared within the weak echoes at 0035 UTC. Thereafter the intensity of echoes increased rapidly and were the early representation of the Winnipeg hailstorm.

Based on our analysis, it appears that the convergence of the low level jet and the outflow from the pre-existing showers had triggered the storm. The convergence produced sufficient lift to raise a parcel from 880 hPa to LFC, breaking the capping inversion. The CAPE from this level was estimated to be  $4220 \text{ Jkg}^{-1}$ , with an estimated storm updraft of  $46 \text{ ms}^{-1}$ .

**c) Developing stage of the storm (0035 to 0105 UTC)**

The convection grew rapidly during its developing stage that lasted from 0035 to 0105 UTC. By 0105 UTC, a peak echo top of 14 km was reached on the southwest flank

of the storm. While the convective cells moved with the mean environmental wind, new cells formed to their southwest. The orientation of the new cells and the southerly direction of the low level jet suggested that the cells developed from the moist air carried by the jet and the outflow of the older cells. After 0050 UTC a new cell veered to the right of the mean environmental flow upwind of the low level jet and intensified very rapidly. By 0105 UTC this particular cell had the strongest echo (52 dBZ) within the entire hailstorm's structure at lower levels.

**d) Maturing stage of the storm (0105 to 0205 UTC)**

After 0105 UTC the low level reflectivity on the southwest flank of the storm intensified further and by 0115 UTC a "hook echo" appeared on the same flank. An area of maximum reflectivity appeared a few kilometres to the northeast of the hook. From 0115 to 0205 UTC, the hook and the associated maximum reflectivity moved to the southeast. Echo tops on the southwest flank of the storm remained steady (14 km) from 0105 to 0155 UTC, but weakened thereafter. The persisting echo tops were consistent with the high reflectivity gradients (hook echo) on the southwest flank of the storm. This indicated that the motion and behaviour of the storm at lower levels were related to the history of the highest echo top. During the maturing stage (0105 to 0205 UTC) the storm moved to the right of the mean environmental wind by 20° and passed across southwestern sections of Winnipeg. Hailstones of 70 mm in diameter were observed. The damage was estimated to be \$111.2 million.

During the maturing stage the precipitation structure of the hailstorm showed the following features on radar:

- 1) a persistent Bounded Weak Echo Region (BWER) at mid levels tracking to the southeast with minor fluctuations in size,

- 2) an area of maximum reflectivity near the BWER which maintained the same orientation with respect to the BWER, and
- 3) a persistent overhang that extended downwind from the reflectivity maximum.

When the characteristics of these features were combined with the storm's relative wind, we found that the likely inflow region of the storm was its southside. This is where the warm moist air carried by the low level jet was injected into the storm. The updraft originated from below the overhang and traversed vertically through the BWER. At higher levels the cross winds tilted the updraft to the right and at 15 km AGL the updraft joined the environmental wind. The downdraft occurred down shear side of the storm and was shown by a column of maximum reflectivity on radar. Analysis of the 5 minute interval radar cross-sections, taken through the centroid of the storm, showed that there were subsiding echoes within the overhang at every 10 to 15 minutes. These echoes seemed to reduce the inflow of the warm moist air into the updraft. During this period a newly formed echo to the left of the collapsing overhang signified the resurgence of another updraft. Therefore, it appeared that a new updraft was being generated at every 10 to 15 minutes on the southwest flank of the storm. The net effect was the propagation of storm to the southeast.

#### **e) Dissipating stage of the storm (0205 to 0245 UTC)**

During the maturing stage (0105 to 0205 UTC) a persistent "hook echo" was displayed on the low level radar. The storm moved to the right of the mean environmental wind and echo tops remained steady near of 14 km. After 0205 UTC the storm moved along with the mean environmental winds. Concurrently, the "hook echo" disappeared from the low levels, the reflectivities weakened and the echo tops declined.

storm moved along with the mean environmental winds. Concurrently, the “hook echo” disappeared from the low levels, the reflectivities weakened and the echo tops declined.

#### **(f) Hail analysis**

Lemon’s (1977) radar criteria for the representation of large hailstones ( $\geq 20$  mm) within a thunderstorm’s structure were met by the maturing stage of the Winnipeg hailstorm. The track of the 45 dBZ echo at 7 km (within the overhang) was compared to the actual hail reports. It was determined that the track of 45 dBZ echo, along the direction of the hailstorm, lay above the majority of hail reports with diameter of  $\geq 20$  mm. This indicated that the quasi-periodic descent of the overhang consisted of the falling hailstones. Further, the swath of hailstones with diameter  $\geq 40$  mm lay within 2 km of the track of peak reflectivity at 7 km. We conclude that the radar reflectivity values of 52 dBZ at 7 km were the likely indication of hailstones with diameters of 40 mm or more.

## **5.2 Comparison to conceptual models**

### **a) Pre-storm condition**

The pre-storm synoptic scale set-up of the Winnipeg hailstorm agreed well with the “classical” conceptual model of Fawbush et al. (1951). In particular the Winnipeg storm exhibited the following “fundamental characteristic”:

- 1) strong warm air advection at low levels ( $\leq 3.0$  km AGL),
- 2) a moderate low level jet, with strong veering,
- 3) the presence of a capping inversion at lower levels and a build-up of (i.e. the “loaded gun” profile),
- 4) a deep layer of potentially unstable air.



## **b) Storm's radar echo characteristics**

The radar structure of the Winnipeg hailstorm, closely resembled the radar structure of the supercell conceptual model of Chisholm and Renick (1972). In particular, at the maturing stage the Winnipeg storm had the following “characteristics”:

- 1) peak echo tops with minor fluctuations,
- 2) track of BWER in nearly straight line with minor fluctuations,
- 3) a persistent radar reflectivity maximum that borders the BWER, and
- 4) the storm's movement to the right of the mean environmental wind.

Furthermore the Winnipeg hailstorm developed in an environment that had the classical supercell hodograph proposed by Chisholm and Renick. The Chisholm and Renick's supercell conceptual model also proposed that the subsiding echoes within the overhang were the precipitation that were eroding the updraft. Therefore, what appeared as generation of new cells on the southwest flank of the storm may have just been the continuous shift of updraft core caused by the precipitation.

Lemon's (1980) conceptual model for the evolution of a supercell hailstorm were also in good agreement with the evolution of the Winnipeg hailstorm, from triggering to the maturing stage. Much like Lemon's model the evolution of the hailstorm had two distinct phases. At the initiation the hailstorm echoes were vertically aligned with more intense echoes at higher levels (no weak echo regions and overhang present). At this stage the storm consisted of several cells and moved to the east in the direction of the mean environmental wind. Within 30 minutes of its initiation the low level reflectivity on the southwest flank increased as the storm veered to the right. The storm's radar cross section was characterised by a weak echo region. 15 minutes later the storm attained the supercell characteristics.

the southwest flank increased as the storm veered to the right. The storm's radar cross section was characterised by a weak echo region. 15 minutes later the storm attained the supercell characteristics.

### **5.3 Discussion**

A comprehensive analysis of the 16 July 1996 hailstorm event over Winnipeg, Manitoba was feasible using the operational observations collected by Environment Canada. Based on this data set we evaluated the pre-storm condition of the atmosphere over southern Manitoba and determined the dynamic processes that affected the evolution of the hailstorm, from triggering to dissipating stages, in three dimensions. The analysis revealed that;

- 1) Warm air advection at lower levels destabilised the troposphere.
- 2) Advection of moisture below a capping inversion led to potentially unstable atmosphere at lower levels ("loaded gun" sounding).
- 3) The storm grew to its maturing stage as the result of the continuous feed of instability carried by the low level jet.
- 4) The low level windshear produced by the low level jet may have separated the updraft core from the downdraft at its maturing stage. As a result the storm reached a quasi-steady structure that lasted for 60 minutes.

The evolution of intense precipitation echoes, at the maturing stage of the hailstorm, revealed that the large hailstones had originated from the overhang. It is concluded that radar echo values of 52 dBZ at 7 km AGL were likely reflected from hailstones with diameters of 40 mm or more.

al. (1972) and Lemon (1980) closely described the evolution of the Winnipeg hailstorm. We concluded that the hailstorm had supercell characteristics at its maturing stage and that it evolved from a multicellular structure within 30 minutes.

Even though the operational data set of Environment Canada enabled us to examine the major storm features, some additional observations would have been useful for a more complete investigation. The following measurements would have been useful:

- 1) The synoptic charts with higher spatial resolution would have provided a better temperature and dewpoint distribution analysis. Also, the strength of the outflow from the pre-existing showers and areas of surface convergence would have been better defined.
- 2) For this case study, a wind profiler in the vicinity of the hailstorm's initiation would be useful in clarifying the dynamic effects of the low level jet. Furthermore, as the type of storm depends on the environmental windshear and instability (Weisman and Klemp, 1985), the transition of the hailstorm from a multicell to a supercell would have been better monitored with a wind profiler.
- 3) A dense network of soundings would have provided a more accurate estimate for CAPE and storm relative winds. Also, more frequent balloon releases (say every 3 hours) would better capture the changing storm environment.
- 4) A Doppler radar would have measured the air flow patterns near and within the hailstorm's structure. This coupled with the maximum reflectivities detected by the conventional radar would have provided a

better data set for the analysis of the hailstorm's evolution. Further, dual-wavelength radar would have detected the large hailstones within the storm more accurately (Rinehart, 1997).

#### **5.4 Recommendation for further research**

Our analysis revealed that the lift and instability associated with the low level jet over southern Manitoba played a key role in the evolution of the Winnipeg hailstorm. We also showed that the supercell characteristics of the hailstorm evolved from a multicellular storm structure. As the type of storm depends on the environmental instability and low level windshear (Weisman and Klemp, 1985), the transition from a multicell to a supercell may have resulted from the approaching low level jet. A future research recommendation would be to verify this transition. This task may be achieved by using a cloud scale numerical model such as ARPS (The Advanced Regional Prediction System) to perform sensitivity tests on the parameters associated with the low level jet. ARPS is a 3 dimensional non-hydrostatic model that is developed by the University of Oklahoma. The reader is referred to Xue et al. (1995) for further information on ARPS. The numerical simulation of the storm may also be used to clarify how the internal flow pattern is related to precipitation zones. The flow circulation may then be compared to conceptual models of hailstorms.

A useful extension of this study would be to build a database of Manitoba hailstorm cases and their synoptic conditions. Ambient kinematic and thermodynamic conditions for each storm could be extracted from weather charts and radiosondes data. A systematic analysis of this data would help to clarify which environmental factors control development of hailstorms. These data, in conjunction with the simulations from a numerical cloud model, would improve understanding and prediction of storm evolution and hailfall in Manitoba.

**Table 1 Maximum hailsize and damage as reported by weather watchers in Winnipeg**

| <b>report #</b> | <b>hail size</b> | <b>damages reported</b>                     |
|-----------------|------------------|---|
| 1               | 20 mm            | tree branches broken                        |
| 2               | 40 mm            |   |
| 3               | 5-10 mm          |   |
| 4               | 50-55 mm         |   |
| 5               | 50-55 mm         |   |
| 6               | 40-50 mm         |   |
| 7               | 30 mm            |   |
| 8               | 30-40 mm         |   |
| 9               | 30 mm            |   |
| 10              | 40-50 mm         |   |
| 11              | 40 mm            | cars and shingles damaged                   |
| 12              | 5-10             |   |
| 13              | 5-10 mm          |   |
| 14              | 5-10 mm          |   |
| 15              | 40-50 mm         |   |
| 16              | 25 mm            |   |
| 17              | 50 mm            |   |
| 18              | 40-50 mm         |   |
| 19              | 40-50 mm         |   |
| 20              | 40-50 mm         |   |
| 21              | 40-50 mm         | cars, windows and shingles damaged          |
| 22              | 45 mm            |   |
| 23              | 50 mm            |   |
| 24              | 25 mm            |   |
| 25              | 40 mm            |   |
| 26              | 30 mm            |   |
| 27              | 30 mm            |   |
| 28              | 50-70 mm         |   |
|                 |                  | broken windows, metal yard furniture dented |

**Table 2** Area of 45 dBZ at 7 km (CAPPI) and its longest width perpendicular to the track of the hailstorm, together with the peak echo within the area and along the width.

| <b>time<br/>(UTC)</b> | <b>area of 45 dBZ<br/>radar echo<br/>(km<sup>2</sup>)</b> | <b>width of 45 dBZ<br/>radar echo<br/>(km)</b> | <b>peak radar echo<br/>at 7.0 km<br/>(dBZ)</b> | <b>peak radar echo<br/>along the width<br/>(dBZ)</b> |
|-----------------------|---|--|--|--|
| 0105                  | 68  | 12   | 57   | 57   |
| 0110                  | 49  | 7  | 60   | 60   |
| 0115                  | 66  | 9  | 60   | 60   |
| 0120                  | 81  | 10   | 60   | 52   |
| 0125                  | 63  | 9  | 57   | 57   |
| 0130                  | 120   | 12   | 60   | 60   |
| 0135                  | 65  | 9  | 57   | 57   |
| 0140                  | 54  | 9  | 57   | 57   |
| 0145                  | 84  | 14   | 60   | 60   |

Table 3 List of 14 atmospheric parameters ranked (in order of importance) by Miller (1972) and their magnitudes. (mb is equivalent to hPa, Kts = knots and nm = nautical miles)

| Rank | Parameter                         | Weak                           | Moderate  | Strong   |
|------|-----------------------------------|--------------------------------|---|--|
| 1    | 500 mb Vorticity                  | neutral or negative            | contours cross vorticity 30 degrees   | contours cross at more than 30 degrees                                       |
| 2    | Stability LI Totals               | -2<br>50                       | -3 to -5<br>50 to 55  | -6<br>55   |
| 3    | Middle Level Jet Shear            | 35 kts<br>15 kts/90 nm         | 35-50 kts<br>15-30 kts/ 90nm  | 50 kts<br>30 kts/90 nm   |
| 4    | Upper Level Jet Shear             | 55 kts<br>15 kts / 90 nm       | 55 to 85 kts<br>15-30 kts/90 nm   | 85 kts<br>30 kts/90 nm   |
| 5    | Low-level Jet                     | 20 kts                         | 25-35 kts   | 35 kts   |
| 6    | Low-level Moisture (g/kg)         | 8                              | 8 to 12   | 12   |
| 7    | 850 mb Max Temp Axis              | East of Moist Ridge            | Over Moist Ridge  | West of Moist Ridge  |
| 8    | 700 mb No-Change Line             | Winds cross line 20 degrees    | Winds cross line 20-40 degrees  | Winds cross line 40 degrees  |
| 9    | 700 mb dry air intrusion          | Not available or weak winds    | Winds from dry to moist intrude at an angle of 10 to 40 degrees and at least 15 kts | Winds intrude at an angle of at least 40 degrees and are greater than 25 kts |
| 10   | 12 Hour Sfc P Fall                |                                | 1 to 5 mb   | 5 mb   |
| 11   | 500 mb height change              | 30 m                           | 30 to 60 m  | 60 m   |
| 12   | Height of Wet-Bulb-Zero Above Sfc | Above 11000ft<br>Below 5000 ft | 9000 to 11000<br>5000 to 7000   | 7000 to 9000 ft  |
| 13   | Surface Pressure over Threat Area | 1010 mb                        | 1010 to 1005  | 1005 mb  |
| 14   | Surface Dewpoint                  | 12 C                           | 12 to 18 C  | 18 C   |

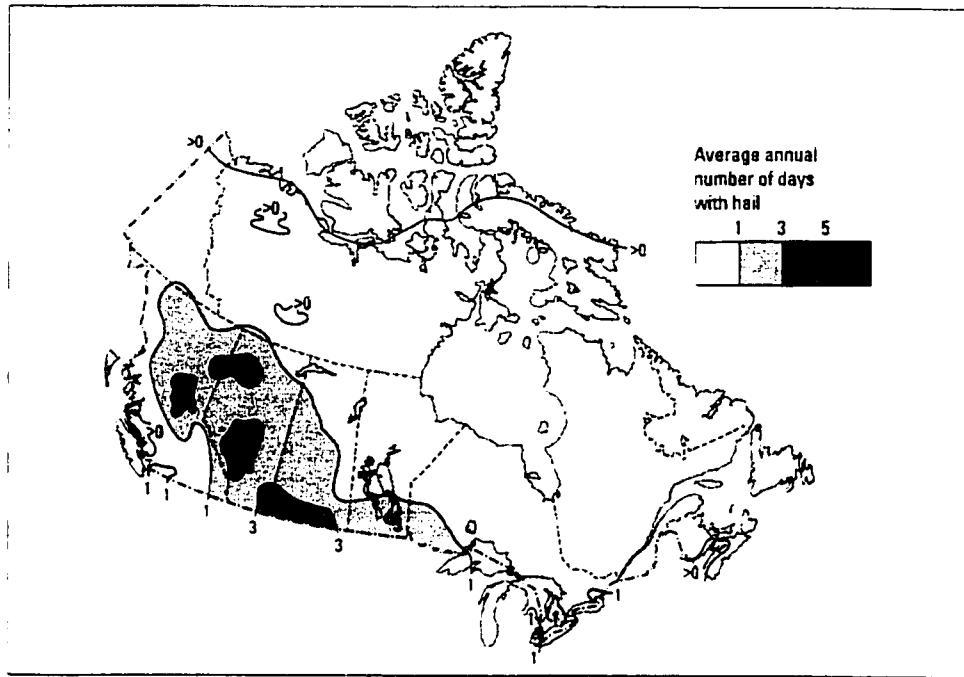


Fig 1.1 Average annual number of days with hail in Canada (Environment Canada, 1977)



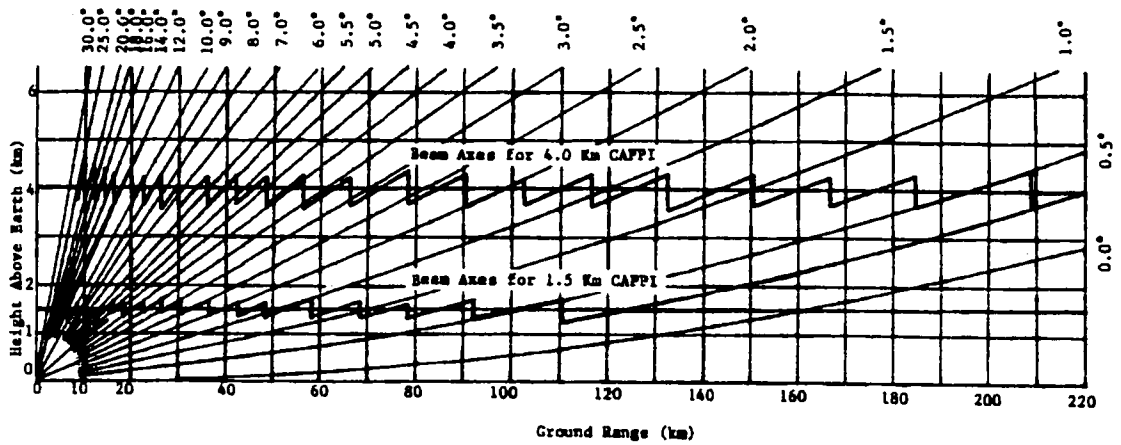


Fig. 2.1 Illustration of how a CAPPI is made. The radar beam is corrected for the earth's curvature and normal refraction. (from Crozier et al., 1986 ).

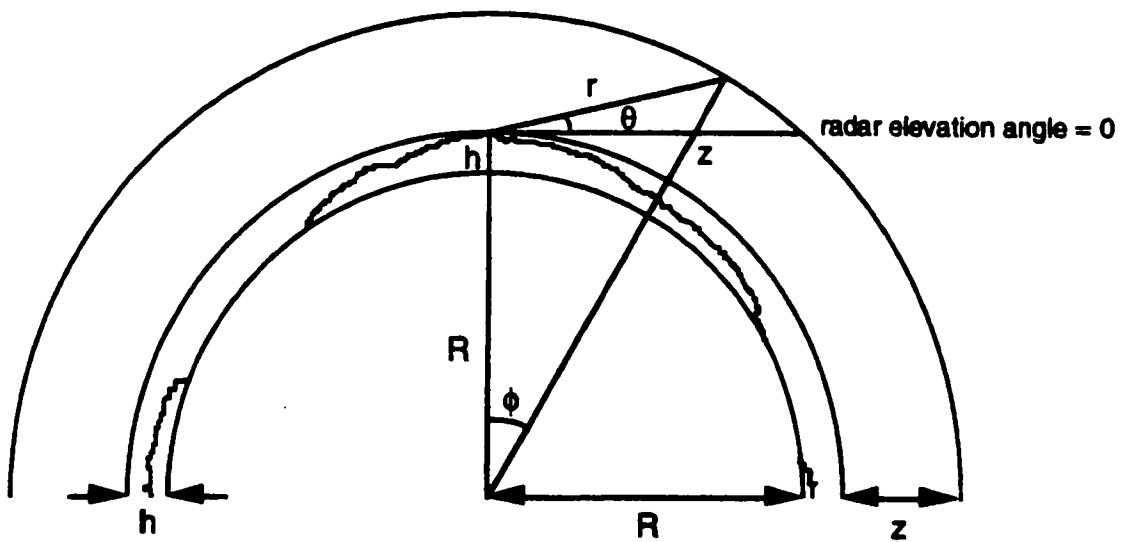


Fig. 2.2 Geometric relation of the height ( $z$ ) of a point above the ground and its radial range ( $r$ ) from the antenna. (from Environment Canada, 1997)

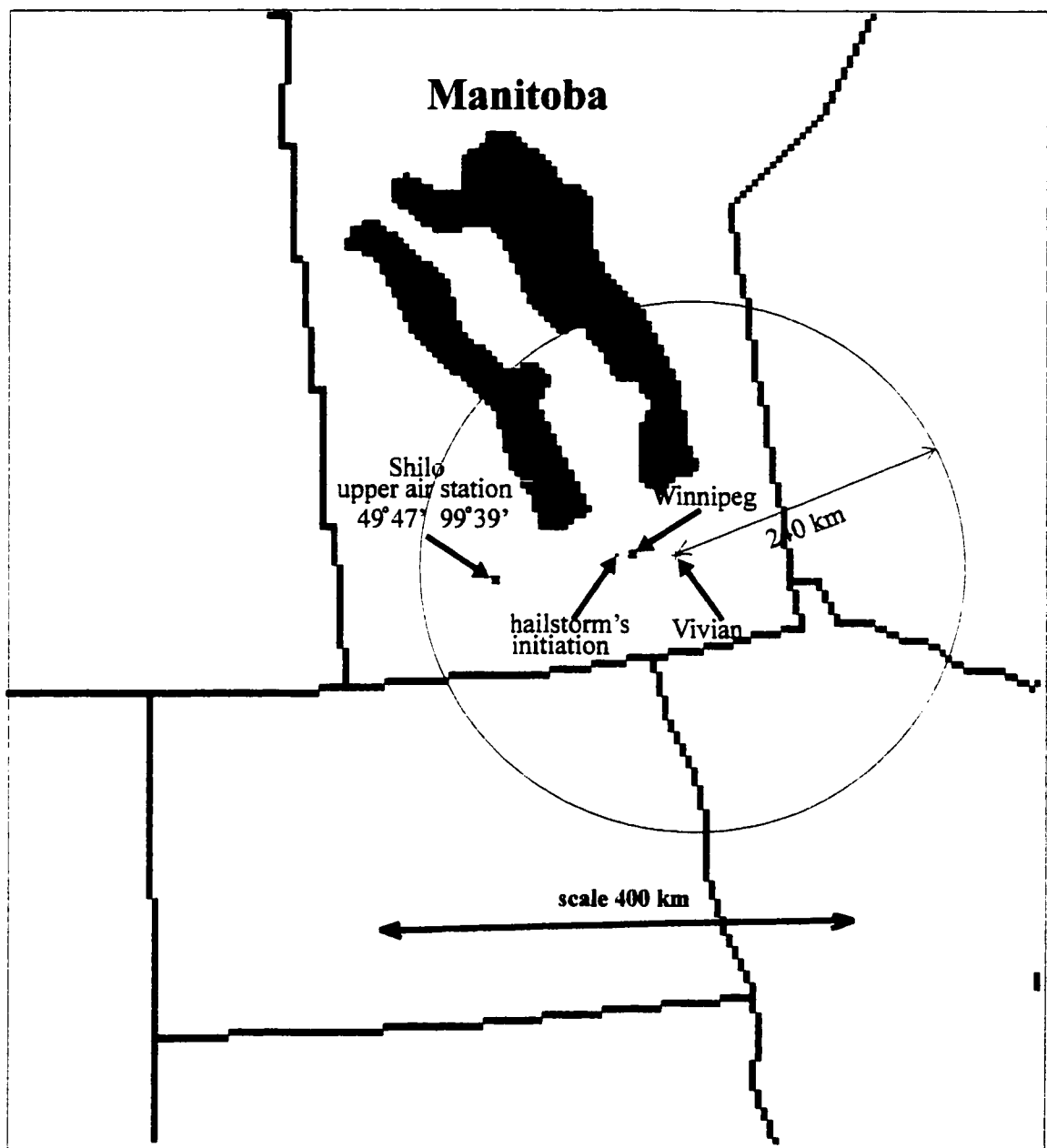


Fig. 3.1 Relative locations of Shilo upper air station, Winnipeg and Vivian radar (range 240 km) with respect to the hailstorm's initiation position.

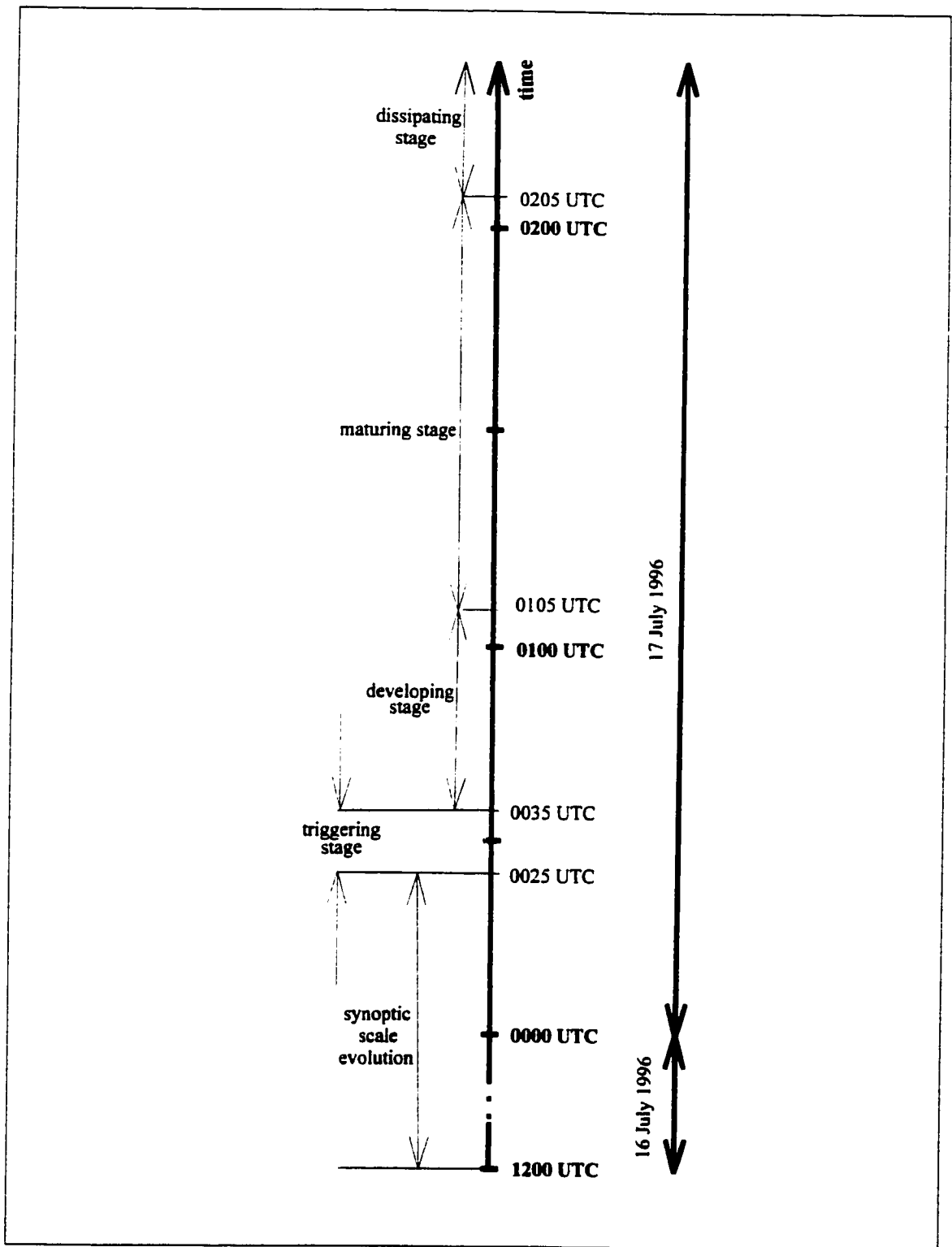


Fig. 3.2 Time line for the evolution of the Winnipeg hailstorm.

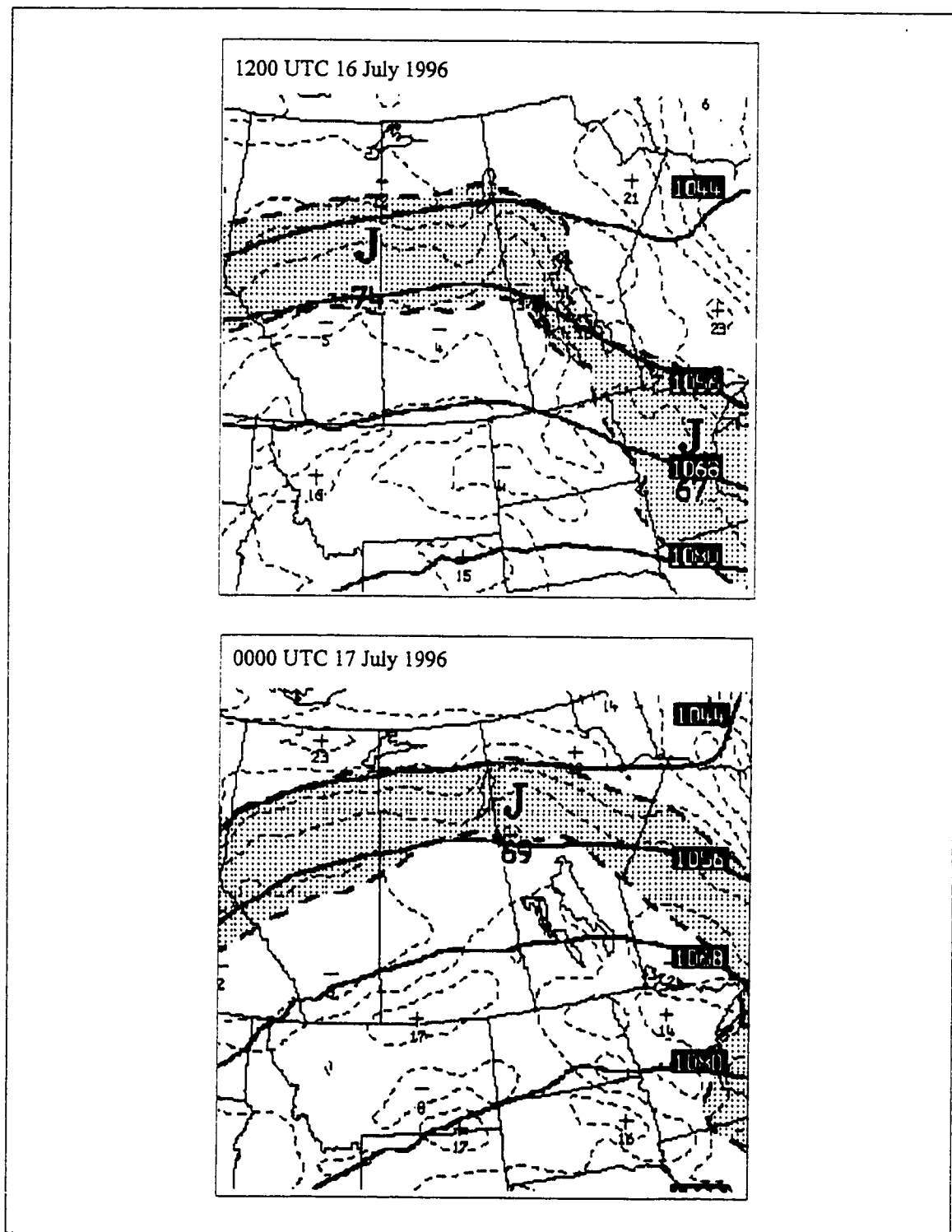


Fig. 3.3 250 hPa heights at 1200 UTC, 16 July 1996 and 0000 UTC, 17 July 1996 depicting contour heights (solid lines, dam), area of maximum winds (shaded, knots) and vorticity (dashed lines).

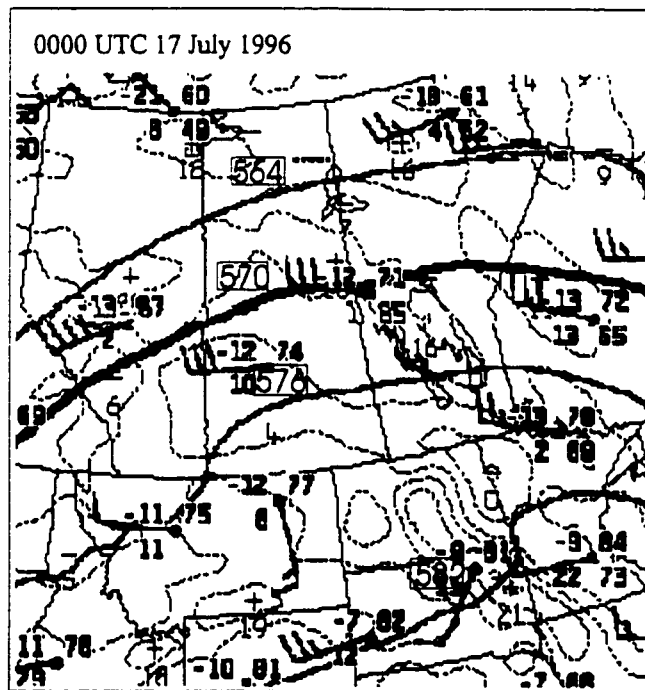
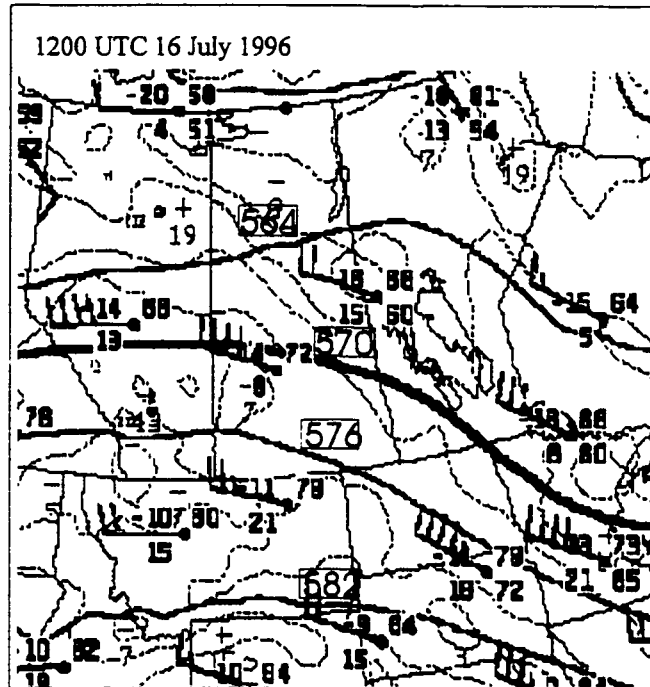


Fig. 3.4 500 hPa heights at 1200 UTC, 16 July 1996 and 0000 UTC, 17 July 1996 depicting contour heights (solid lines, dam), vorticity (dashed lines).

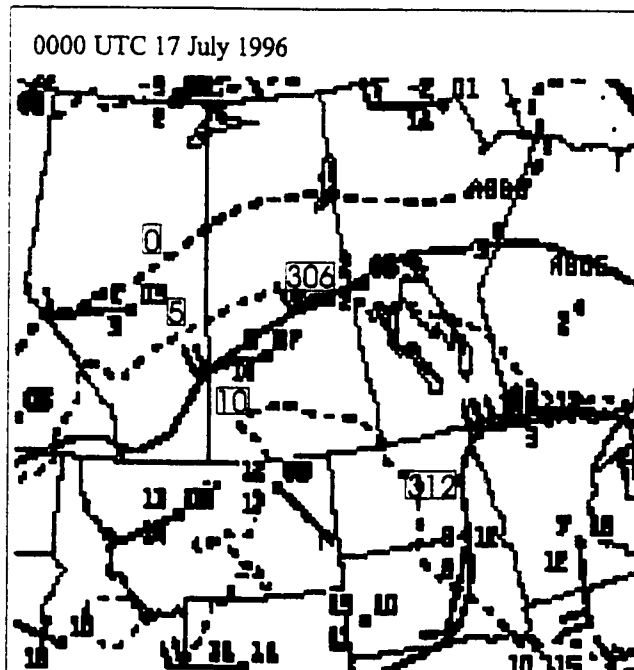
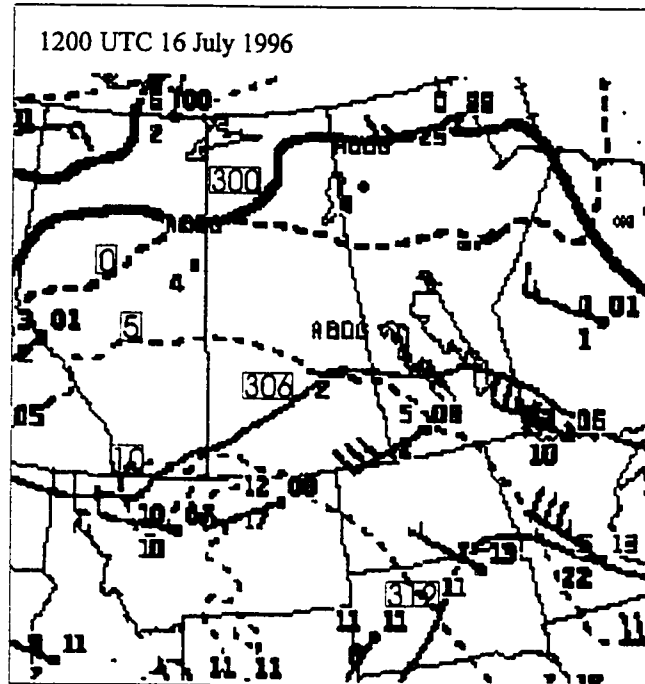


Fig. 3.5 700 hPa heights at 1200 UTC, 16 July 1996 and 0000 UTC, 17 July 1997 contour heights (solid lines, dam) and temperature (dashed lines, °C).

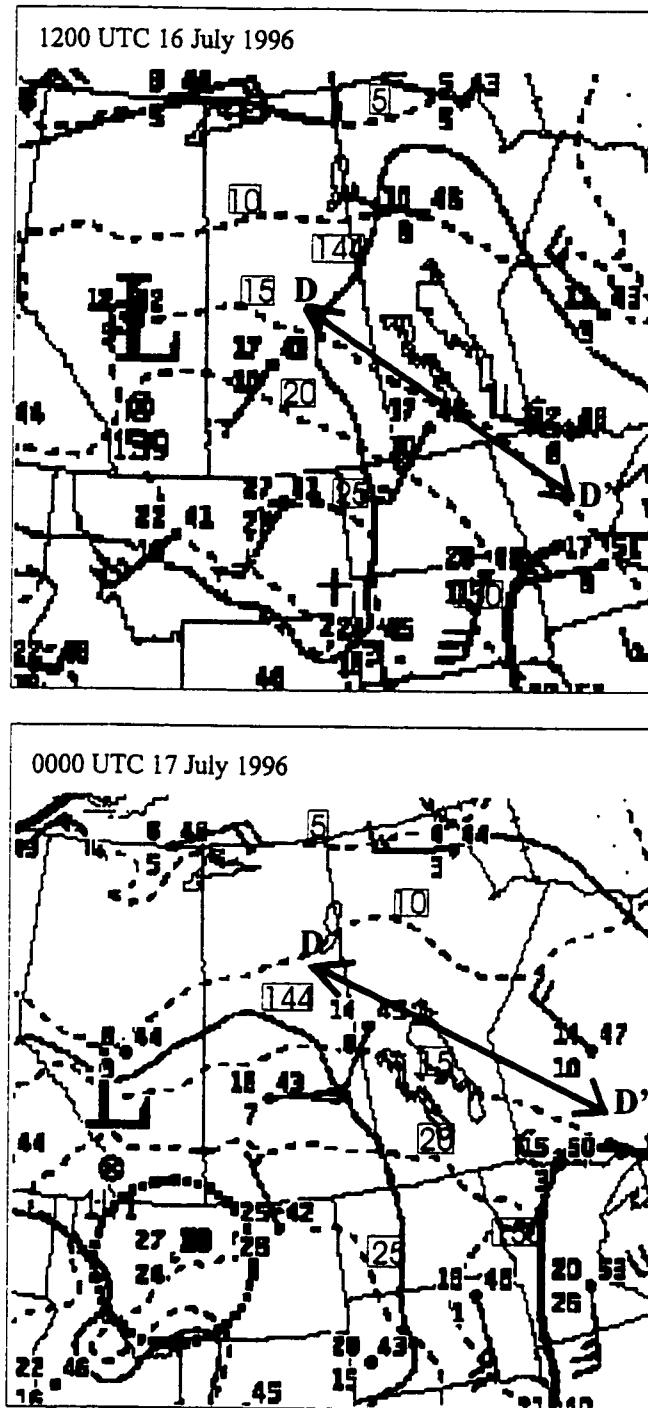


Fig. 3.6 800 hPa heights at 1200 UTC, 16 July 1996 and 0000 UTC, 17 July 1996 contour heights (solid lines, dam) and temperature (dashed lines, °C). The axis of dilatation is shown as DD'.

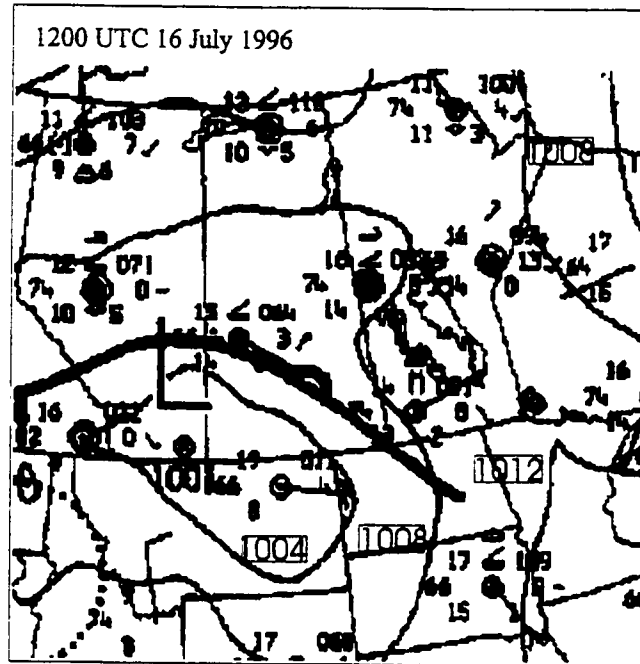


Fig. 3.7 Surface analysis at 1200 UTC, 16 July 1996 depicting isobars and an upper front..



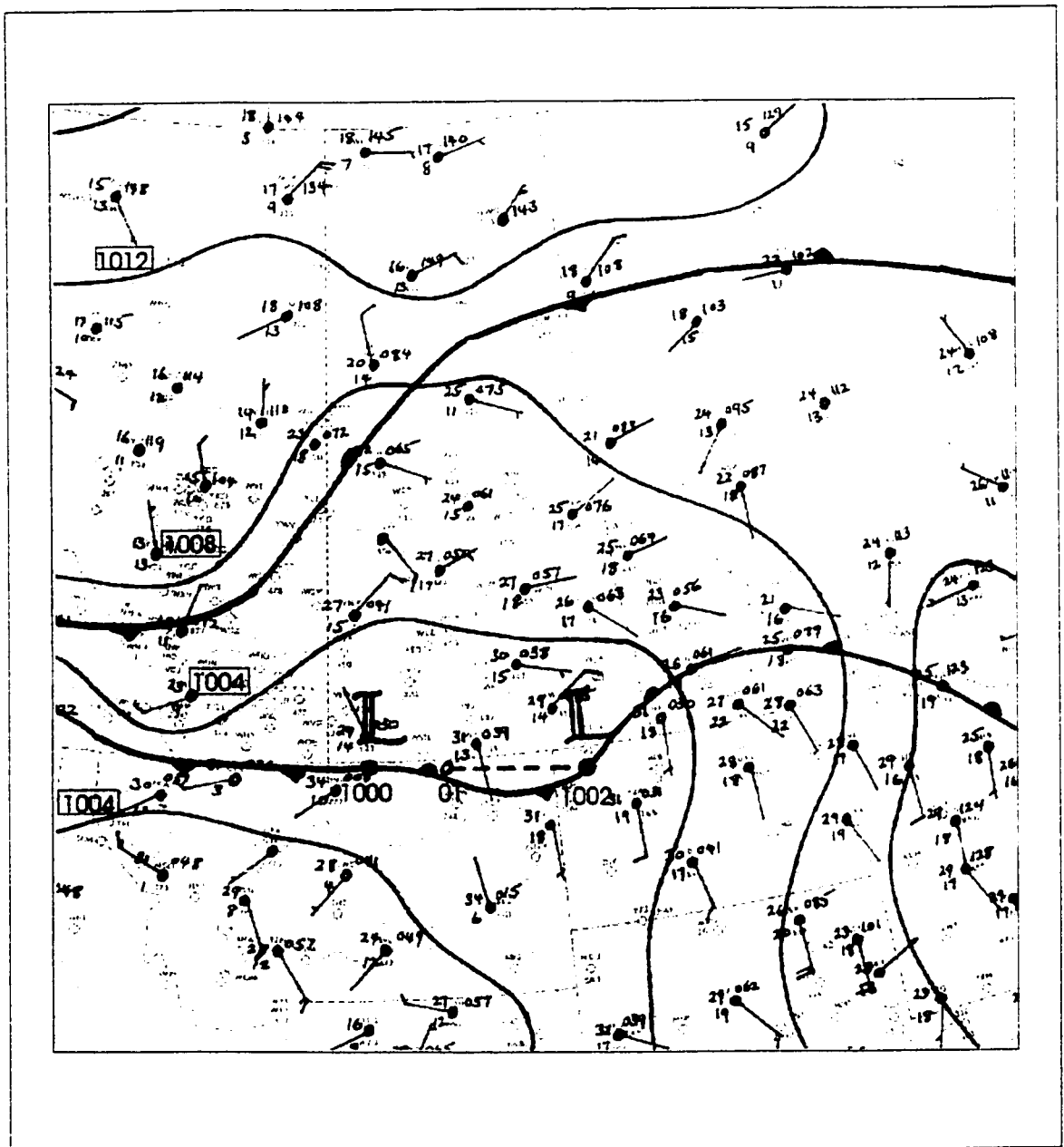


Fig. 3.8 Surface analysis at 0000 UTC, 17 July 1996 depicting isobars and surface fronts.

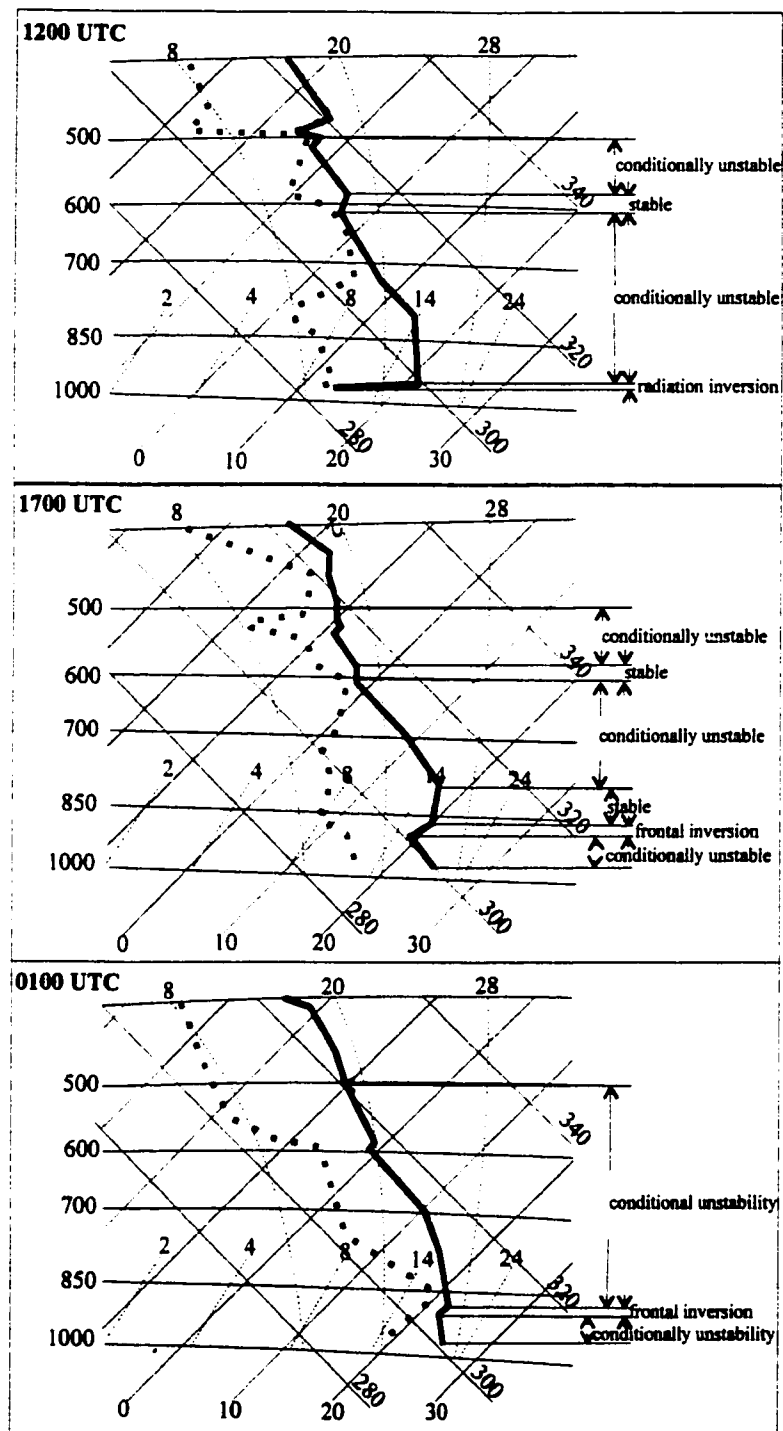


Fig. 3.9 Tephigrams for soundings at Shilo (WLO) taken at 1200, 1700 UTC 16 July 1996 and 0100 UTC, 17 July 1996 depicting temperatures (thick solid curve) and dewpoint (dotted curve). Horizontal lines are isobars (hPa), straight lines skewed to the right are isotherms ( $^{\circ}\text{C}$ ), straight lines skewed to the left are dry adiabats ( $^{\circ}\text{C}$ ), long dashed lines are moist adiabats ( $^{\circ}\text{C}$ ) and short dashed lines are mixing ratios (g/kg).

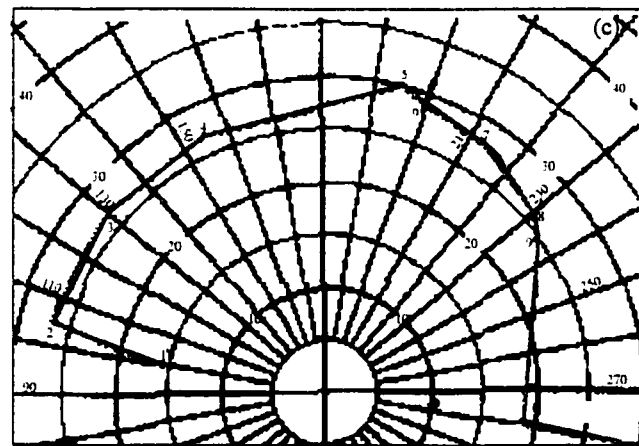
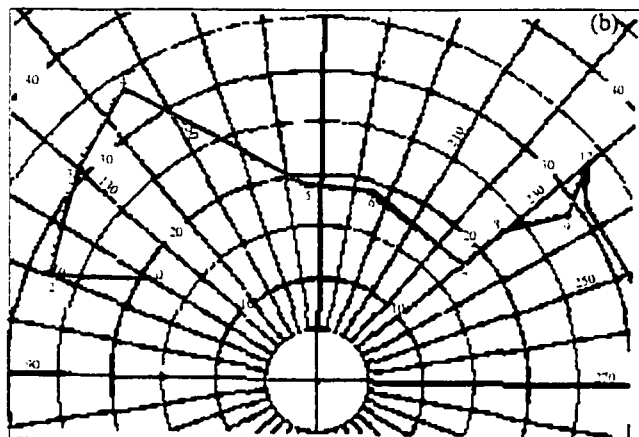
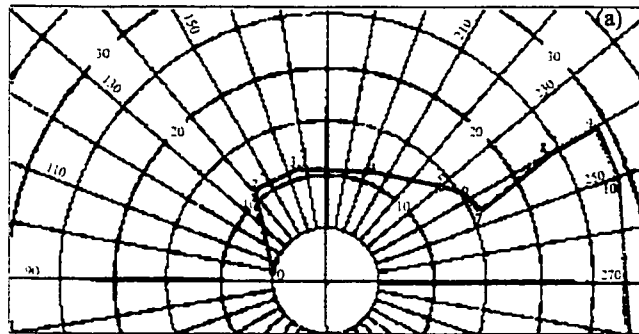
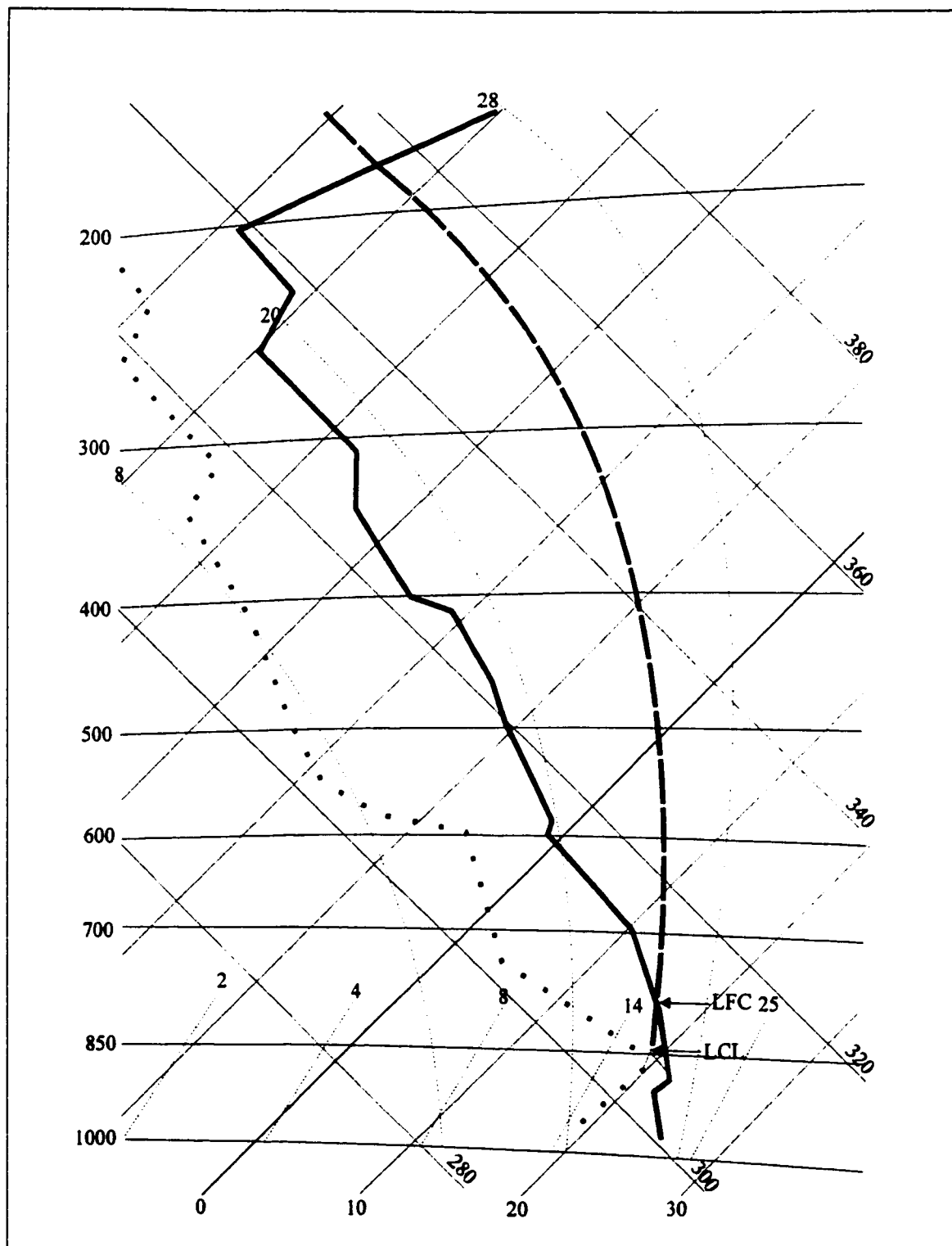


Fig. 3.10 Hodographs for the soundings at Shilo (WLO) taken at (a) 1200 UTC, (b) 1700 UTC, 16 July 1996 and (c) 0100 UTC, 17 July 1996 depicting the wind profile (blue line). Heights are in thousands of feet. Rings are in 5 knots intervals.



**Fig. 3.11** Modified Shilo (WLO) sounding at 0100 UTC 17 July 1996. Measurements from the 1200 UTC 16 July 1996 sounding above 400 hPa is attached to that of 0100 UTC below 400 hPa. The thick dashed line is the track of the lifted parcel along the corresponding wet adiabat.

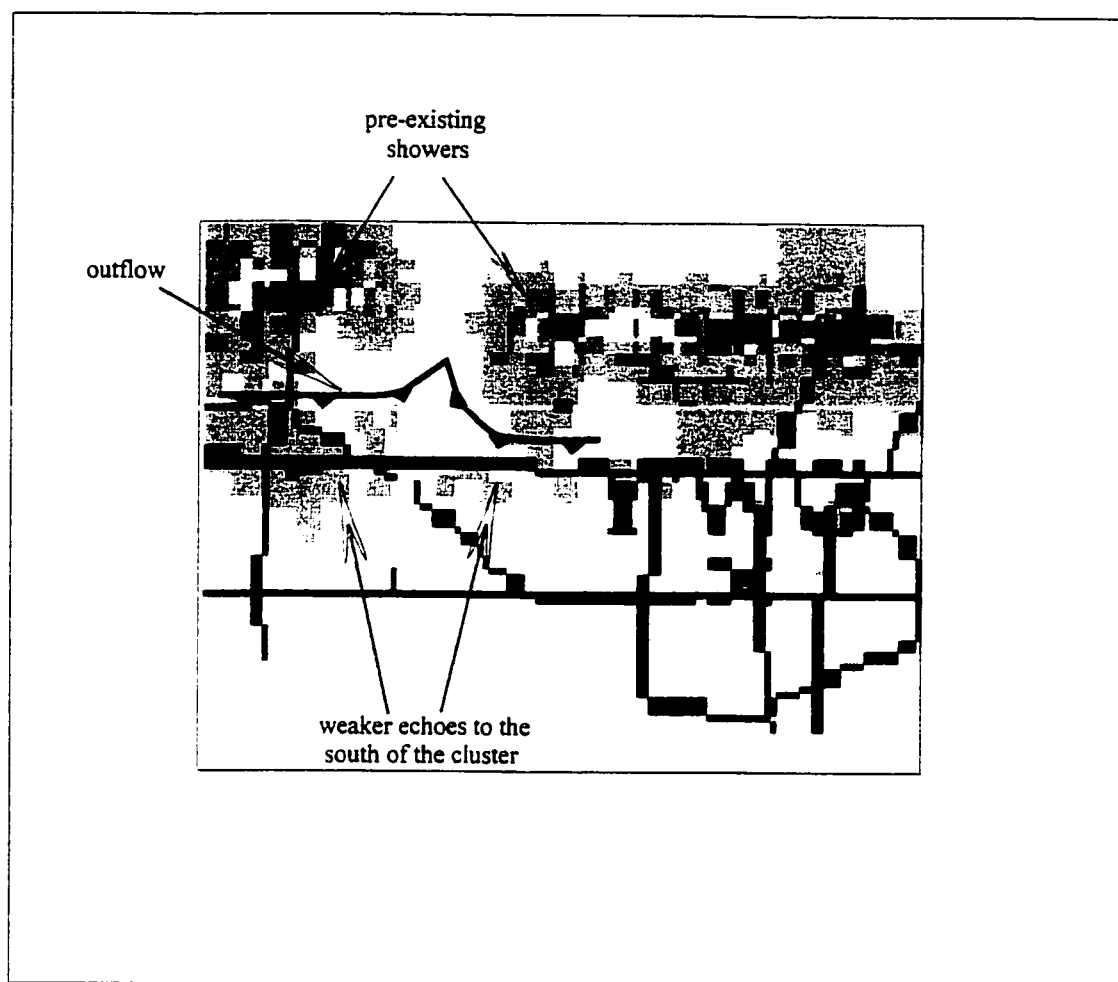
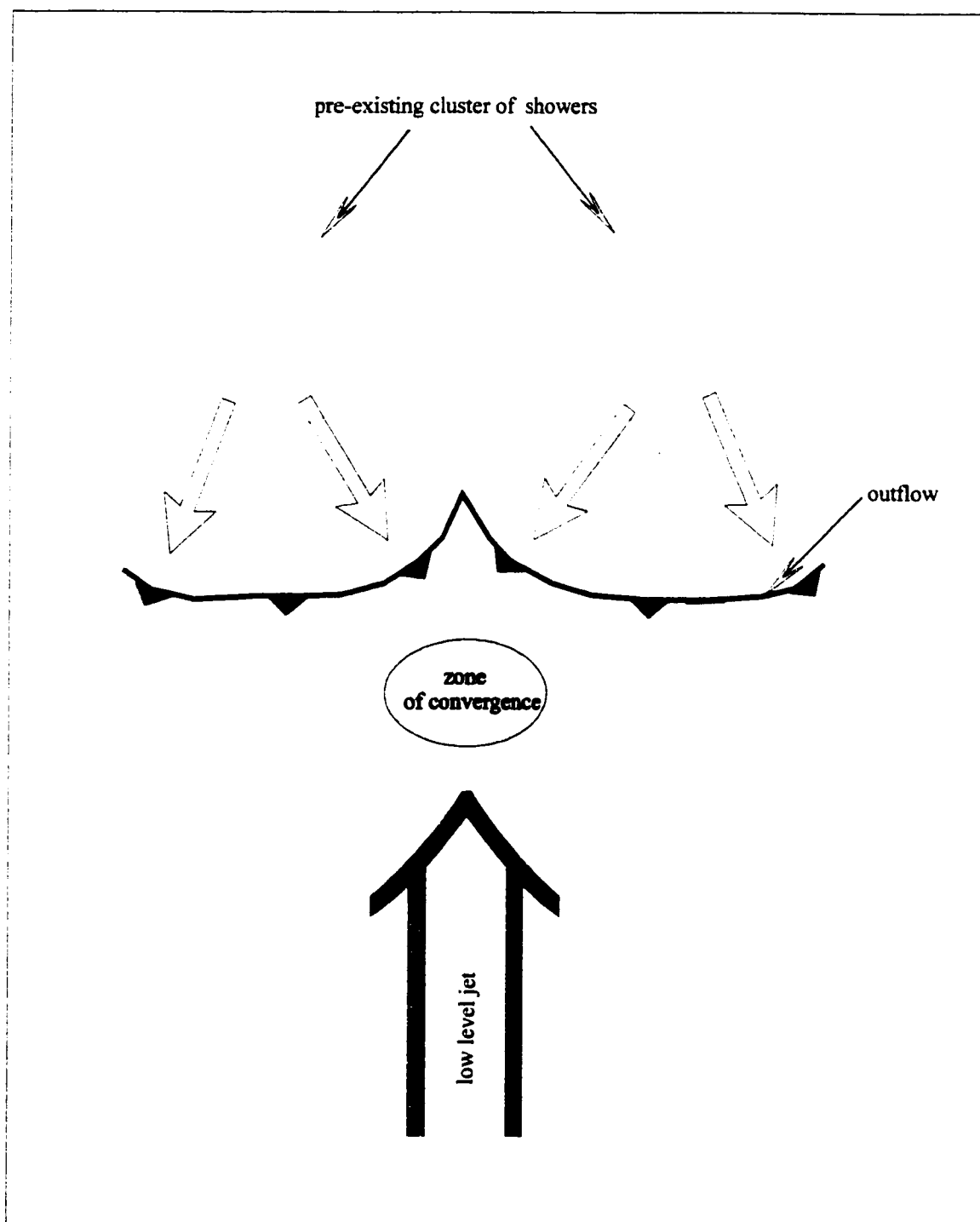


Fig. 3.12 Vivian Radar CAPPI at 1.5 km for 0025 UTC, 17 July 1996. Rings are spaced 50 km apart. The colour scheme for rainfall rates (in mm/h) is shown in Fig. 3.32.



**Fig. 3.13** Conceptual diagram for the triggering of the Winnipeg hailstorm.

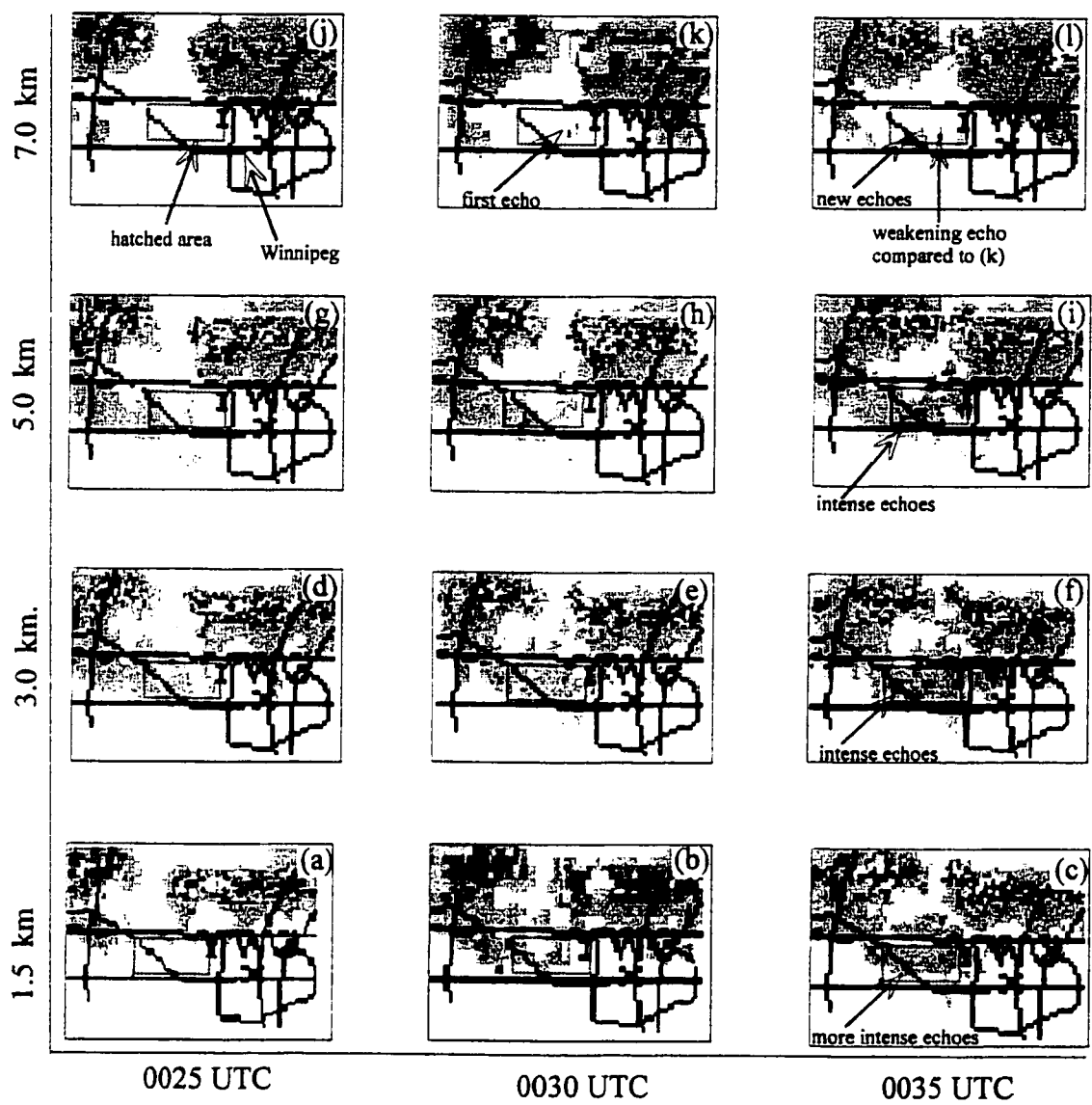


Fig. 3.14 Five minute sequence of 1.5, 3, 5 and 7 km Vivian radar CAPPIs from 0025 to 0035 UTC, 17 July 1996.

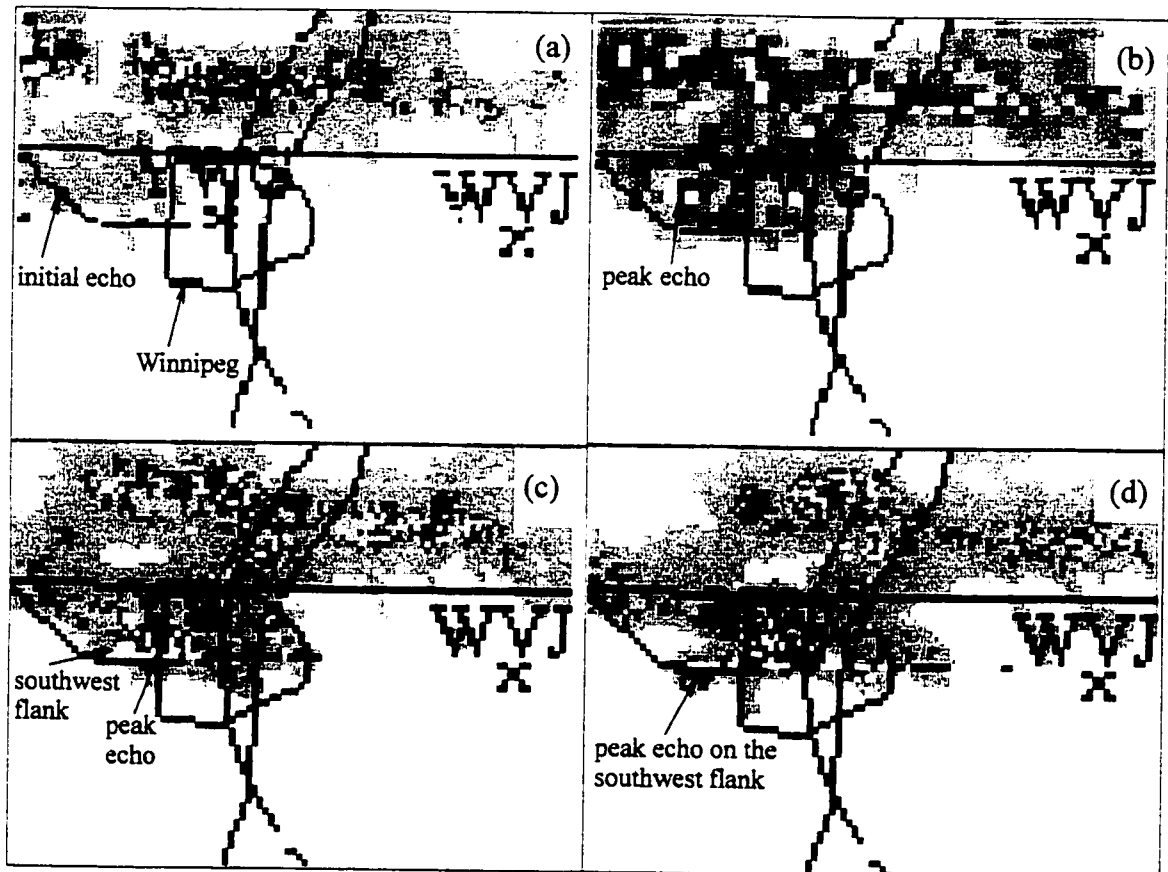


Fig. 3.15 Vivian radar (WVJ) CAPPIs at 1.5 km for (a) 0035, (b) 0045, (c) 0055 and (d) 0105.



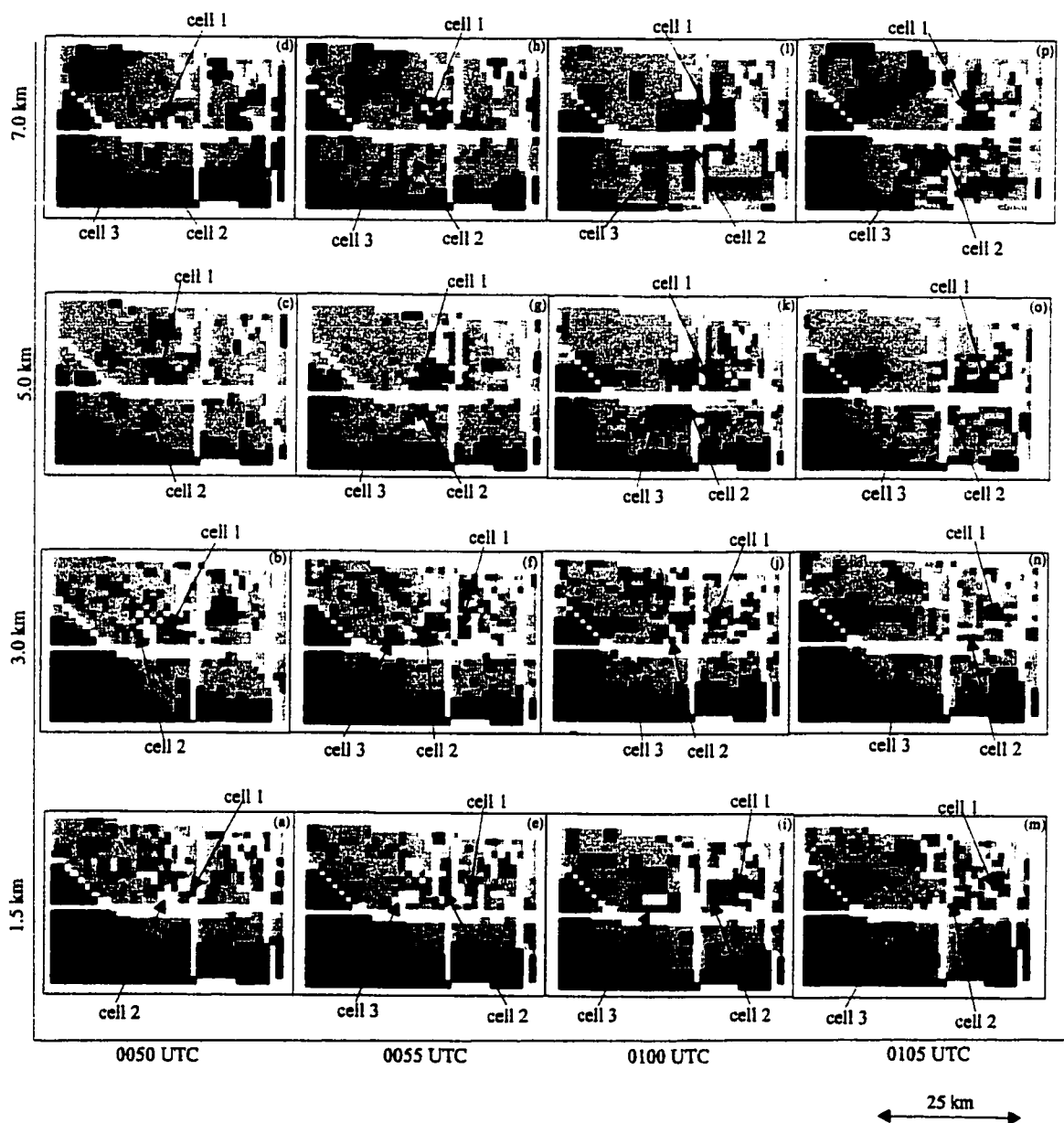


Fig. 3.16 Five minute time sequence of 1.5, 3, 5 and 7 km Vivian radar CAPPIs from 0050 to 0105 UTC 17 July 1996.

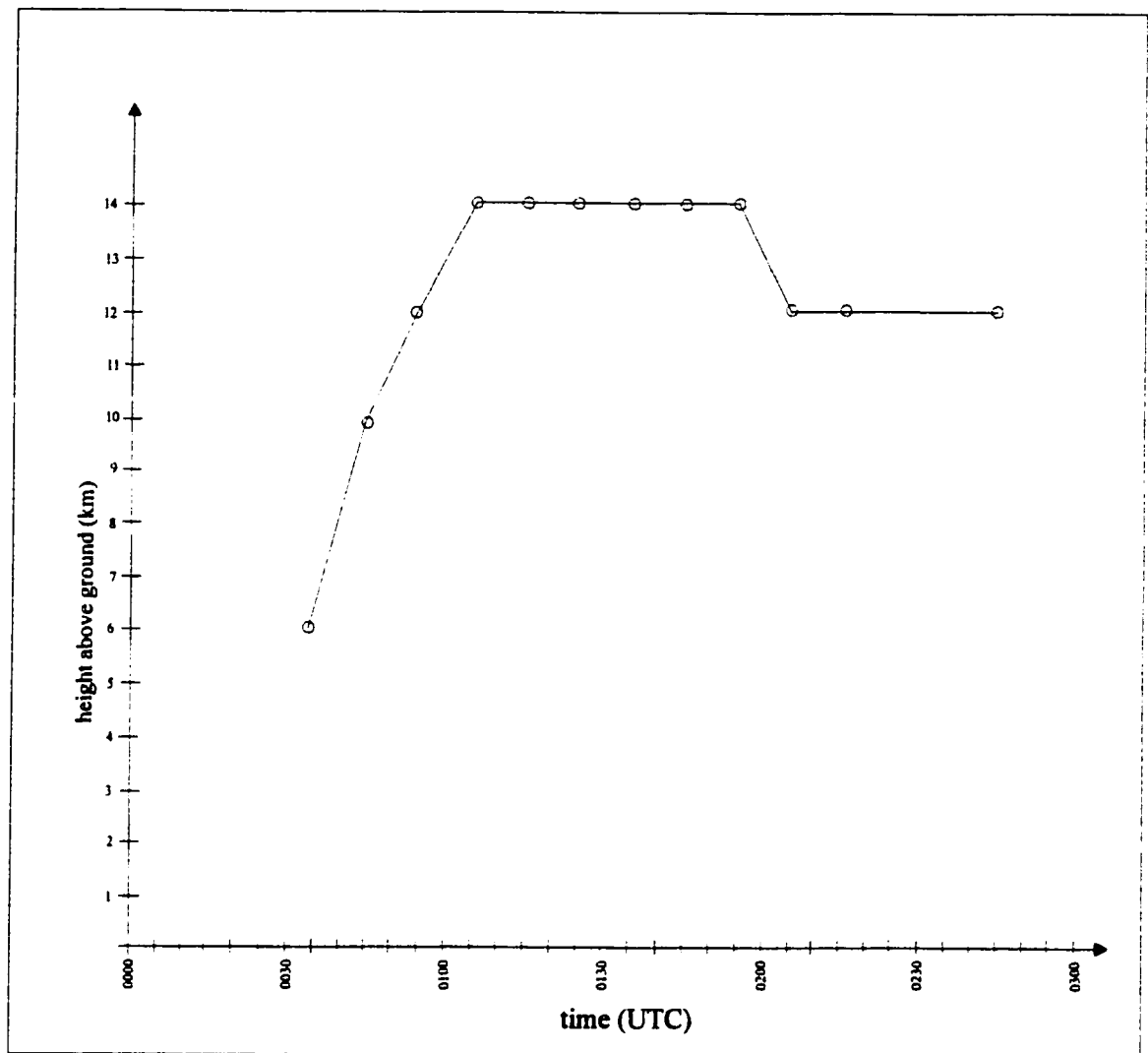


Fig. 3.17 Time variation of height of maximum radar storm tops, 17 July 1996.

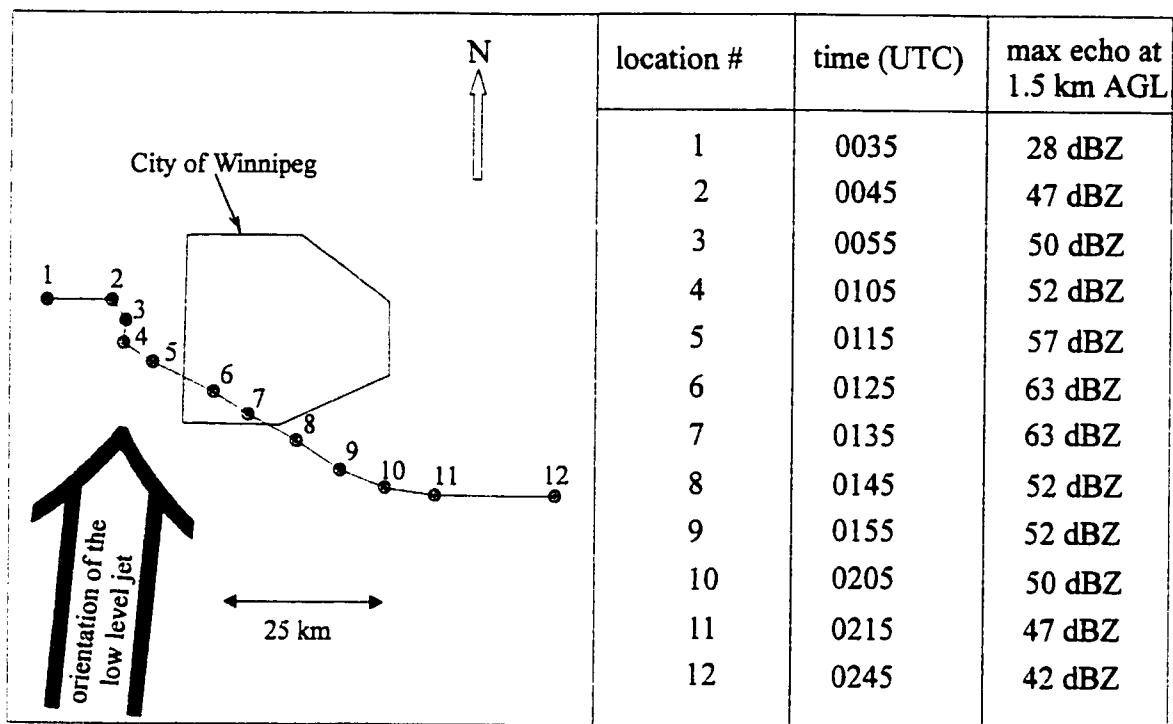


Fig. 3.18 Track of the strongest reflectivity on the southwest flank of the Winnipeg hailstorm and the orientation of the low level jet (not in scale). Blue circles show the locations of the peak echoes and their path is shown by small dashed lines.

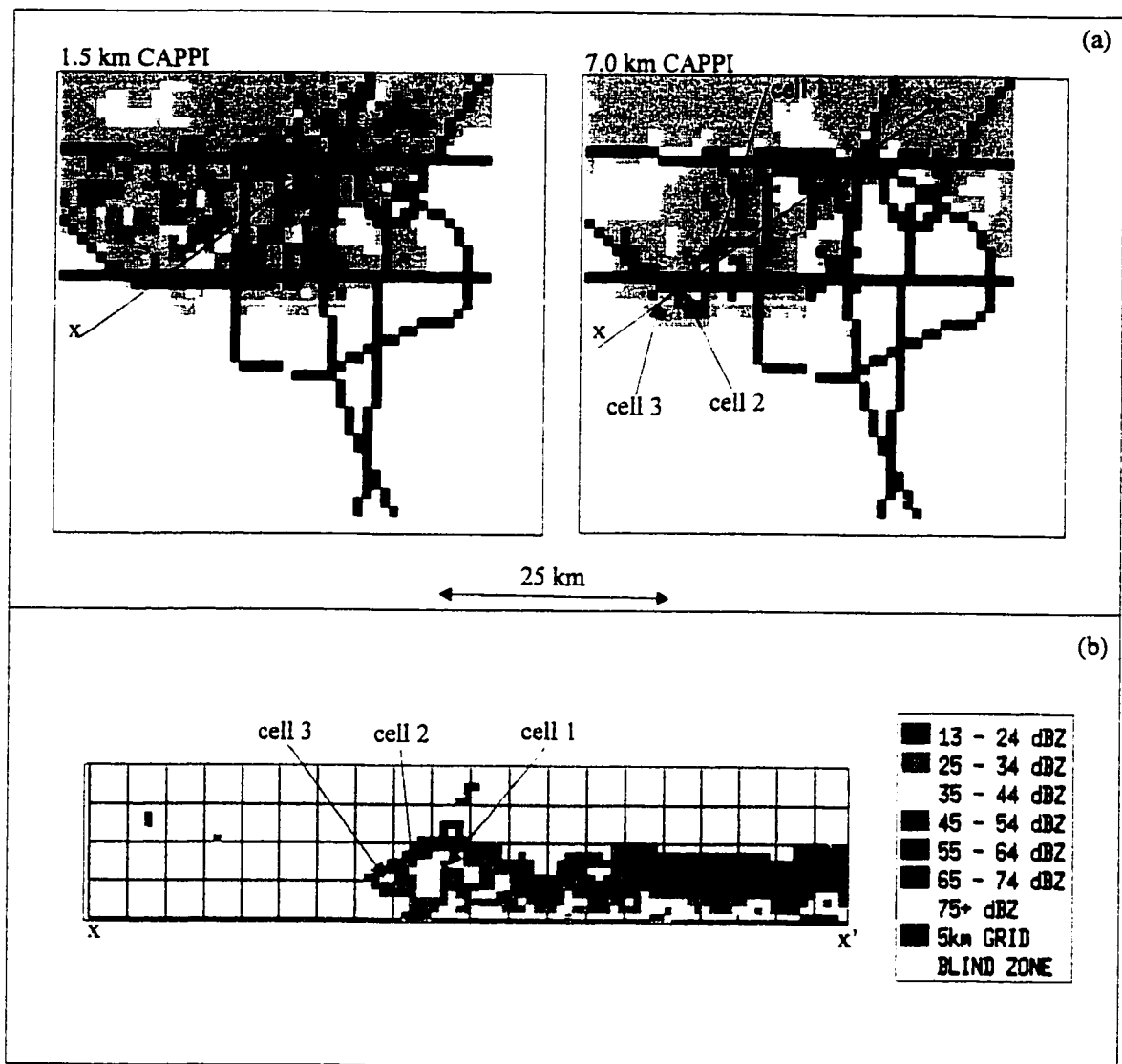


Fig. 3.19 (a) 1.5 and 7 km Vivian radar CAPPIs at 0050 UTC, (b) cross section presented by RDSS through the southwest flank of the storm (shown as  $xx'$  in (a)).

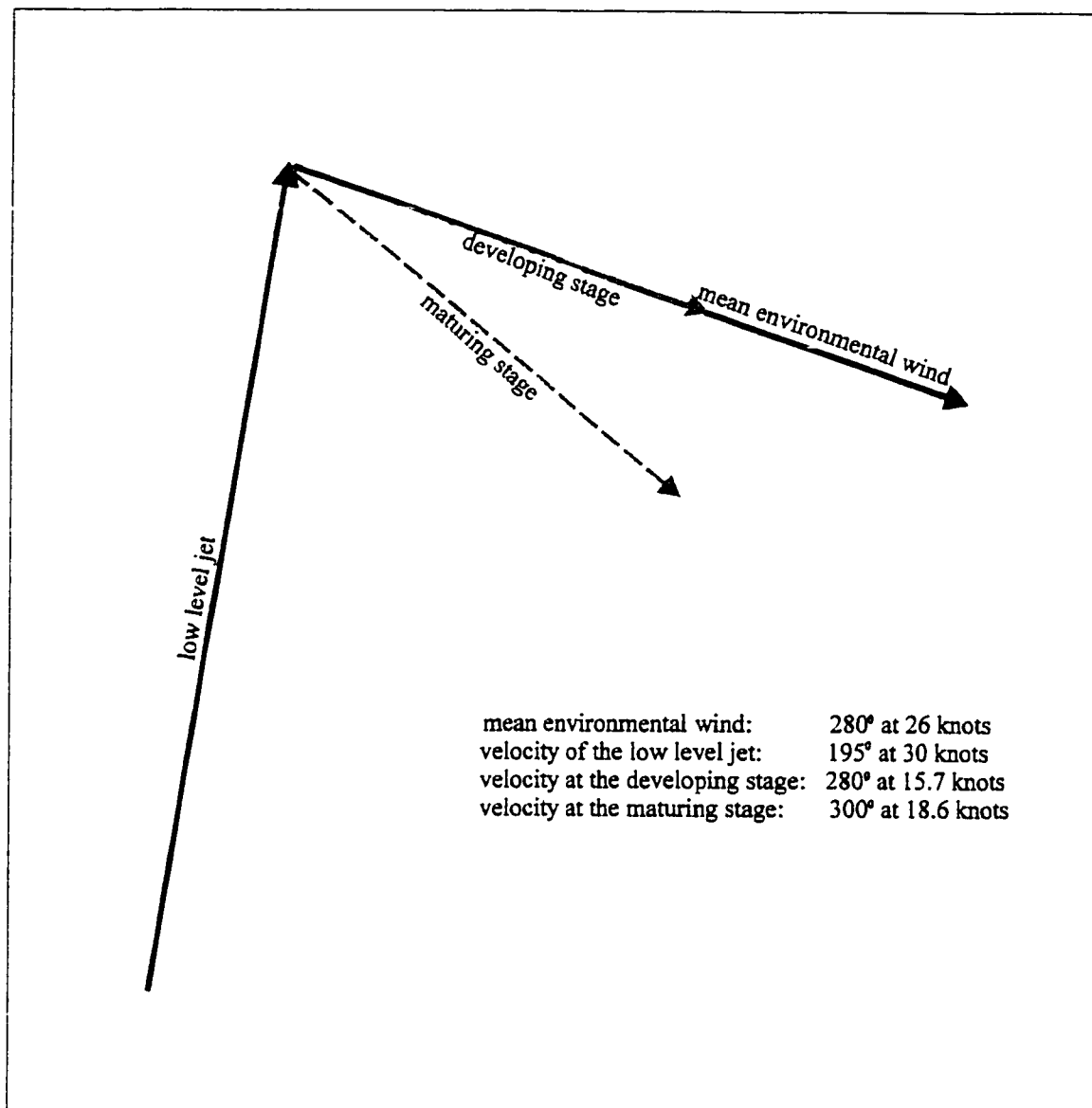


Fig. 3.20 Vector composite for the velocity of the low level jet, mean environmental wind and the hailstorm at its developing and maturing stage.

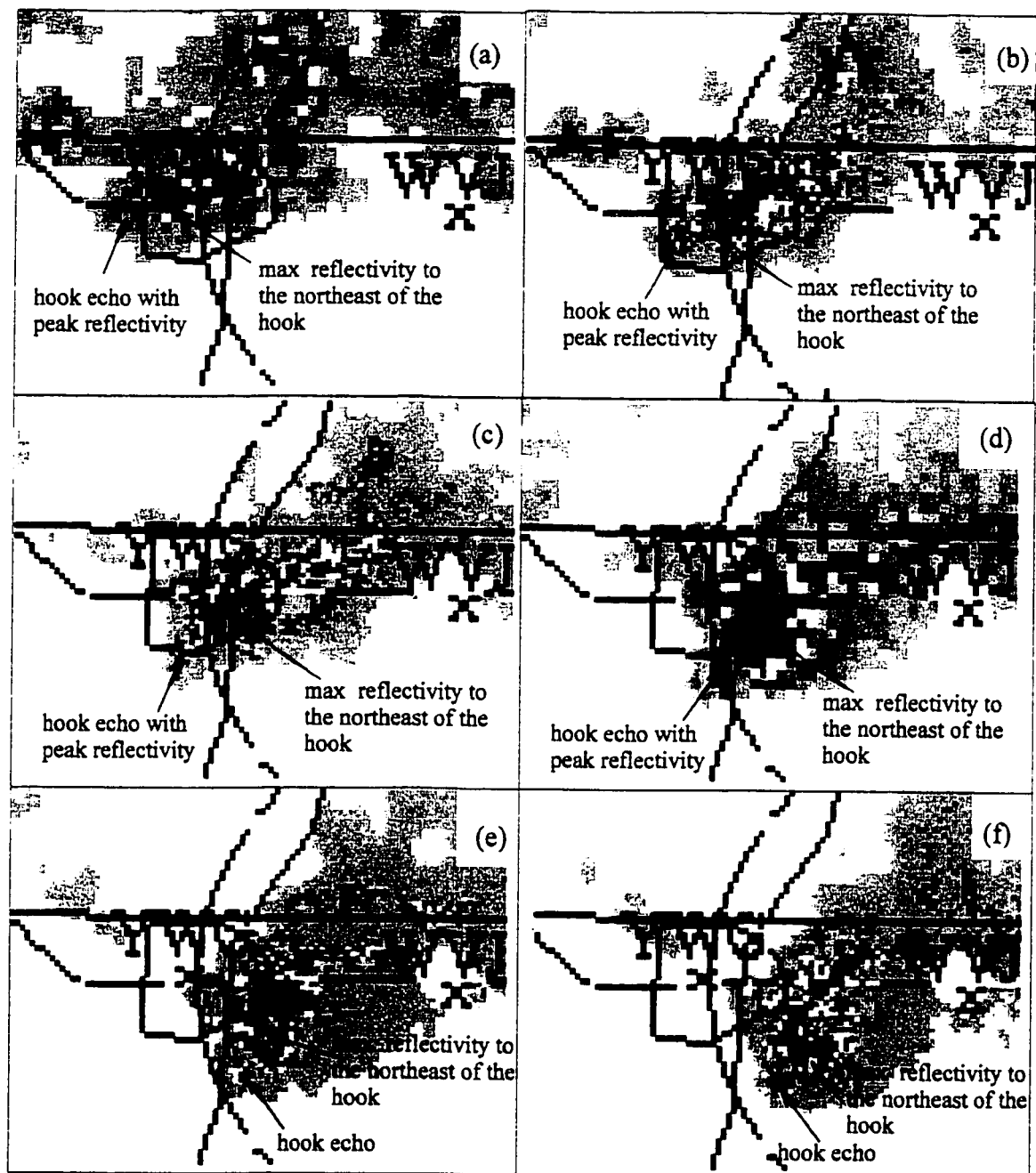


Fig. 3.21 Vivian radar CAPPIs at 1.5 km for (a) 0115, (b) 0125, (c) 0135, (d) 0145, (e) 0155 and (f) 0205 UTC.



Fig. 3.22 16 July 1996 Winnipeg hailstorm - photo by Eugene Kowaluk.

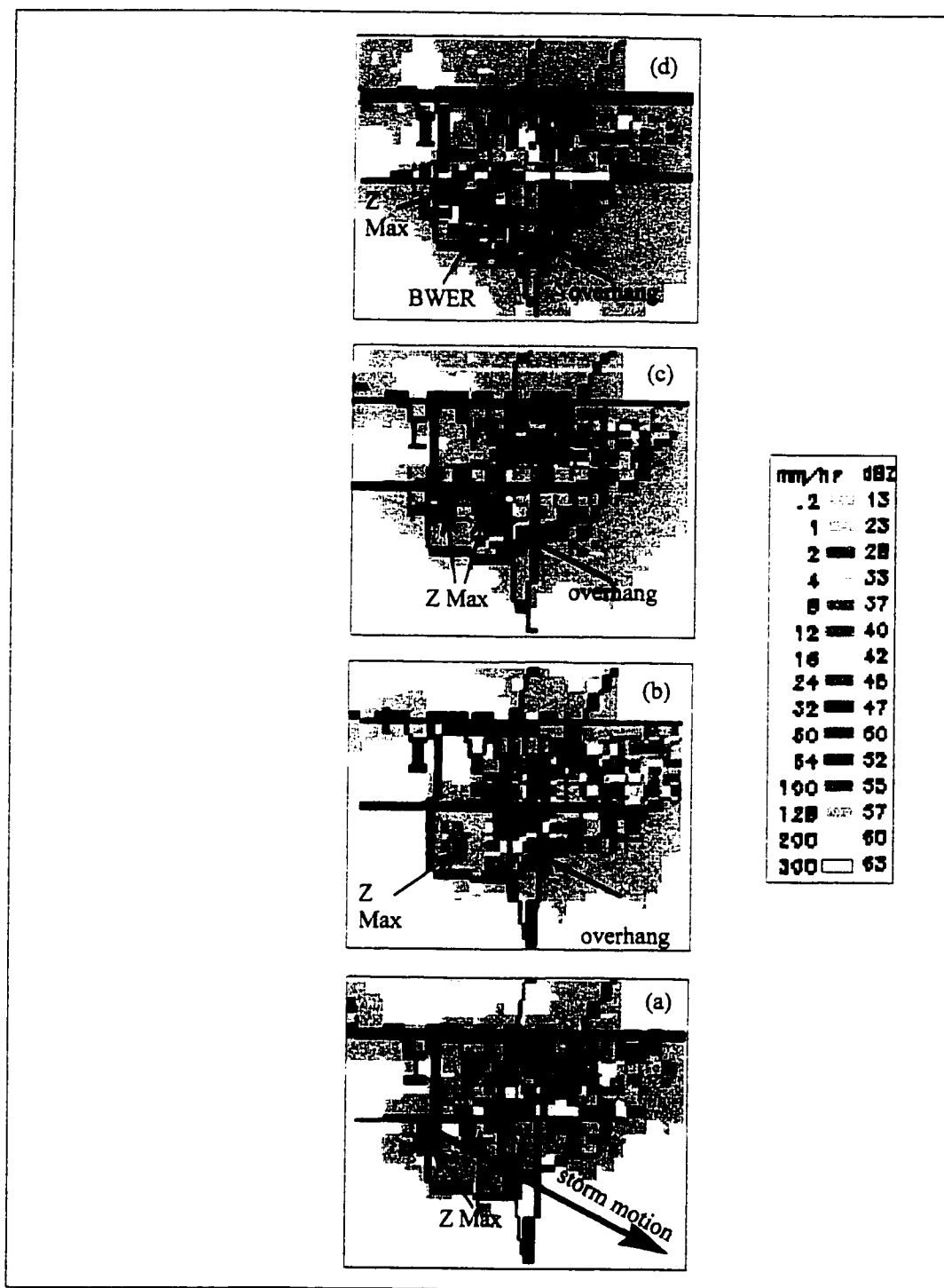


Fig. 3.23 Vivian radar CAPPIs at (a) 1.5, (b) 3.0, (c) 5.0 and 7.0 km for 0120 UTC, 17 July 1996. Areas of maximum radar reflectivity are labelled by Z Max .



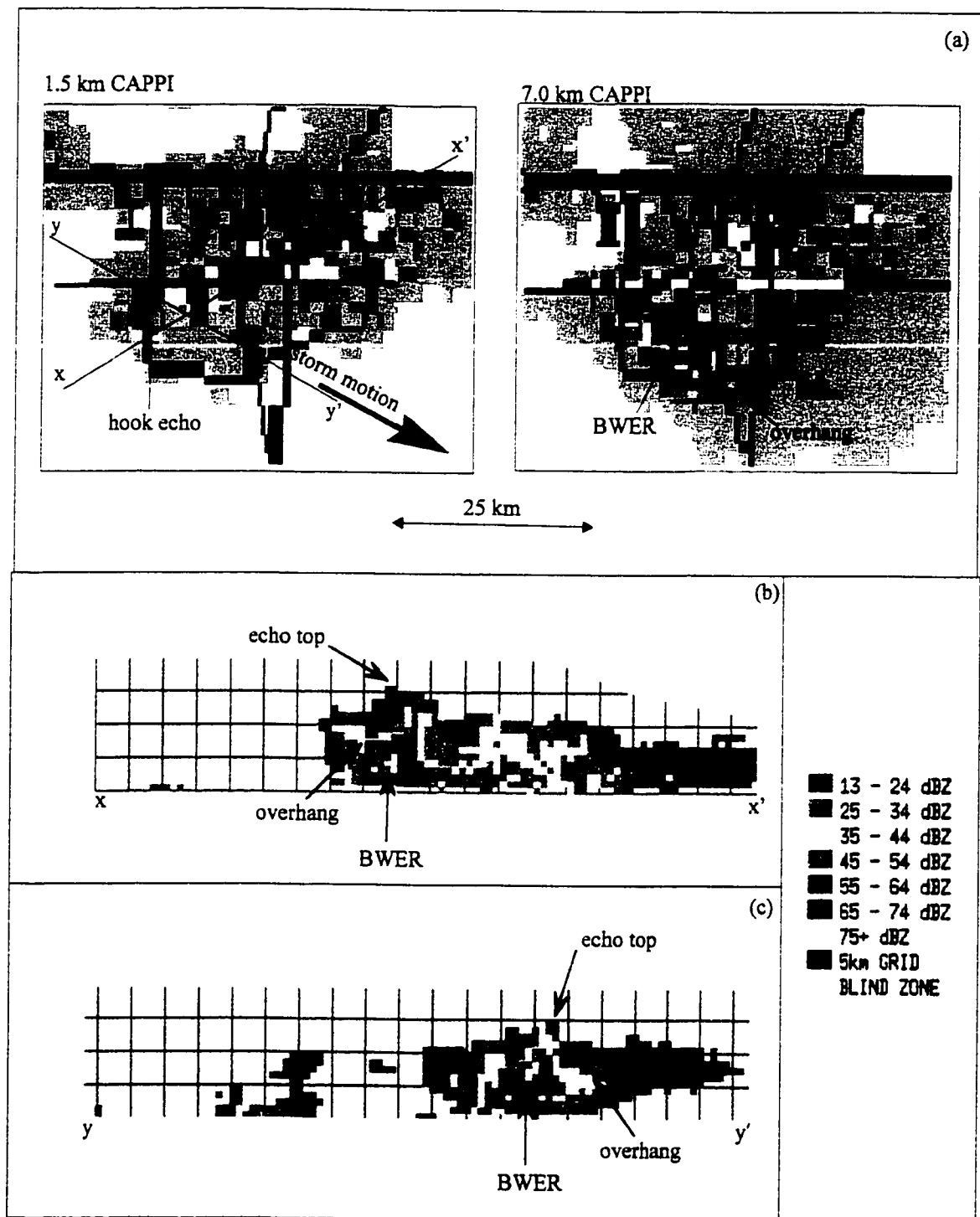


Fig. 3.24 (a) Vivian radar CAPPIs at 0120 UTC for 1.5 km altitude (left top) and 7 km altitude (right top). The colour scheme for rainfall (in mm/h) is shown in Fig. 3.32. (b) Vertical cross section showing radar reflectivity in dBZ along the line segment  $xx'$  shown in (a). (c) Vertical cross section along  $yy'$ .

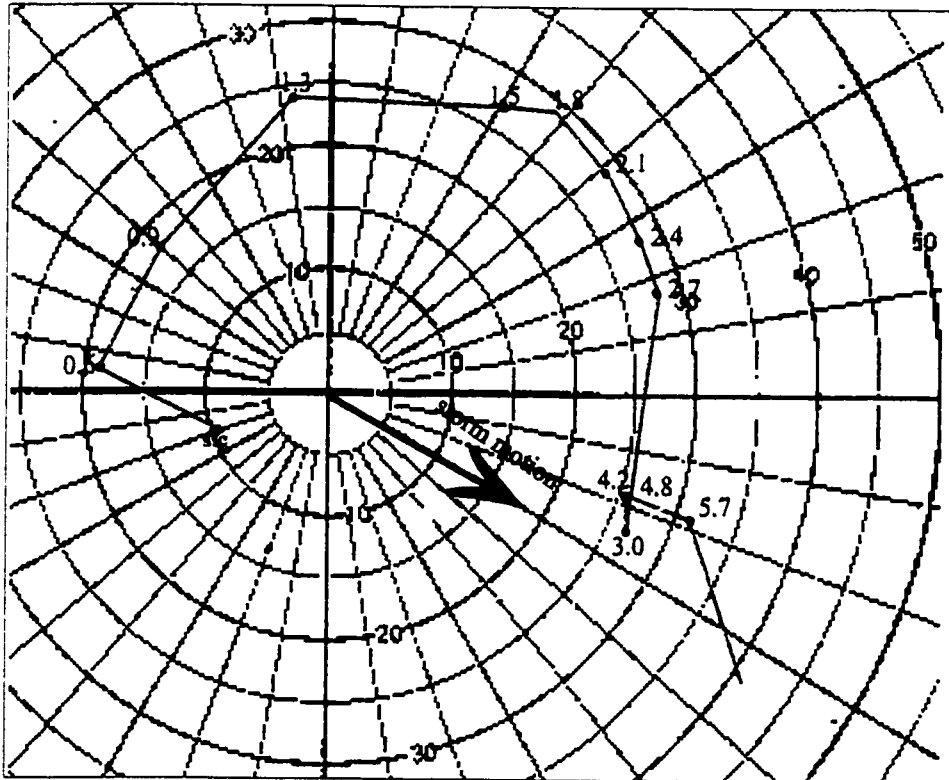


Fig. 3.25 Hodograph illustrating the environmental wind relative to the storm at 0100 UTC (blue). Heights are indicated in km AGL (red numbers), wind speed relative to storm are in knots (black numbers).

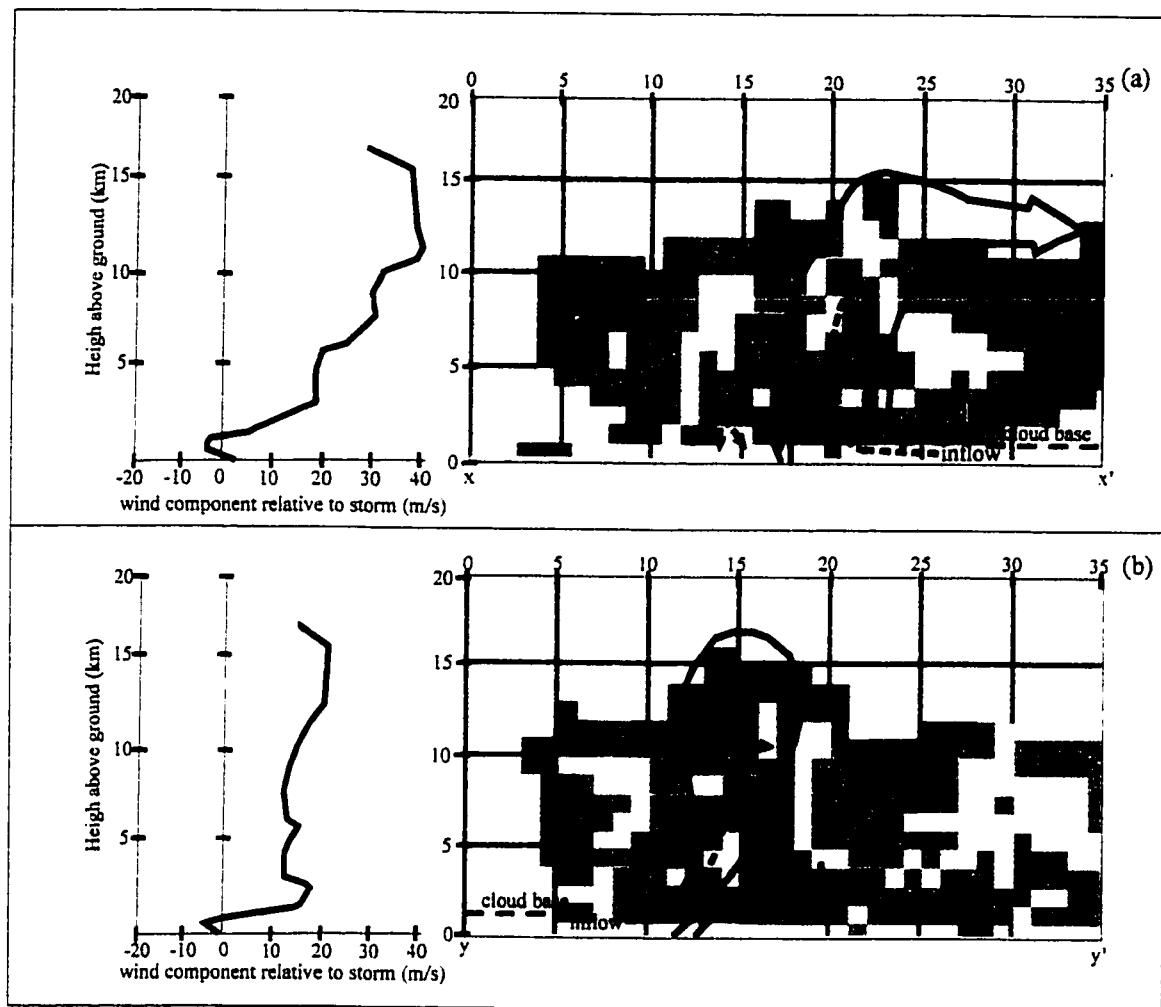


Fig. 3.26 Schematic air flow in the direction (a) and across (b) the plane of the hailstorm's motion, 0120 UTC 17 July 1996, superimposed on the vertical cross sections displayed by RDSS (refer to Fig. 3.24). Wind components relative to the storm (in the plane and across of storm motion) are shown on the left side of each display (a and b).

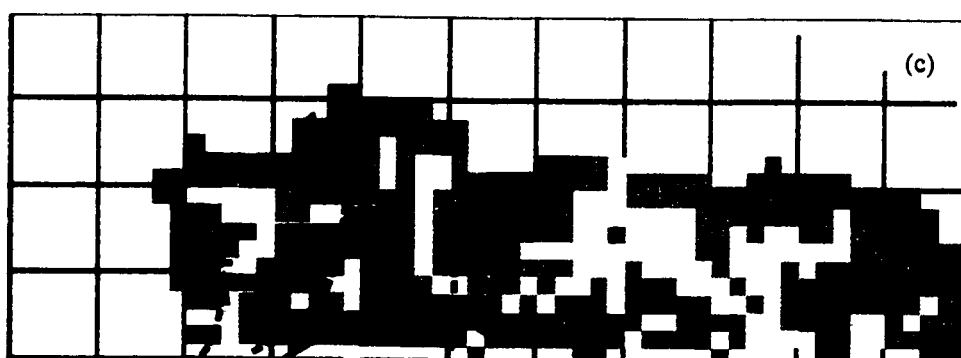
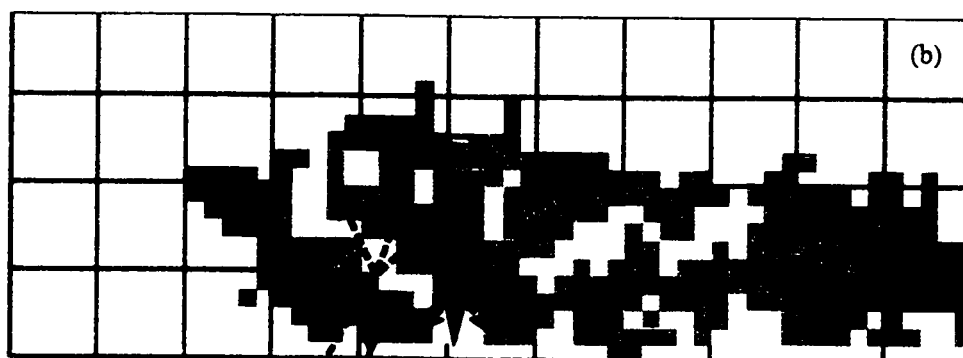
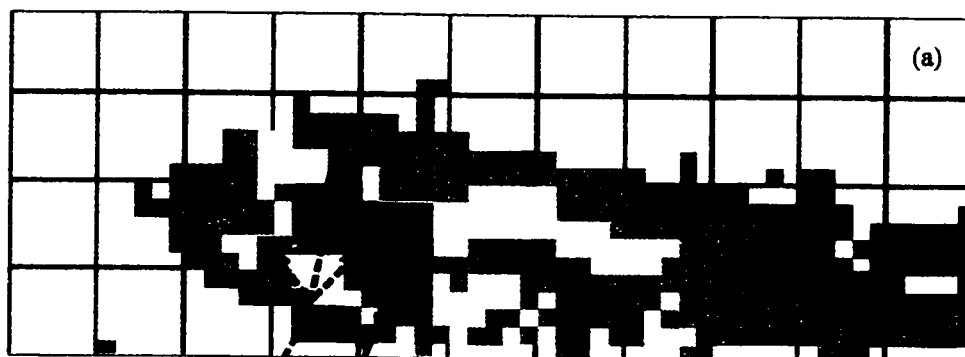


Fig. 3.27 Five minute sequence of cross sections (through the southwest flank of the storm) displayed by RDSS from 0110 to 0135 UTC, 17 July 1996. (continued in the next page)

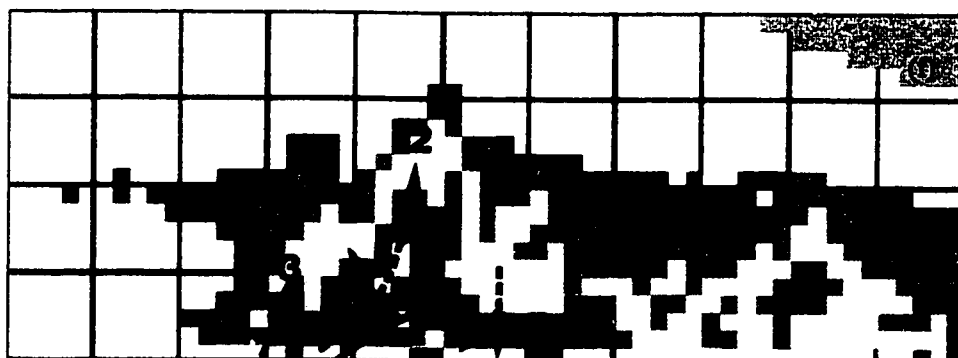
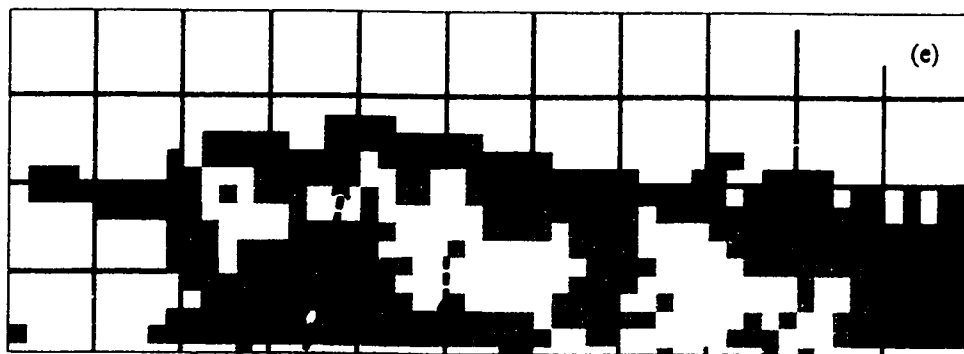
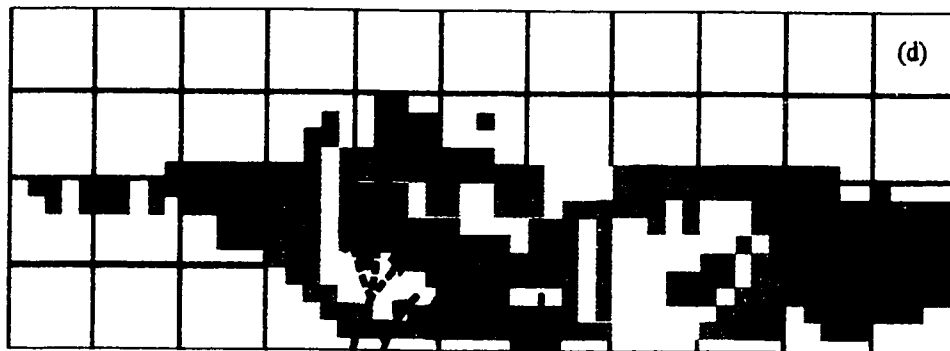


Fig. 3.27(continued) Formation and decay of three cells (1-3) are shown in the severe hailstorm complex.

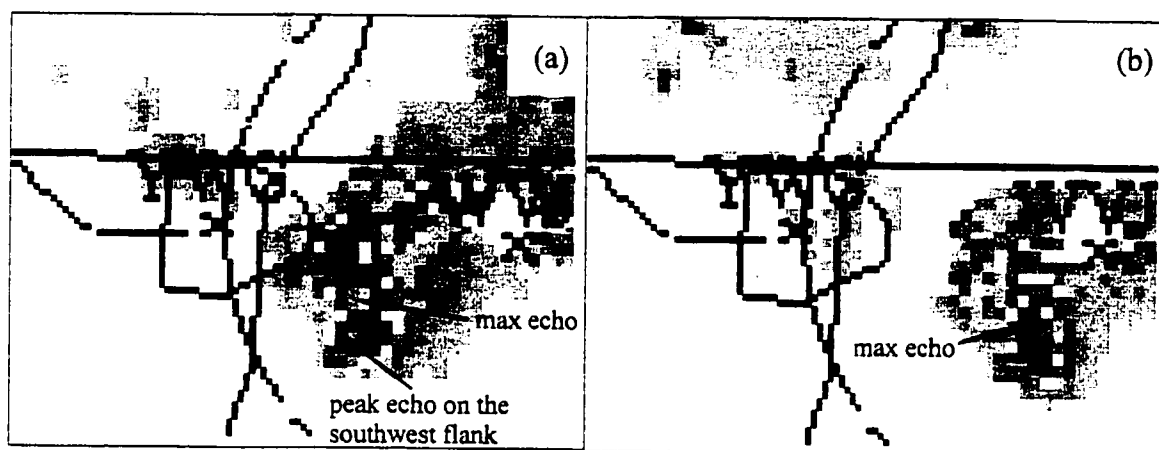


Fig. 3.28 Vivian radar CAPPIs at 1.5 km for (a) 0215 and (b) 0245.

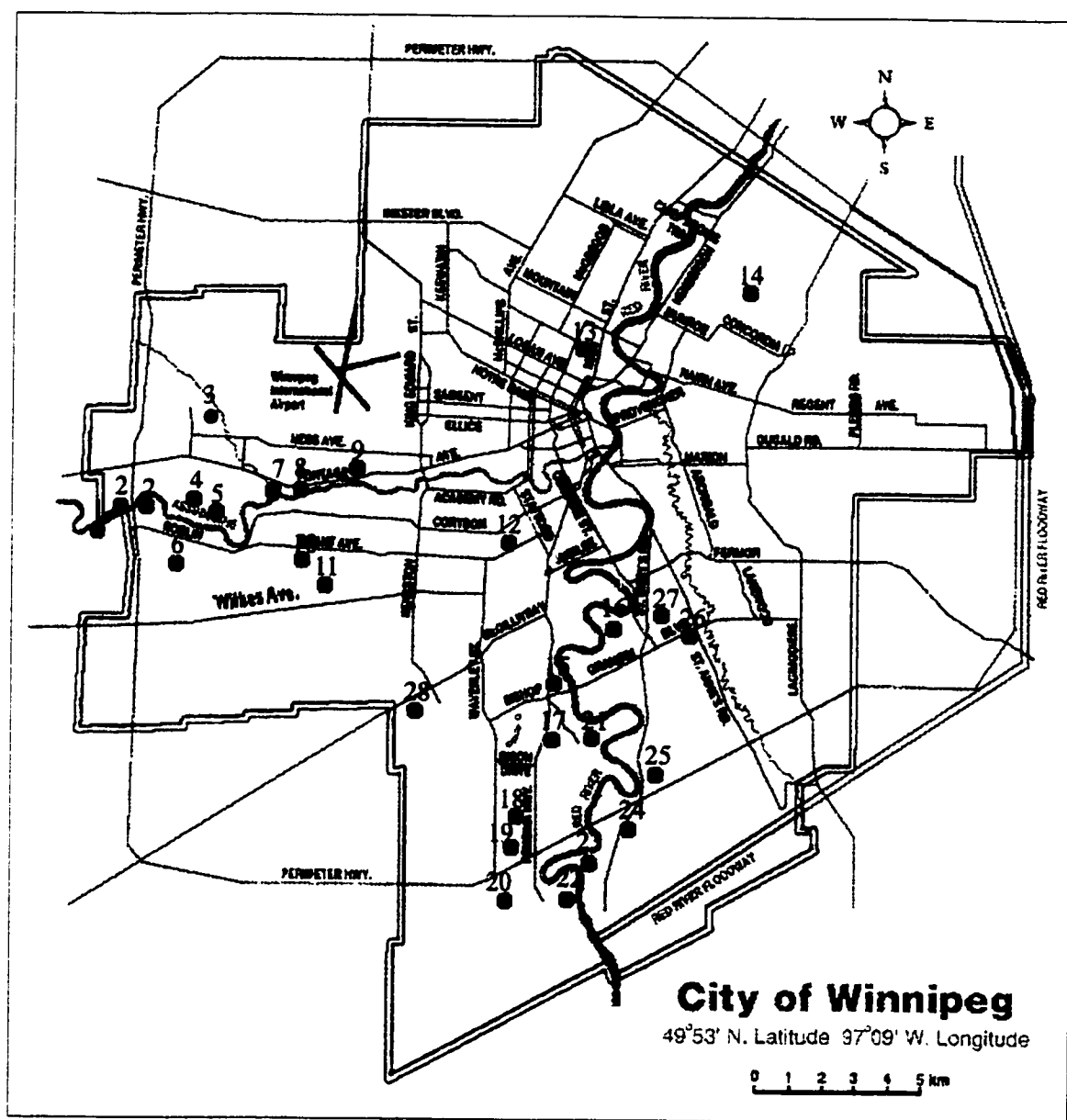


Fig. 3.29 The locations of the reported large hailstones over the city of Winnipeg. Refer to Table 3.1 for the size and the possible damage caused to property.

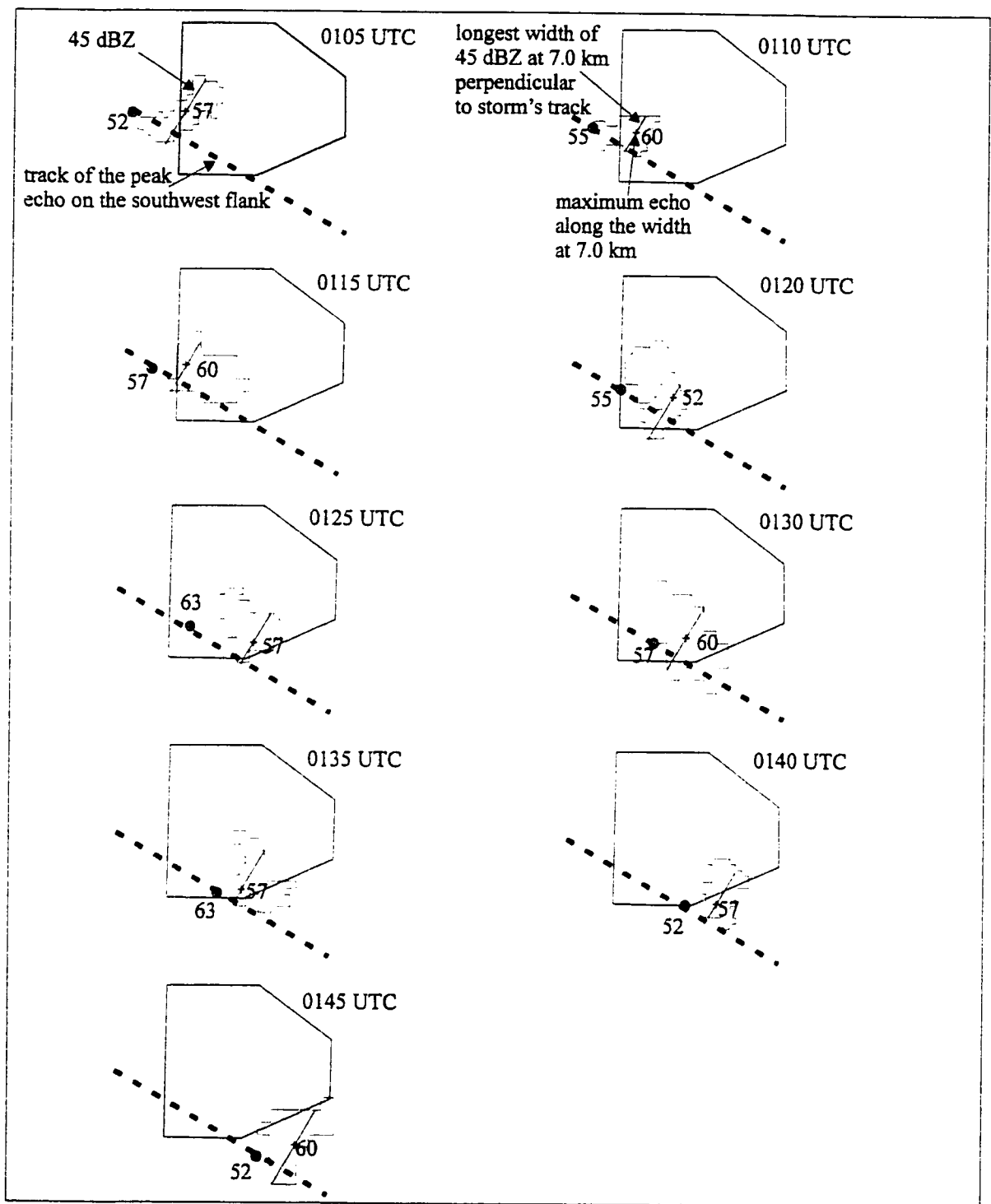


Fig. 3.30 Five minute sequence of 45 dBZ boundary (red) obtained from 7.0 km CAPPIs and peak echoes (blue) on the southwest flank of the storm at 1.5 km. The dashed is the path of the storm, the solid line is the longest width of the 45 dBZ at 7 km perpendicular to the track of storm and the cross indicate the maximum echoes along the width.



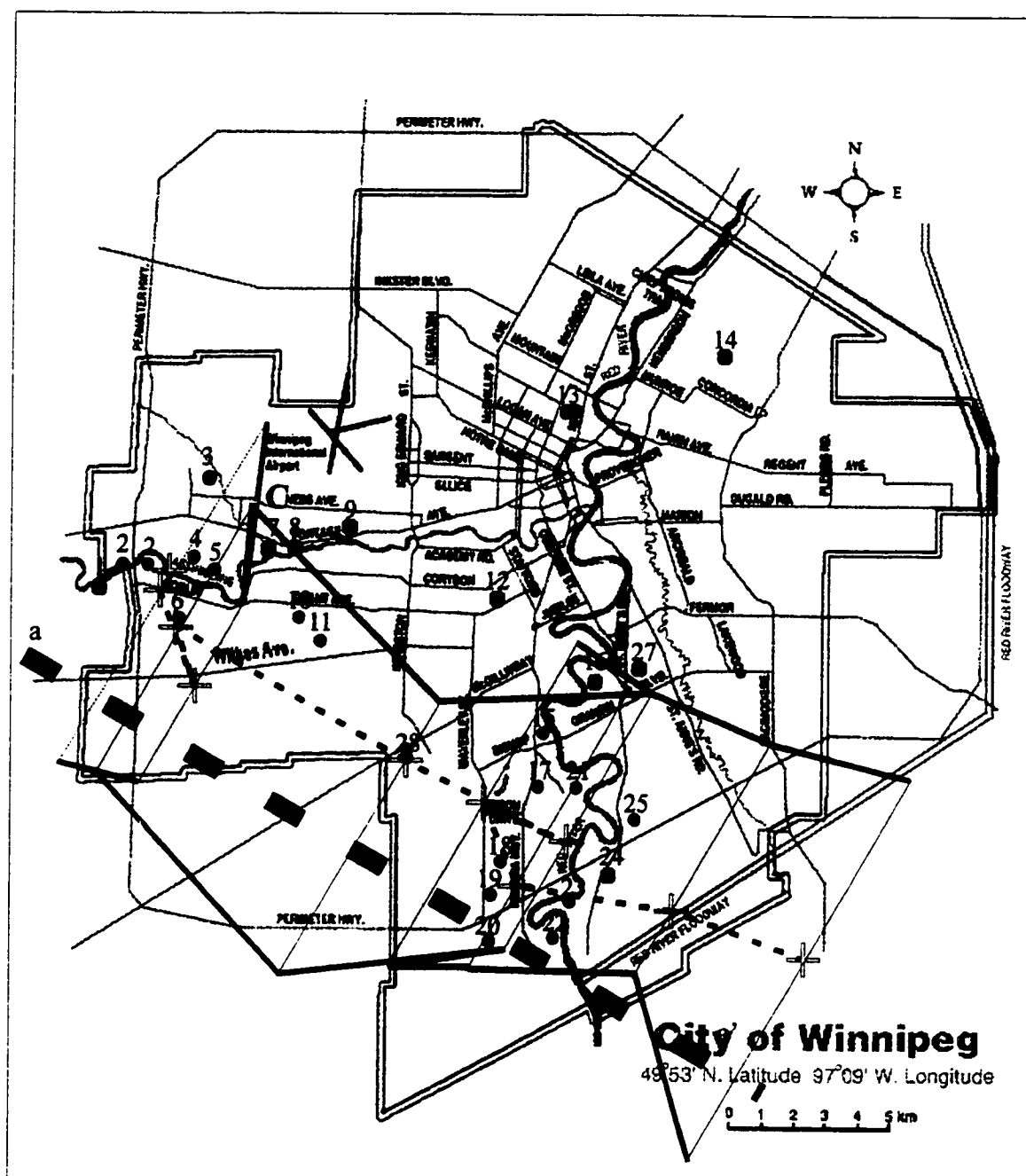


Fig. 3.31 Track of the longest width of 45 dBZ at 7 km (thick black) perpendicular to the the storm's motion (aa') (refer to Fig. 3.29). The crosses are the maximum echoes along the width. The thin dashed line (black) is the track of the maximum echoes. Red circles are the location of hailstones greater than 40 mm.

| mm/h | dBZ |
|------|-----|
| .2   | 13  |
| 1    | 23  |
| 2    | 28  |
| 4    | 33  |
| 8    | 37  |
| 12   | 40  |
| 16   | 42  |
| 24   | 45  |
| 32   | 47  |
| 50   | 50  |
| 64   | 52  |
| 100  | 55  |
| 128  | 57  |
| 200  | 60  |
| 300  | 63  |

Fig. 3.32 Colour scheme for converting radar reflectivity (in dBZ) to rainfall rate (in mm/h) based on the Marshall Palmer Z-R relationship.

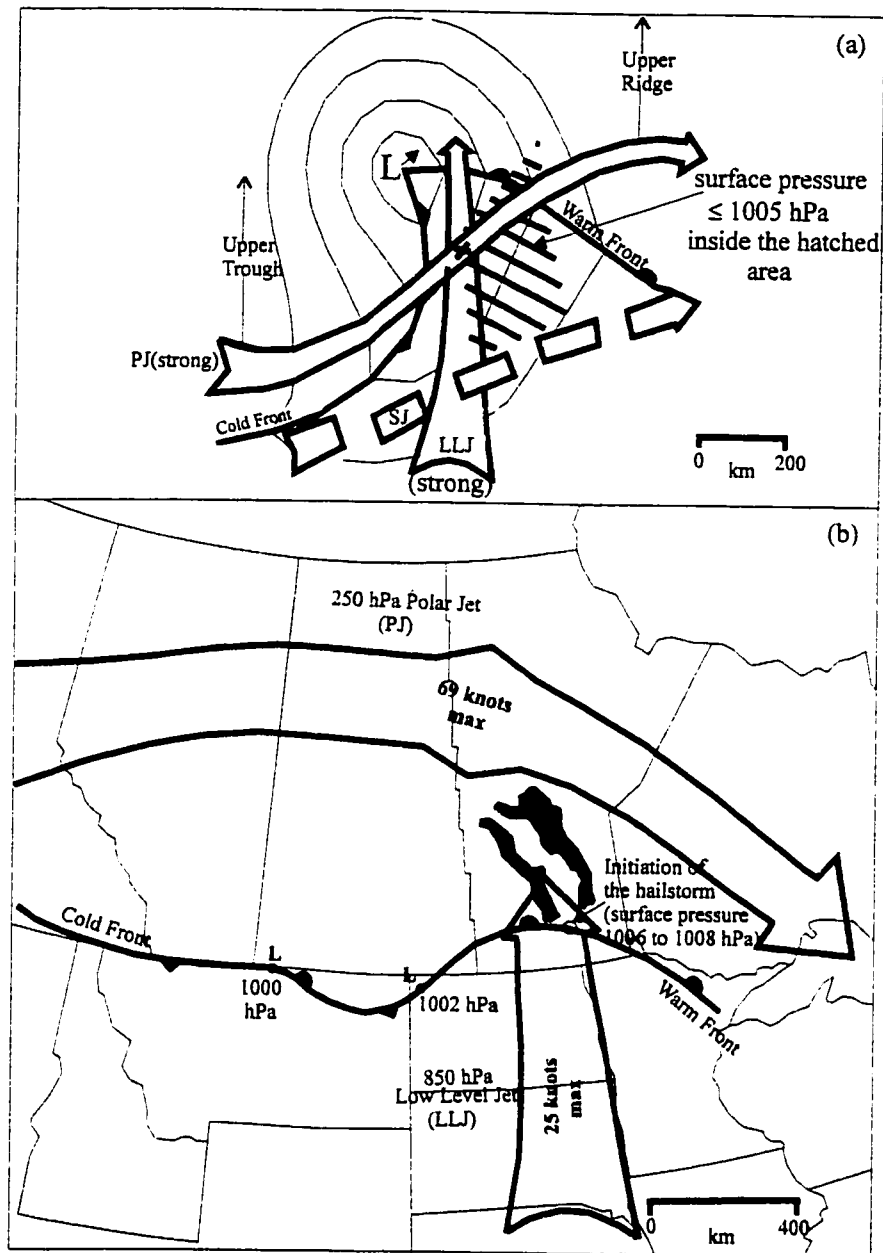
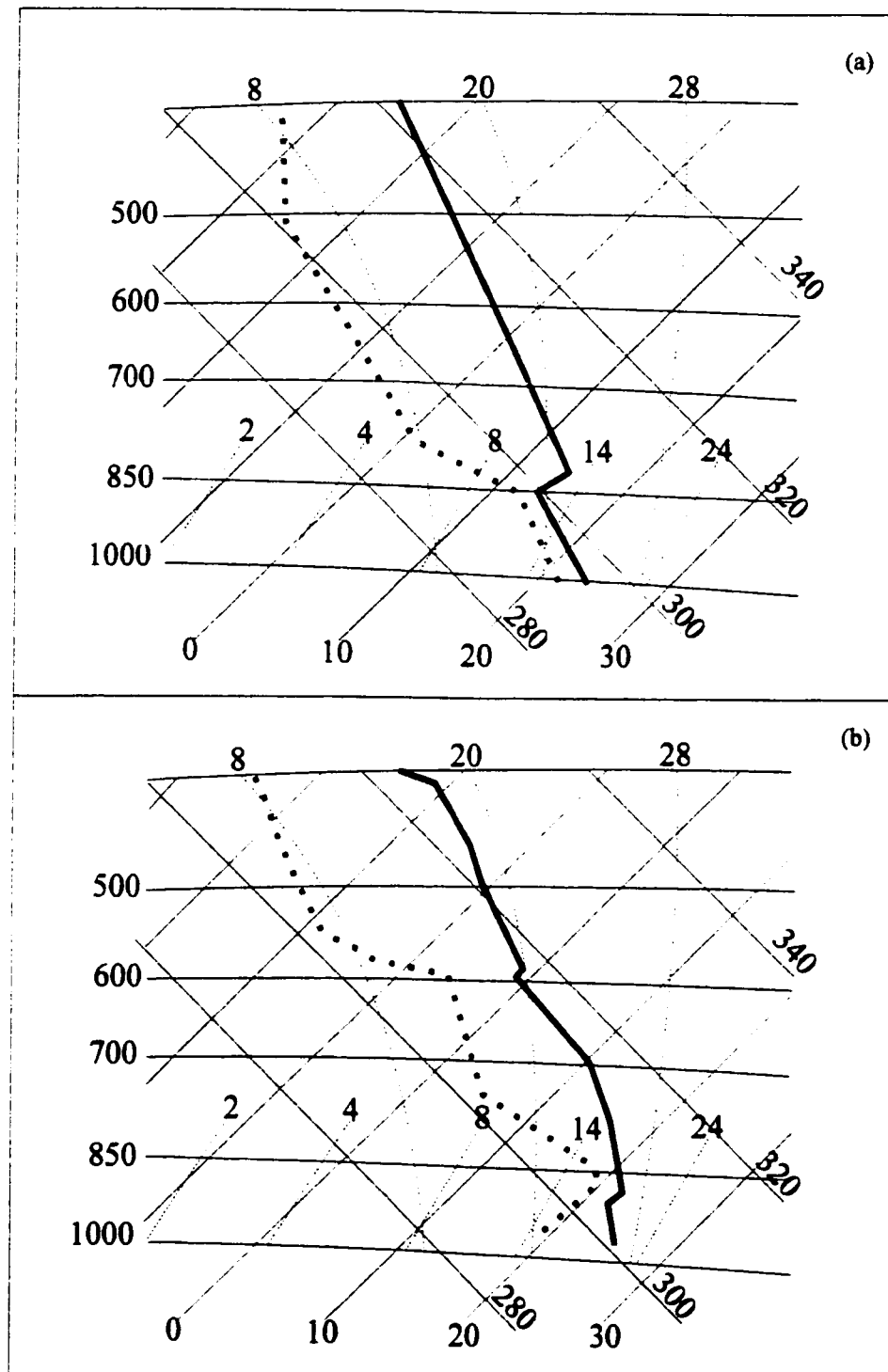
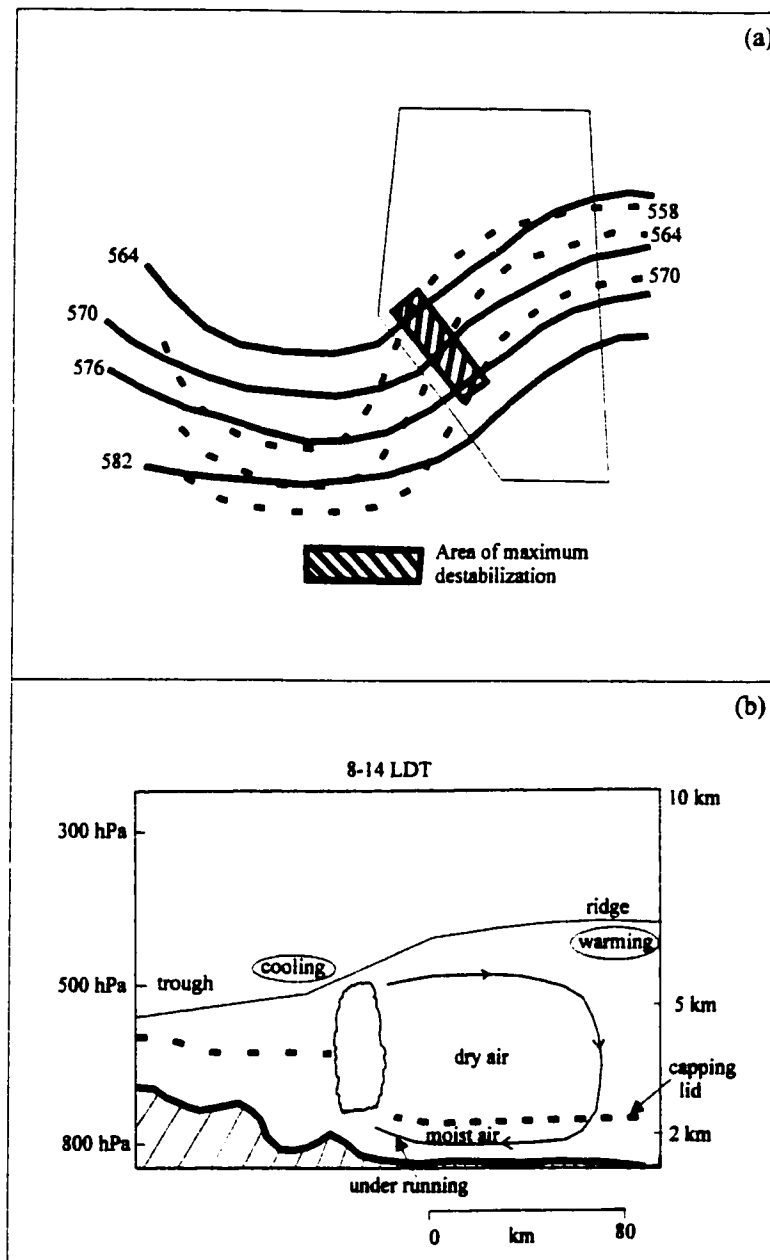


Fig. 4.1 (a) Classical pattern of a mid-latitude, synoptic scale situation favourable for the development of a severe thunderstorm. Thin line denote sea level isobars. Broad arrows represent low level jet (LLJ), polar jet (PJ) in the upper troposphere, and subtropical jet (SJ) at a slightly higher level in the upper tropical troposphere. Severe storms (hatched areas) are most likely to start near "x". (from Barnes and Newton, 1986)

(b) The composite dynamic features, in the synoptic scale, over Manitoba at 0000 UTC, 17 July 1996 (approx. 30 minutes prior to the hailstorm's initiation).



**Fig. 4.2** (a) The classical "loaded gun" sounding of temperature and dewpoint plotted on a tephigram (from Johns and Doswell 1992).  
 (b) The Winnipeg hailstorm sounding (from Shilo at 0100 UTC 17 July 1996).



**Fig. 4.3** a) Typical 500 hPa heights (solid, dam) and 100-500 hPa thickness (dashed, dam) fields associated with severe convective outbreaks in Alberta.  
b) East - west daytime cross section showing exaggerated mountain-plain circulation produced by the upper level cooling and surface heating over the foothills. (from Smith and Yau, 1993b)

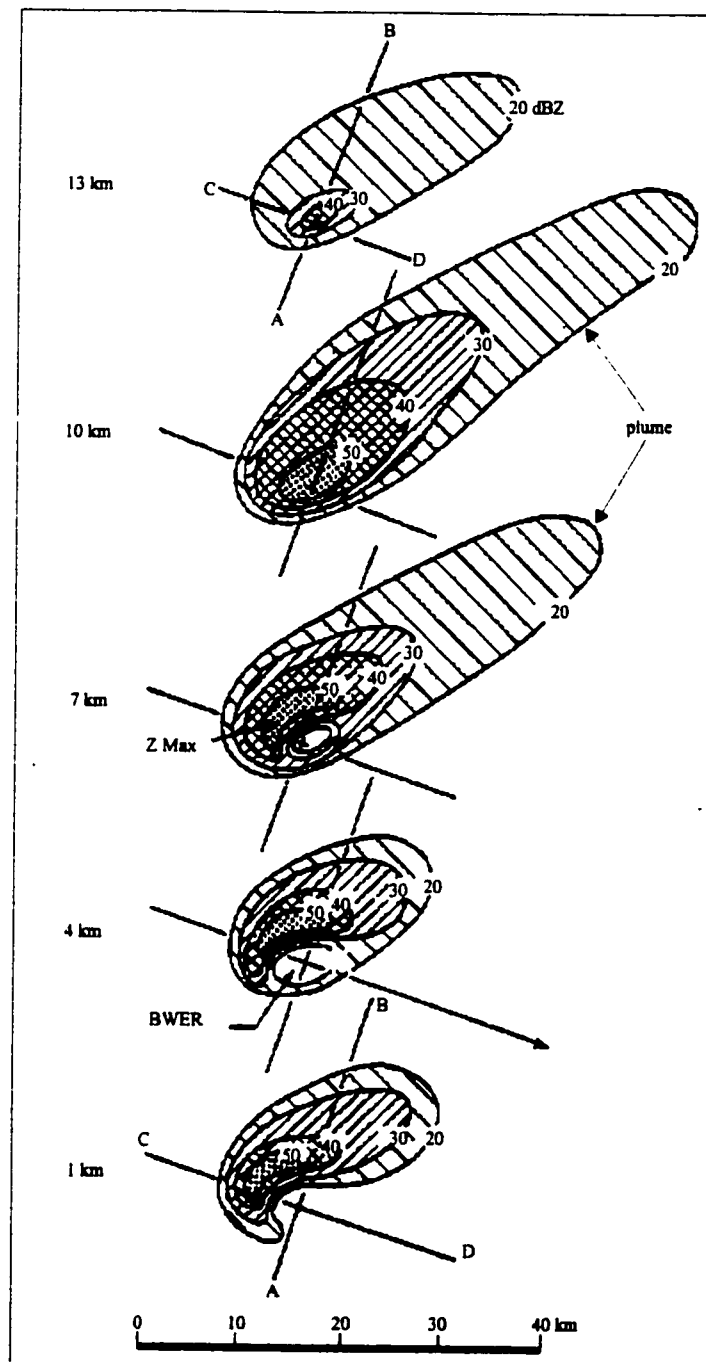


**Fig. 4.4** Schematic horizontal sections of the radar showing the radar structure of a supercell storm at 1, 4, 7, 10 and 13 km AGL. Reflectivity contours are in dBZ. Note the indentation on the right front quadrant of the storm at 1 km which appears as a BWER at 4 and 7 km. On the left hand side of the BWER, is a Z maximum, extending from the top of the BWER to the surface. (from Chisholm and Renick, 1972)

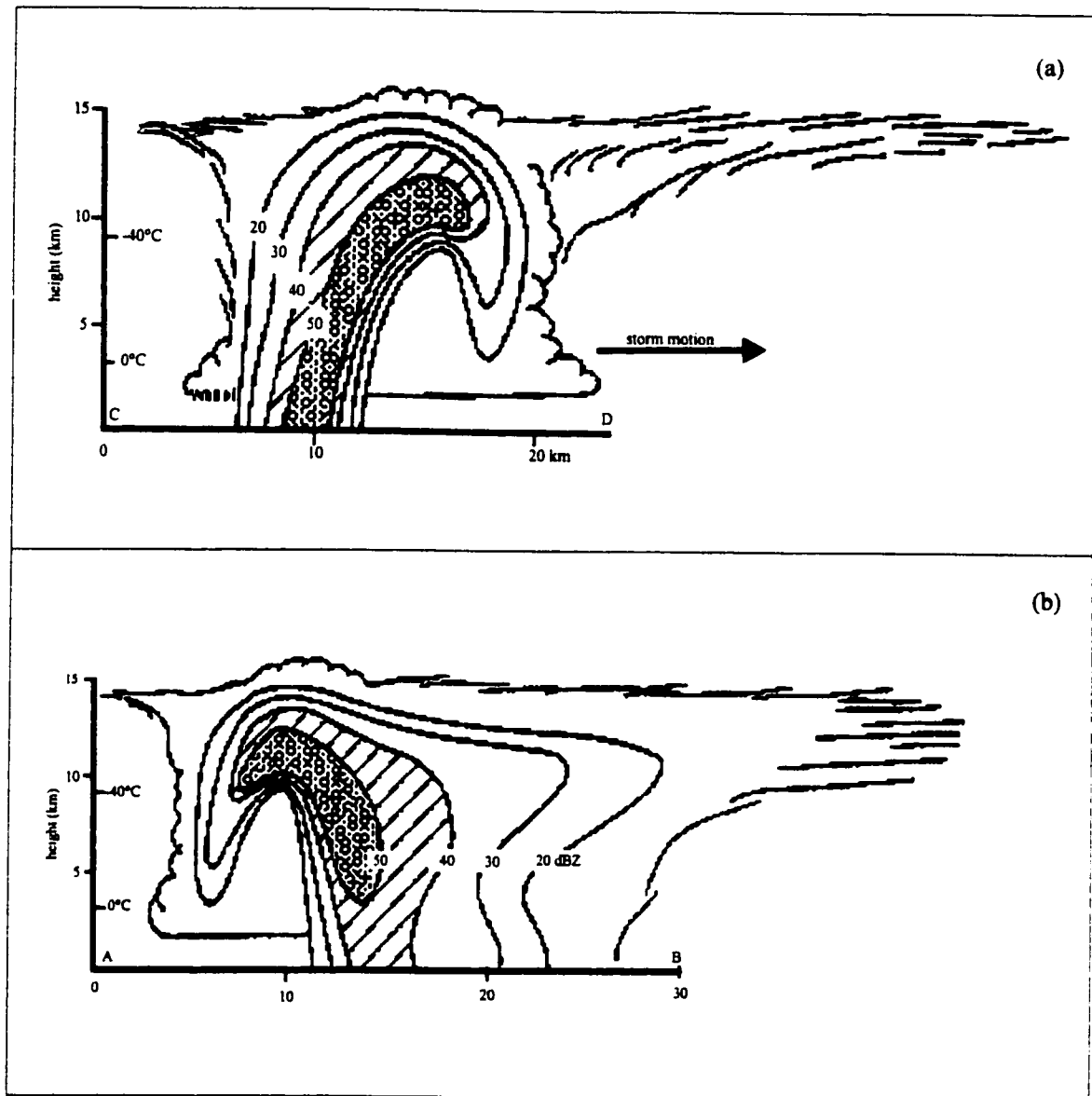


**Fig. 4.5 Schematic vertical sections through a supercell storm:**  
 (a) normal to the plane of storm motion. The cross section is taken through line AB in Fig. 4.6 and viewed in the upwind direction. Note that the BWER extends to a height of 9 km AGL and the high gradient of reflectivity on the Left side of the BWER.  
 (b) in the plane of storm motion, along line CD of Fig. 4.6. Note the Z maximum caps the BWER and extends to the surface on the rear of the BWER. (from Chisholm and Renick, 1972)

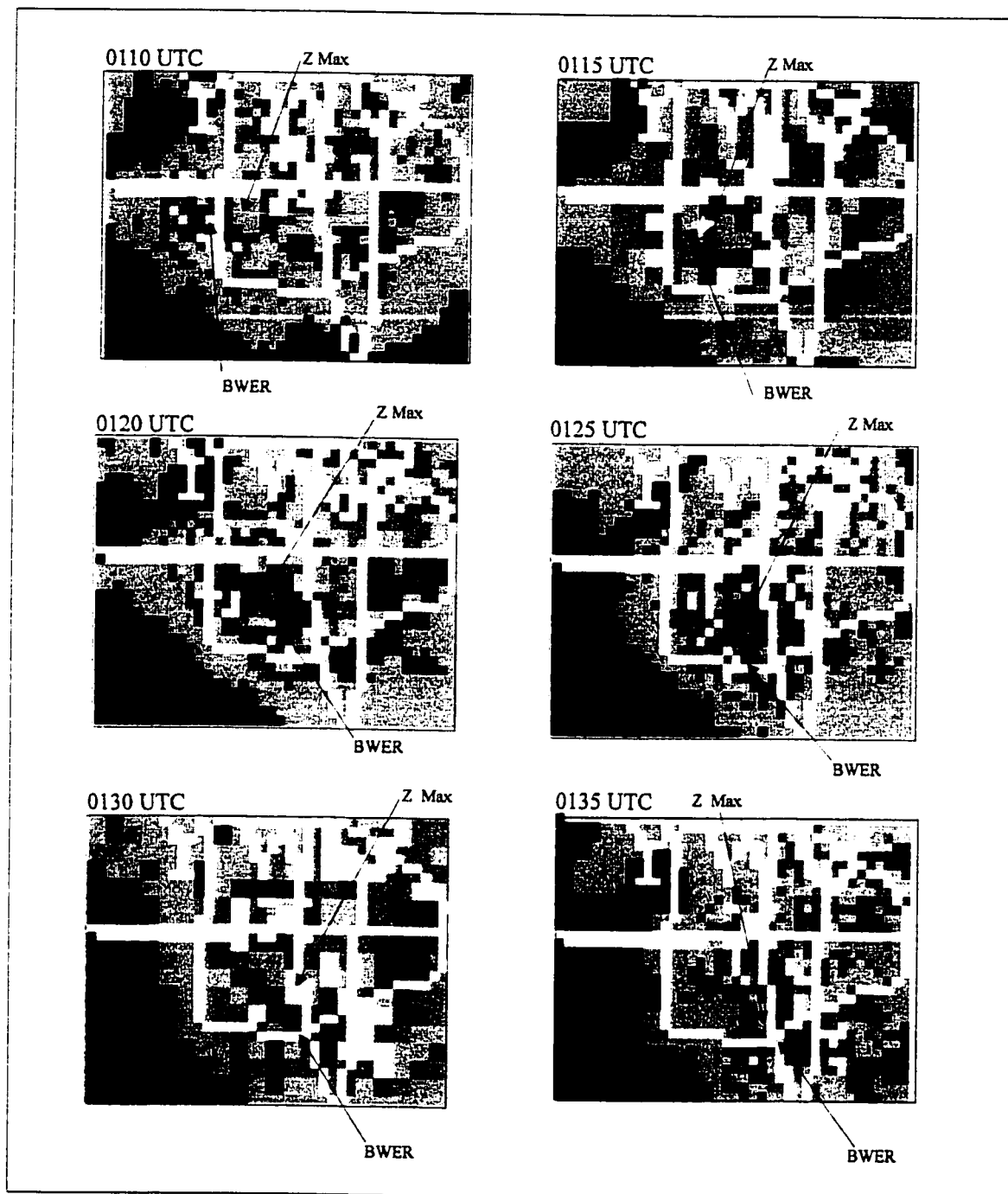


Fig. 4.6 Five minute time sequence, from 0110 to 0135 UTC, of 7 km CAPPI.



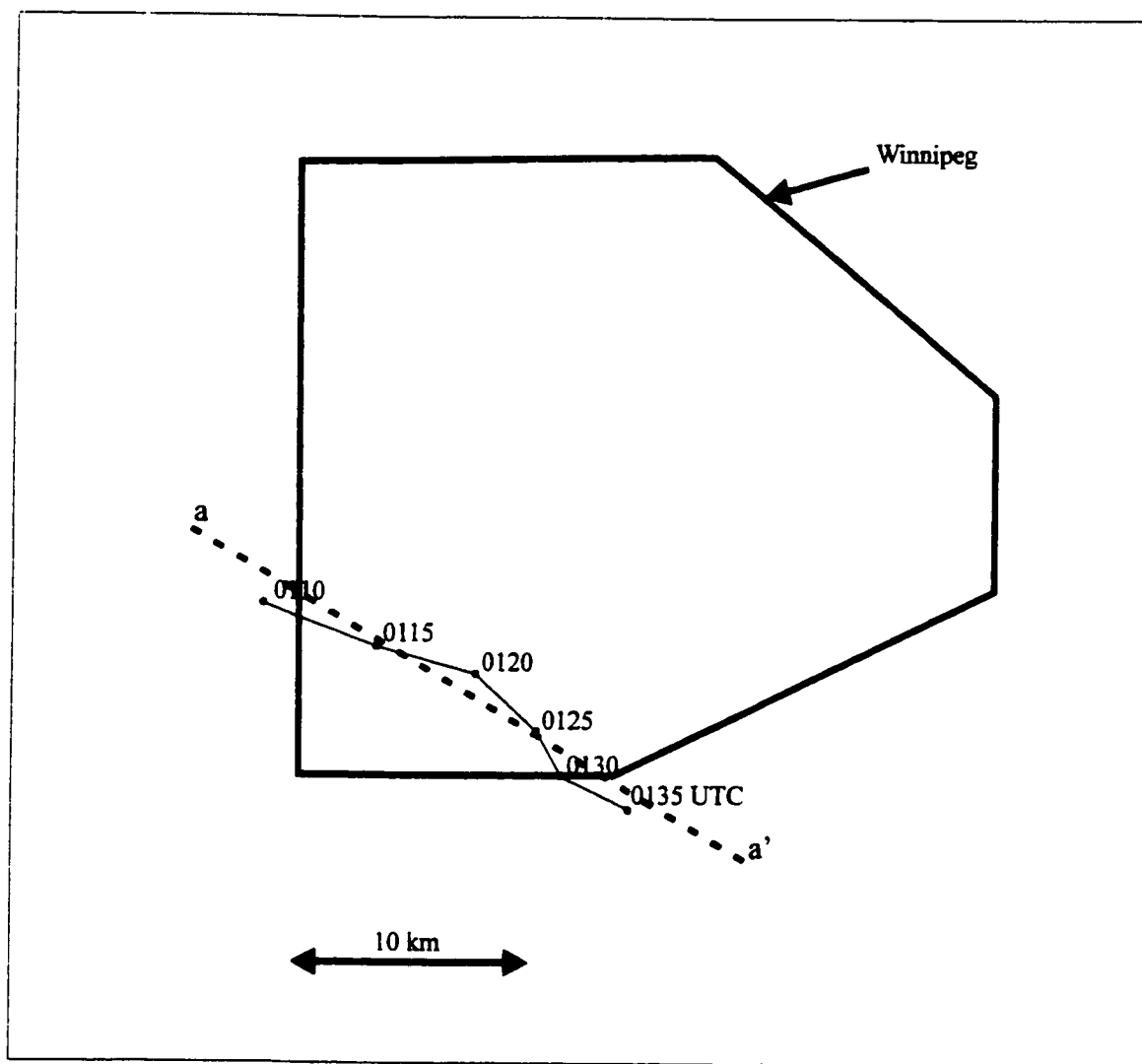


Fig. 4.7 The location (circles) of the BWER centers from 0110 to 0135 UTC. These centers are obtained from the 7 km CAPPIs shown in Fig. 4.6. The solid lines joining the centers illustrate the track and the dashed line, aa', is the best fit line through the centers.

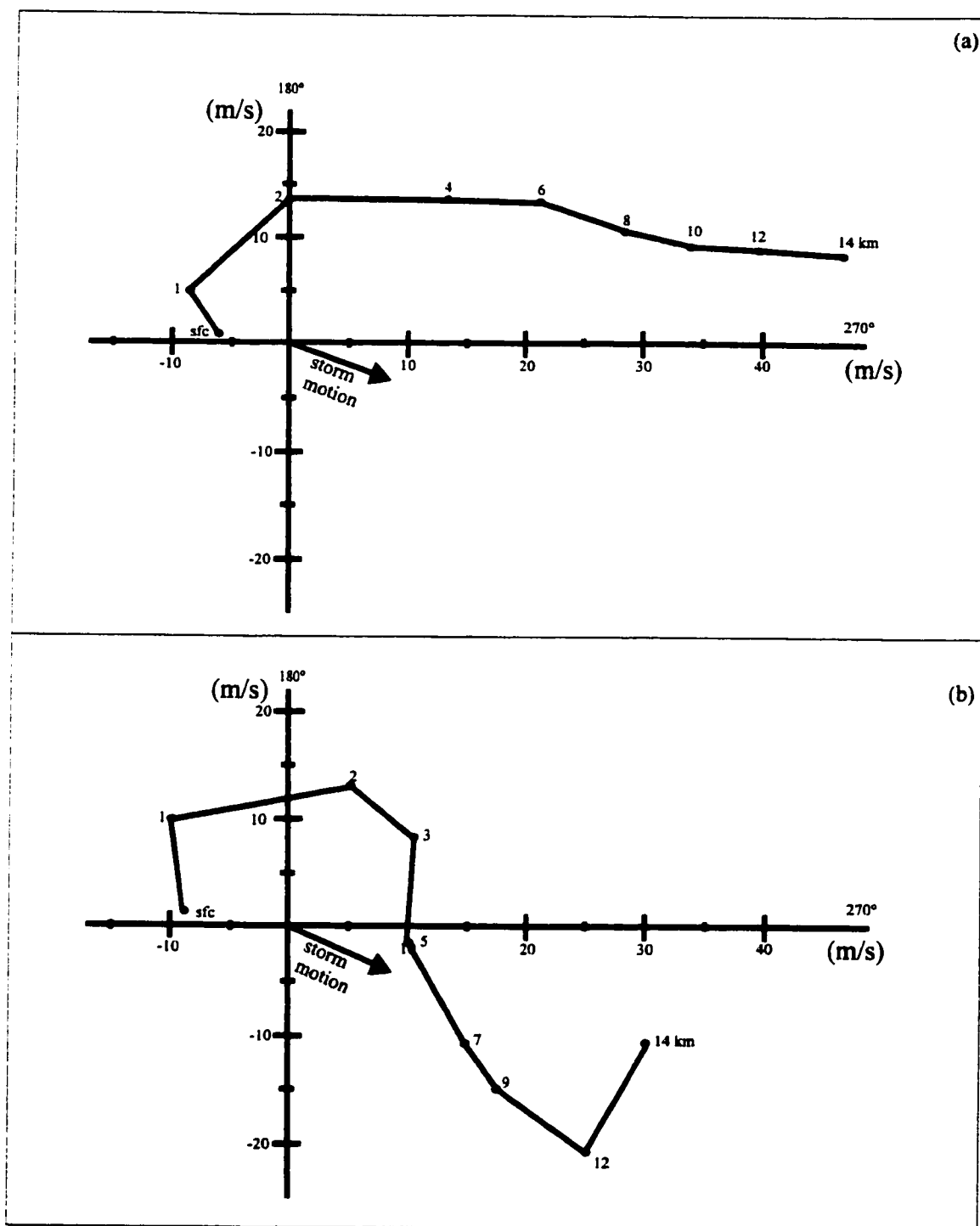


Fig. 4.8 (a) Classical supercell wind hodograph (from Chisholm and Renick, 1972)  
 (b) Winnipeg hailstorm wind hodograph (at 0100 UTC 16 July 1996).

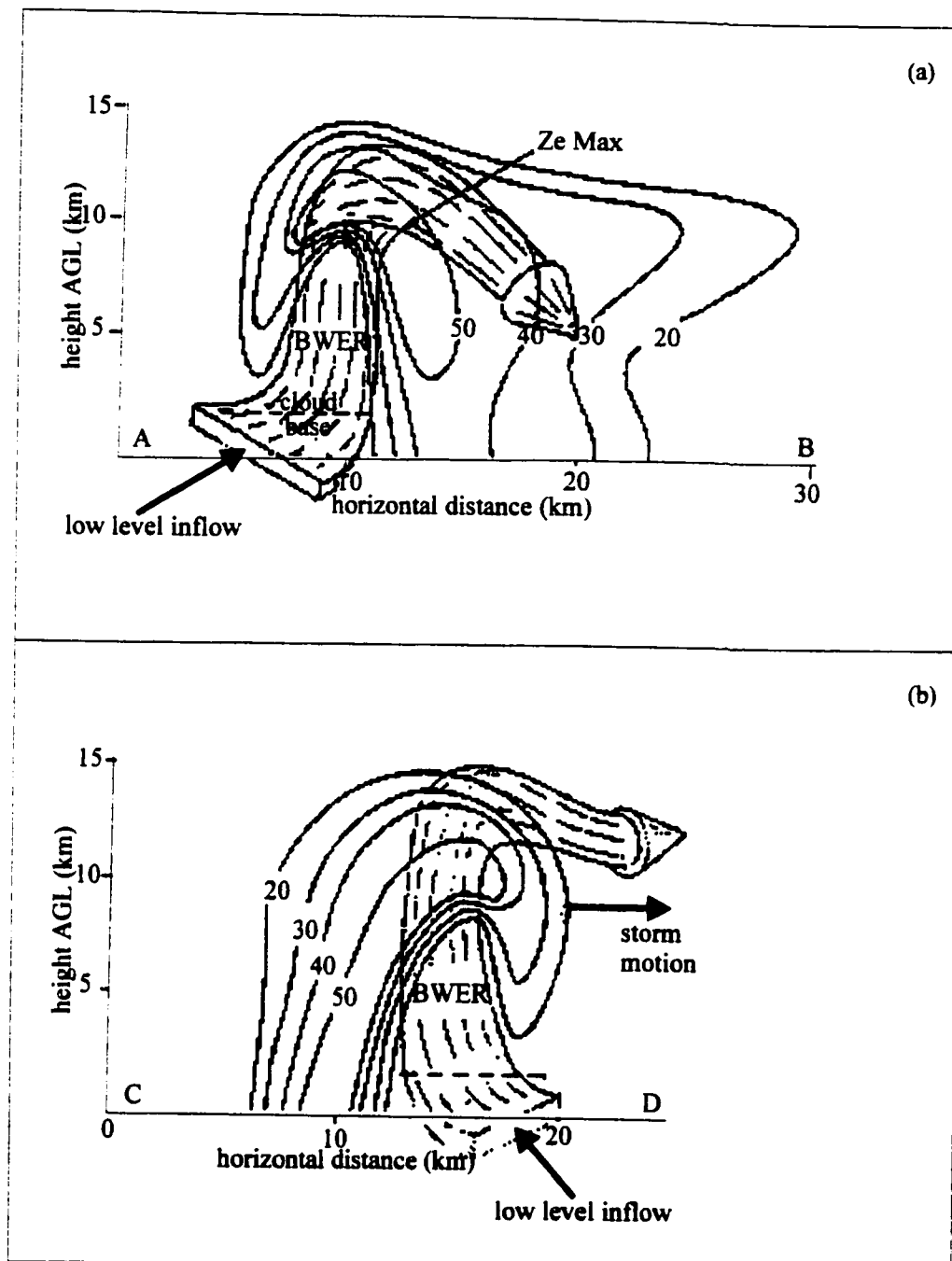


Fig. 4.9 Schematic airflow pattern for a supercell hailstorm (refer to Fig. 4.6 for location of cross sections). (from Chisholm and Renick, 1972)

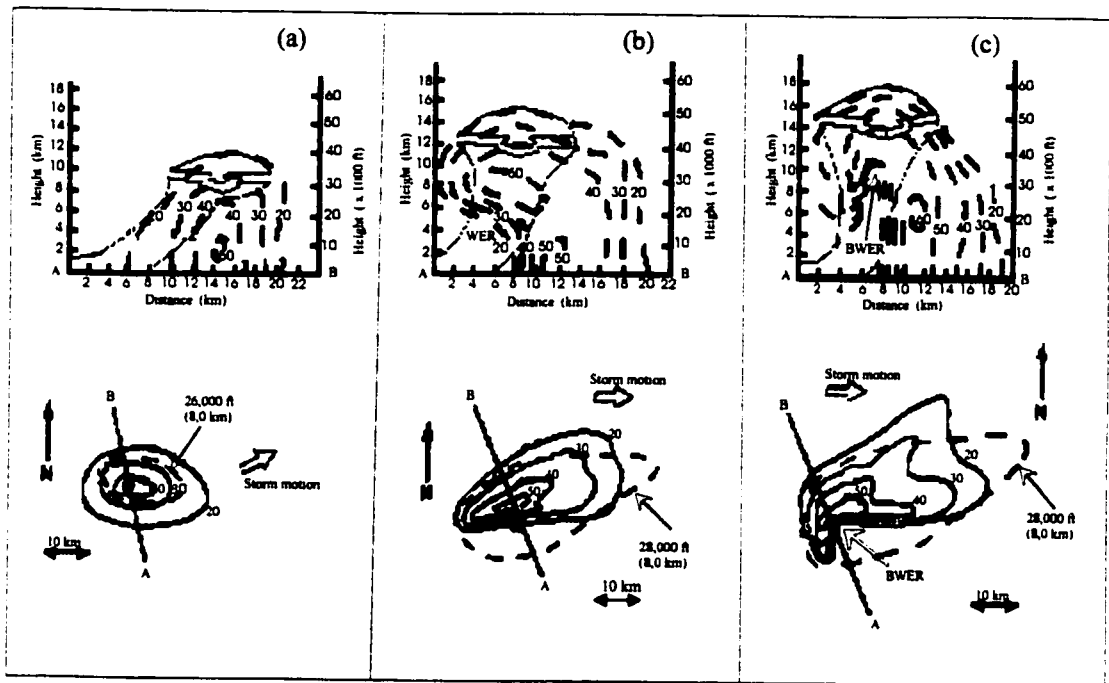


Fig. 4.10 (Above) Vertical Sections as it might be observed on a radar scope during the (a) early, (b) middle, and (c) mature phases of a supercell storm. Low-level inflow, updraft, and outflow aloft (solid lines) are superimposed on the radar reflectivity (dashed lines). The updraft becomes more intense as the storm evolves to its mature phase. WER implies a weak echo region and BWER implies a bounded weak echo region. (below) Composite tilt sequences. Solid lines are the low-level reflectivity contours, dashed lines outlines the echo > 20 dBZ derived from the middle-level elevation scan, and the black dot is the location of the maximum top from the high-levels scan. (from Weisman and Klemp, 1986)

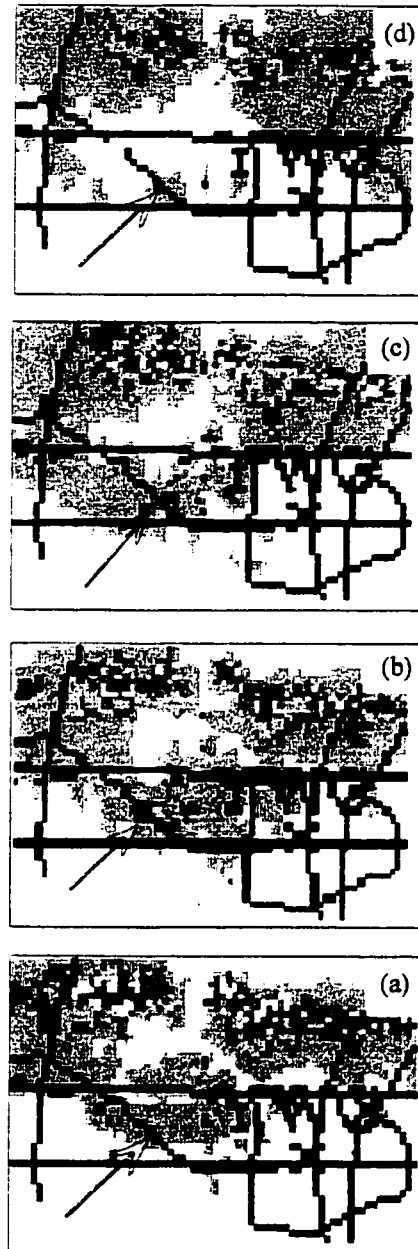


Fig. 4.11 Vivian radar CAPPIs for (a) 1.5, (b) 3, (c) 5, and (d) 7 km AGL at 0035 UTC, 17 July 1996 (triggering stage).

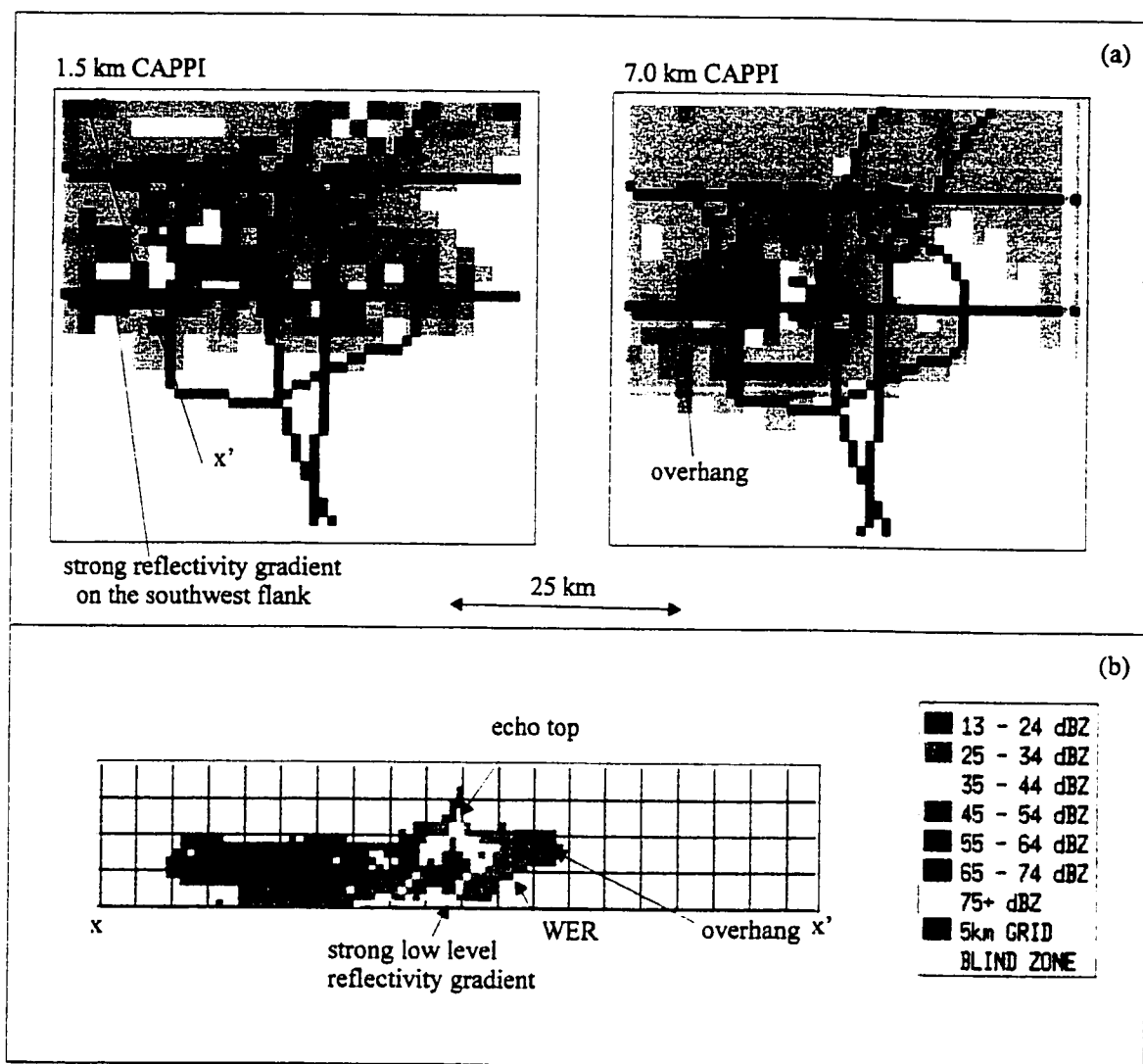


Fig. 4.12 (a) 1.5 and 7 km Vivia radar CAPPIs at 0100 UTC (refer to Fig. 3.32 for the key the reflectivity), (b) cross section presented by RDSS through the southwest flank of the storm (shown as  $xx'$  in (a)).

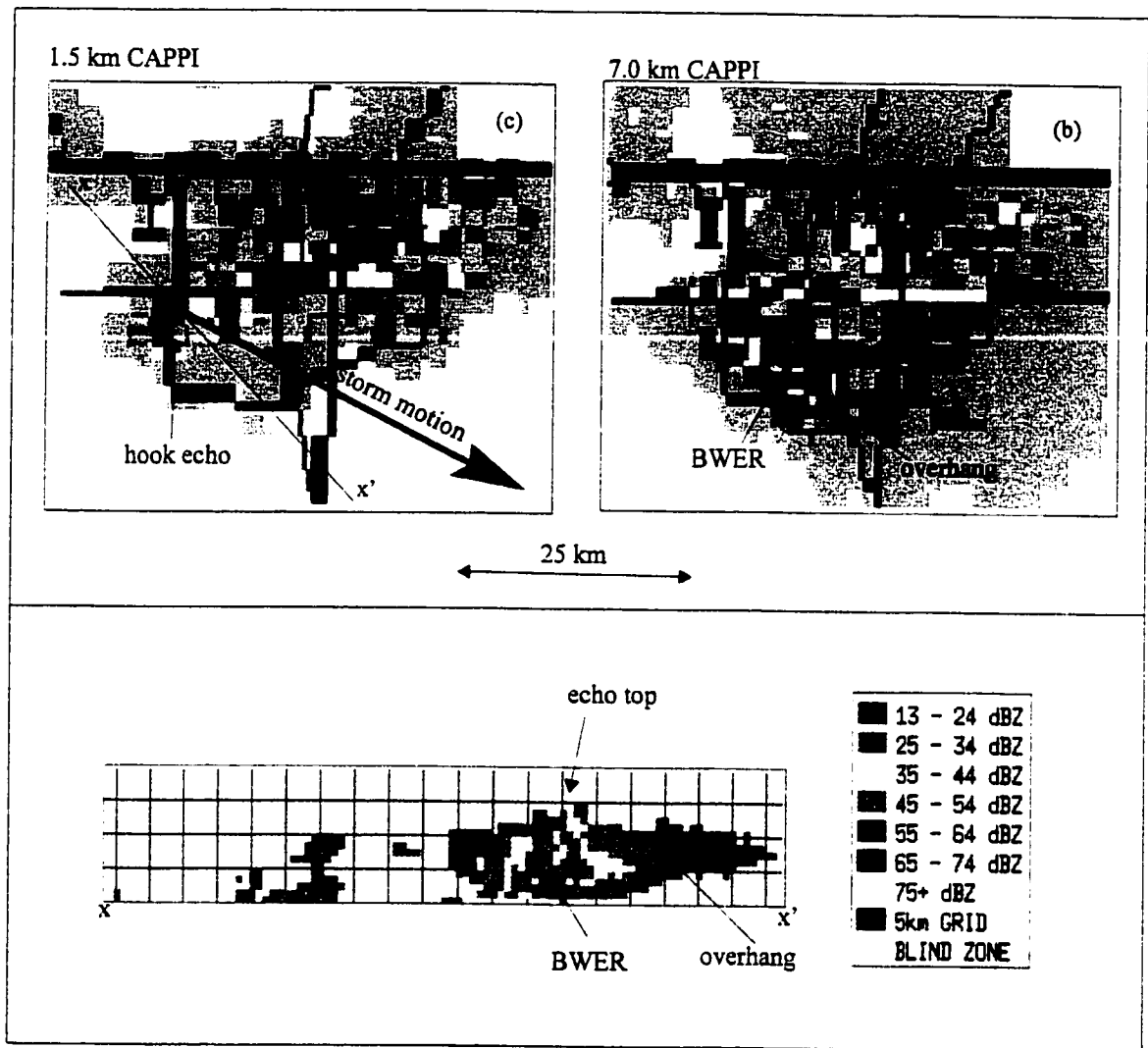


Fig. 4.13 (a) 1.5 and 7 km Vivian radar CAPPIs at 0120 UTC, (b) cross section presented by RDSS through the southwest flank of the storm (shown as  $xx'$  in (a)).

## **Bibliography**

- Barnes, S. L., 1978: Oklahoma thunderstorm on 29-30 April 1970: Part I. Morphology of a tornadic storm. *Mon. Weather Rev.* 106, 673-684.
- Barnes, S. L., and C. W. Newton, 1986: Thunderstorms in the synoptic setting. *Thunderstorm: A Social, Scientific, and Technological Documentary*. Vol. 2: Thunderstorms Morphology and Dynamics, 2<sup>nd</sup> edition, E. Kessler, Ed., University of Oklahoma Press, 75-111.
- Browning, K. A. and F. H. Ludlam, 1962: Airflow in convective storms. *Quart. J. Roy. Meteor. Soc.*, 102, 499-534.
- Browning, K. A., 1964: Airflow and precipitation trajectories with severe local storms which travel to the right of the winds. *J. Atmos. Sci.*, 4, 634-639.
- Browning, K. A., and G. B. Foote, 1976: Airflow and hail growth in supercell storms and implications of hail suppression. *Quart. J. Roy. Meteor. Soc.*, 102, 499-534.
- Browning K. A., 1977: The structure and mechanism of hailstorms. *Meteor. Monogr.*, No. 38, 1-39.
- Chalon, J. P., J. C. Fankahauser, and P. J. Eccles, 1976: Structure of an evolving hailstorm: Part I. General characteristics and cellular structure. *Mon. Weather Rev.* 104, 564-575.



- Chappel, C. F., 1986: Mesoscale Meteorology and Forecasting; Quasi-Stationary Convective Events, American Meteorological Society., Boston, Chapter 13., 289-309.
- Chisholm, A. J., and J. H. Renick, 1972: The kinematics of multicell and supercell Alberta hailstorms. Research council of Alberta, Hail studies Reports 72-2, 24-31.
- Chisholm, A. J., 1973: Alberta Hail Storms. Part I: Radar Case Studies and Airflow Models. Meteor. Monograph, Vol. 14, No. 36. American Meteorological Society, Boston, 1-36.
- Cotton, W. R., and R. A., Anthes, 1989: Storm and Cloud Dynamics, Vol. 44. Academic Press Inc., San Diego, CA, 524 pp.
- Crozier, C. L., 1986: King weather operations manual and users guide, Internal publication, Atmospheric Environment Services, Toronto, 423 pp.
- Doswell , III., C. A., 1985: The Operational Meteorology of Convective Weather, Vol. II: Storm Scale Analysis., NOAA Technical Memorandum ERL ESG-15. Boulder, 59-79, 130-135.
- Djuric, D., 1994: Weather Analysis, Prentice-Hall, Inc., New Jersey, 201-224.
- English, M., 1973: Alberta Hail Storms. Part II: Growth of Large Hail in the Storm. Meteor. Monograph, Vol. 14, No. 36. American Meteorological Society, Boston, 37-98.

- Environment Canada, 1997: High level design of the Radar Decision Support System, EC-6-0524, 37 pp.
- Fawbush, E. J., R. C. Miller, and L. G. Starrel, 1951: An empirical method of forecasting tornado development. Bull. Amer. Meteorol. Soc. 32,1-9.
- Fankhauser, J. C., 1982: Case Studies Of The National Hail Research Council Experiment. Part II: The 22 June 1976 Case Study: Large-Scale Influences, Radar Echo Structure, and Mesoscale Circulations. Colorado Associated University Press, Boulder, 1-34.
- Foot, G.B and C.G. Wade., 1982: Case Studies Of The National Hail Research Council Experiment. Part II: The 22 July 1976 Case Study: Radar Structure and Evolution. Colorado Associated University Press, Boulder, CO, 93-113.
- Johns, R.H. and C. A. Doswell III, 1992: Severe local storms forecasting. Wea. and Forecasting. 7, 588-612.
- Houze, Jr., R. A., 1993: Cloud Dynamics, Academic Press Inc., San Diego, CA, 268-292.
- Lemon, L. R., 1977: On the Use of Storm Structure for Hail Identification. Preprints, 18<sup>th</sup> Conference on Radar Meteorology, American Meteorological Society, Boston, MA, 203-206.
- Lemon, L. R., 1980: Severe thunderstorm radar identification techniques and warning criteria, National Oceanic and Atmospheric Administration, National Severe Storms Forecast Center; Springfield, Va, 60 pp.

- Maddox, R.A. and C. A. Doswell, 1982: An examination of jet stream configuration, 500 mb vorticity advection and low level thermal patterns during extended periods of intense convection. *Mon. Weather Rev.* 110, 184-197.
- Miller, R. C., 1972: Notes on Analysis and Severe Storm Forecasting Procedures of the Air Force Global Weather Central. Technical Report 200 (Rev), Air Weather Service (MAC), USAF, Nebraska.
- Marwitz, J. D., 1972: The structure and motion of severe hailstorms. Part I: Supercell storms. *J. Appl. Meteor.*, 11, 166-179.
- Nelson, S. P., 1976: Characteristics of multicell and supercell hailstorms in Oklahoma. Preprints, International Conf. On Cloud Physics, Boulder, Colorado, 335-340.
- Newton, C. W., 1963: Dynamics of severe convective storms, *Meteor. Monogr.*, 5, No. 27, 33-58.
- Paul, A.H., 1973: The heavy hail of 23-24 July 1971 on the Western Prairies of Canada. *Weather*, 28, 463-471.
- Rinehart, E. R., 1997: Radar for Meteorologists, Rinehart Publications, Grandforks, ND, 428 pp.
- Reuter, G. W. and M. K. Yau., 1987: Mixing mechanisms in cumulus congestus clouds. *J. Atmos. Sci.*, 44, 798-827.
- Rogers, R. R., and M. K. Yau, 1989: A Short Course In Cloud Physics, 3<sup>rd</sup> Ed. Pergamon Press., Toronto, ON, 222-234.

- Smith, S. B. and M. K. Yau, 1993a: The Causes of Severe Convective Outbreaks in Alberta . Part I: Comparison of a Severe Outbreak with Two Non severe Events. Mon. Weather Rev. 121, 1099-1125.
- Smith, S. B. and M. K. Yau, 1993b: The Causes of Severe Convective Outbreaks in Alberta . Part II: Conceptual Model and Statistical Analysis. Mon. Weather Rev. 121, 1126-1133.
- Strong, G. S., 1986: Synoptic to mesoscale dynamics of severe thunderstorm environments: A diagnostic study with forecasting applications. Ph.D. thesis, University of Alberta, Edmonton, 345 pp.
- Summers, P. W., 1972: Project hailstop: A review of accomplishments to date in Alberta. Hail Studies Report 72-2, 47-53.
- Weisman, M. L., and J. B. Klemp, 1986: Mesoscale Meteorology and Forecasting; Characteristic of Isolated Convective Storms. American Meteorological Society., Boston, Chapter 15., 331-358.
- Xue, M., K. K. Droegemeier, V. Wong, A. Shapiro and K. Brewster. 1995: ARPS Version 4.0 User's Guide. Available from Center for Analysis and Prediction of Storms, University of Oklahoma, Norman OK 73072. 380 pp.

## **Appendix 1**

**Winnipeg Free Press 17 July 1996 issue. Page A1 and A3**

Gale-Force winds, torrential rains and golf ball-sized hail tore through Winnipeg last night, leaving behind blackouts, thousands of dented cars and millions of dollars in damages. Charleswood and St. James took the brunt of the hail, which piled up like snow. Rain deluged streets and underpasses—where some drivers sought shelter from the hail—leaving cars stranded in water as deep as 1.5 metres. In some areas, the 100-minute storm smashed gardens and ripped so many leaves off trees it looked like the seasons had suddenly changed from summer to fall. Although the entire city was hit by thundershowers and winds up to 100 kilometres per hour, the hail cut a swath southeast from Headingley, through St. James, Charleswood and Waverly Heights before moving through south St. Vital. “I’ve never seen hail larger than walnuts myself,” said Mark Melsness, an Environment Canada meteorologist. “It’s a rare event.”

Golf ball-sized pits were left in the metal of cars and Autopac officials were scrambling last night trying to get ready for an expected flood of complaints today. Jim Kingdon, a Manitoba Public Insurance spokesman, said Autopac was trying to marshal more telephone complaint worker’s for duty today. “The hail was so strong we know it took out some car windshields in Charleswood,” he said. Kingdon said he couldn’t estimate what the hail damage could cost the insurance corporation, but he said a hail storm last year in Brandon, a city of 39,000, rang up \$5 million worth of vehicle damage. Kingdon said motorists with hail damaged cars will have to pay their deductible, but insurance covers the rest. “Unless there is an emergency we are asking people to with us because there will be delays on the phone. We are asking people to wait until Thursday to call us if they can.”

Wes Redekopp of Corydon Auto Body said he sympathizes with motorists, but knows hail means increased business. "Obviously, we hope no one gets damaged, but unfortunately it will create more business," he said. "The guys at Autopac will be crying." Redekopp said it costs an average of \$1,200 to \$1,500 to repaint a damaged car and a further \$1,200 to \$3,000 to pound out metal damage. "Yes it is amazing what mother nature can do." He said. Motorists did what they could to prevent hail damage.

"I covered my car with sleeping bags, rugs, anything I could get my hands on," a Haney Street resident said. "My car is 3 weeks old today and I didn't want anything to happen to it. I ran out and did anything I could. I just panicked. I was trying to cover myself, but I didn't care what happened to me—just my car."

Other motorists raced for protection at gas stations with overhangs over the pumps. Gary Labossiere, who works at the Shell station at 2501 Portage Avenue, said more than 10 motorists attempted to cram their cars under his gas pump roof.

"Some were getting gas, but most were just trying to protect their cars," He said.

"We even had others using the car wash to get out of the hail."

Lightning is being blamed for a \$35,000 duplex fire in Transcona. Police said the fire, at 752 McMeans Ave., was sparked by lightning hitting the attic and then passing through the wires. The duplex was vacant and there were no injuries.

Hours after the storm, police were still detouring motorists away from the McPhillips Street underpass. "Why people for some unknown reason try to get through 5 feet of water I'll never know," Duty Insp. Alex Katz said. Katz said there were no major storm accidents.

Police and fire crews were swamped with false alarms triggered by the storm. Anita Mitchell, a spokeswoman for Manitoba Hydro, said 2,000 customers in areas of East Kildonan were without power for up to 60 minutes, while 1,400 customers in West Kildonan and Garden City were out for 2 hours. Mitchell said 1,600 Whiteshell Provincial Park residents also lost power for about an hour.

Kevin Houd, an assistant pro at the Charleswood Golf Club, said he braved the golf ball-sized hail to protect equipment on the course. "I got hit a few times, but I'm OK," he said. "For a while there it looked like snow out there on the course. It was white covered over the course. It took 20 minutes to melt."

Meteorologists said hail was ankle deep in some parts of Winnipeg. Home owners were amazed at the force of the hail. "I really thought the hail was going to break the windows," Island Lakes resident Debra Preece said. "It just sounded like rocks hitting the window." Gary Johnson of Haney Street in Charleswood said he saw hail half the size of a baseball outside.

Keith Hoas said "the hail sounded like bombs hitting the side of the building" at South Park Drive apartment. "Ice was hitting and just exploding," said Hoas, a former meteorologist technician who is now a purchaser with Environment Canada. "When you have 2 inch hail, some holes in the screen you can put your pinkie right through ". He was outside surveying the damage after the storm. "I've got some chrome damage and 20 or 30 nice dimples in my roof," he said of his assault on his 1984 Dodge Ram pickup truck. "Some people with fiberglass bodies had holes in them."

Environment Canada meteorologists were fielding dozens of calls and trying to assess the impact of the storm at press time. Gerald Machnee said one St. James resident

called in a report of 62 millimetres of rain at his home near Grace General Hospital. Portage Avenue was awash in water from curb to curb in the area.

He also had a number of reports of hail stones 40-mm to 60-mm in diameter.

“between golf and baseball.” He said. The storm, which hit the city between 7:50 p.m. and 9 p.m., was unusual in how fast it blew in. “It’s not the worst I’ve been through but it had very rapid development,” Machnee said.

And there is was a second storm on its tail; it hit Galdstone at about 10 p.m. and was expected to clip the north end of Winnipeg in a weakened state-around midnight.

Winnipeggers can expect cloud this morning with sunshine in the afternoon, but there could be another thunderstorm late in the day.